An Investigation of the Effect of Erosion Voids on Existing Tunnels

By

Cheehan Leung

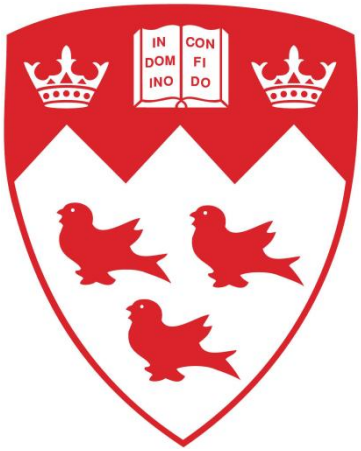

Department of Civil Engineering & Applied Mechanics

McGill University, Montreal, Quebec, Canada

Sept, 2009

This thesis submitted to McGill University in partial fulfillment of the requirements of the degree of Master of Civil Engineering

Abstract

Much of our subsurface infrastructure suffer from aging and is becoming more susceptible to damage due to the deterioration of either the buried structure or the surrounding ground. A known mode of deterioration in tunnels is the formation of erosion voids on the outer surface of the tunnel linings. These are usually caused by the ingress of groundwater through cracks in the tunnel lining that slowly erode the soil surrounding the crack by transporting soil particles. This process may lead to pressure redistribution on the lining and progressive deterioration that could lead to eventual failure. A greater understanding of the impact of these erosion voids can aid in the maintenance of aging infrastructure.

A review of the literature regarding this topic showed that little research has been done beyond numerical analysis and site investigations of failed tunnels. This study presents the results of the experimental investigation that has been conducted to examine the effect of erosion voids on the earth pressure distribution acting on the tunnel liner. The experimental setup allowed for the simulation of the two-dimensional tunnelling process and the tunnelling-induced pressure that results from shield tunnelling. A model tunnel was constructed out of segmented steel pipe to simulate a machine bored tunnel. A controlled contraction of the tunnel diameter was used to simulate a tail void closure and soil movement needed to establish initial conditions. Pressure sensors were placed at various locations along the lining and fine sand was used as the soil medium. A void of known size was then introduced at different locations around the tunnel and the contact pressure on the lining was measured before and after the void introduction. Results indicated significant changes in the magnitude of earth pressure in the close vicinity of the void. The changes in earth pressure differed greatly depending on the placement of the erosion void. Voids placed at a 45^{o} angle between the springline and the invert showed the greatest increase at +29%, whereas voids placed near the springline measured the most change at -60%. This showed considerable change in pressure with the introduction of a relatively small void.

Resume

Notre infrastructure souterraine souffre du vieillissement et devient plus susceptible au dommage grâce à la détérioration de la structure ou la terre enveloppante. Un processus de détérioration des tunnels connu est la création de poches de vide due à l'érosion à la surface extérieure de la doublure du tunnel. Elles sont normalement créer par l'entrée de l'eau souterraine entourant la fissure en transportant des particules de terre. Ce processus pourrait mener à une redistribution de la pression interstitielle sur la doublure et une détérioration progressive qui risque de créer une rupture. Une compréhension plus importante de l'impacte de ces poches de vide peut aider dans la maintenance d'infrastructure vieillissante.

Une revue de la littérature concernant ce sujet montre que peu de recherche a été faite au delà de d'analyse numérique et de l'investigation de site de tunnel. Cette étude présente les résultats de l'investigation expérimentale qui a été mené pour examiner l'effet des poches de vide sur la distribution de pression des terres actant sur la doublure du tunnel. Le montage expérimentale a permit pour la simulation du processus de tunneling en deux dimensions et de la pression induit par le tunneling qui en résulte des travaux de perçage de tunnels protecteurs. Une modèle de tunnel a été construit de tuyau d'acier segmenté pour simuler les machines TBM (Tunnel Boring Machine). Une réduction contrôlée du diamètre du tunnel a été utilisé pour simuler le tassement des machines TBM et le mouvement de terre nécessaire pour établir les conditions initiales. Des capteurs de pression ont été mit à divers emplacements le long de la doublure et de la terre fine a été utilisé en temps que sols. Des poches de vide de taille connue ont été ensuite introduites aux différents emplacements autour du tunnel et la pression sur la doublure a été mesurée avant et après l'introduction de poches de vide. Les résultats indiquent des changements importants dans la grandeur de pression des terres dans les régions de poches de vide. Les changements des points plus loin des poches de vide étaient minimaux. Les changements de pression des terres diffèrent considérablement dépendant de l'emplacement des poches de vide. Celles mises à un angle de 45 ^{o} entre

les côtés et le dessous du tunnel ont montré l'augmentation la plus importante à +29% ; alors que les poches de vide mises près des côtés du tunnel ont mesuré le plus gros changement de -60%. Ceci a montré un changement de pression important avec l'introduction de poches de vide relativement petits.

Acknowledgments

Of everyone that needs to be acknowledged in helping to make this thesis possible, my parents Ying-Wai Leung and Waichuen Lam are the most deserving of thanks, for it has been with their steadfast support, and gentle guidance that has allowed me to reach this goal. An accomplishment that I would not have imagined possible even three years ago. I also want to thank my brother, Cheequn for helping me from afar and providing me with wonderful distraction at times most appropriate.

To Professor M. A. Meguid for giving me this wonderful opportunity and fighting for me from the very beginning. Whose careful direction allowed me many freedoms while pursuing my research that has made me not only grow academically, but personally as well. To the technicians, Damon Kipperchuk, Ron Sheppard, Marek Przykorski and especially John Bartzak, who watched my transformation from a young undergraduate, to an apprentice, and finally to a proven machinist. The experiments would not have been possible without their help. Also, to Dr. William Cook and Jorge Sayat for helping me work through all those many technical issues.

To my colleagues Sherif Kamel and Mahmoud Ahmed for assisting in the backbreaking labour of running the tests. Through your patience and hard work, we were able to overcome. To Miguel Nunes and Tatiana Tobar for providing so much advice and guideance. My work is built directly on the backs of your immense contributions.

And finally, to Claire-Elise Orleach, who, in addition completing the arduous task of translating my abstract, has been a daily source of strength and inspiration, a confidant, and a friend and companion throughout this whole journey.

Nomenclature

Symbol	Definition
a	Tunnel drainage radius
C	Compressibility
c	Cohesion
C_c	Coefficient of curvature
C_u	Coefficient of uniformity
D	Diameter
E	Soil modulus of elasticity
E_s	Lining modulus of elasticity
F	Flexibility ratio
F	Seepage Force
G_s	Specific gravity
h	Depth below ground surface
h_a	Lining energy head
i	Hydraulic gradient
K	Soil permeability
K_o	Coefficient of at rest lateral earth pressure

K_a	Coefficient of active lateral earth pressure
l	Tunnel lining arc length
L_v	Void length
$\mathrm{loss}(\%)$	Percentage difference between lining area and excavation area
M	Moment
P	Measured pressure
P_o	Initial Pressure
q	Drainage flow
r	Lining radius
r_o	Lining outer radius
t	Tunnel lining thickness
T	Thrust
U_{max}	Maximum soil movement
U_r	Radial movement
U_θ	Tangential movement
w	Tail void
x	Axis normal to the y-z plane
y	Axis normal to the x-z plane
z	Axis normal to the x-y plane

γ	Unit weight of soil
γ_w	Unit weight of water
τ	Shear strength
$\tau_{r\theta}$	Polar coordinates shear stress
ν	Soil Poisson's ratio
ν_s	Lining Poisson's ratio
σ_θ	Tangential stress
σ_r	Radial stress
ϕ	Angle of internal friction

Table of Contents

List of Figures

List of Tables

Chapter 1 – Introduction

1.1 General

As urban populations continue to grow around the world, engineers and urban planners are challenged with the task of having to sustain an expected quality of life with an ever decreasing amount of space. This includes the expansion of existing facilities as well as the maintenance and upgrade of existing infrastructure. Accordingly, tunnels have become an indispensible part of a functioning developed society. In dense urban settings, tunnels become economical for various infrastructures such as subways, sewers, power lines and communication cables. In older cities, much of the urban infrastructure is already hidden underground and has been in service for many years. As these tunnels age the need to assess the condition of these structures becomes paramount. The ability to determine whether certain stretches of a tunnel are at a critical state can allow better management of our tunnel infrastructure. With more and more tunnels reaching later stages of their design lives, a better understanding of the deterioration conditions that a tunnel undergoes will allow more efficient allocation of limited resources in maintaining these integral structures.

This thesis will examine one of the modes of deterioration in tunnel linings. That is the effect of formation of local contact loss on the pressure distributions on the lining. Contact loss can develop due to erosion voids caused by the infiltration of water through cracks in the tunnel lining. The water can carry with it small soil particles that will, over time, create voids in the soil surrounding the tunnel. The exact effects of these local erosion voids on tunnel lining are essentially unknown. Figure 1.1 shows the formation of an erosion void in the soil surrounding a subway tunnel.

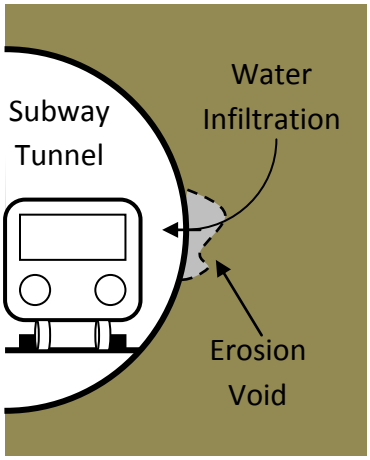

Figure 1.1: Erosion void on a subway tunnel

1.2 Purpose and Scope

The purpose of this thesis is to investigate the changes in earth pressure acting on a circular tunnel subjected to local contact loss on the surface of the tunnel lining. This will be achieved using a small scale model of a tunnel in granular soil. Void creation will be simulated and tested in two-dimensional (plane-strain) conditions.

1.3 Objectives

The research objectives of this thesis are as follows:

- Develop a physical model that simulates the erosion void effect on tunnel linings
- Determine the change in the distribution of stresses around a tunnel lining as a result of local contact loss
- Verify if the laboratory model accurately simulates the forces on a tunnel lining

- Identify areas in the laboratory procedure that would have affected the test values such as boundary conditions
- Determine whether a trend in the subsurface reaction to voids on the tunnel lining can be confirmed

1.4 Thesis Organisation

This thesis is organised into several chapters, each of which is briefly outlined below:

- Chapter 1 introduces the topic and gives some background information about erosion voids.
- Chapter 2 is the literature review. This chapter provides a summary of relevant academic topics relating to the thesis topic. This includes basic tunnel/soil interaction, groundwater seepage in linings, numerical models of erosion voids and tunnel failure field observations.
- Chapter 3 presents the experimental methods and materials. This chapter outlines in detail the model tunnel that was developed for this experiment as well as the container built to house it. Also covered are the data acquisition program and the experimental procedure.
- Chapter 4 presents the data resulting from the experiments and offers some analysis. Also discussed are possible sources of error.
- The conclusions reached in this thesis are presented in Chapter 5. This chapter discusses recommendations for future studies into erosions voids on linings.
- The appendices contain supplemental materials include sensor specifications and additional data.

Chapter 2 – Literature Review

2.1 General

Groundwater infiltration has been a problem of growing concern for engineers and owners of underground infrastructure alike. The potential problems that are caused by water infiltration can range from being a minor nuisance to extremely damaging. The *Highway & Rail Transit Tunnel Maintenance & Rehabilitation Manual* released by the U.S. Department of Transportation: Federal Highway Administration on Aug, 2006 stated that with groundwater infiltration, "fine soil particles can be carried through cracks with water, creating voids behind the liner, which can cause settlement of surrounding structures and/or cause eccentric loading on tunnels that can lead to unforeseen stresses." ITA (1991), Asakura and Kojima (2003), MacDonald and Zhao (2001) and Davis et al. (2005) have all mentioned soil voids on the lining as a serious problem to the service life of tunnels.

In this chapter a review of case studies of voids around pipes will be presented. This is because pipe infrastructure is more extensive than tunnel infrastructure and therefore more case studies have been reported. Damaged buried pipes can be excavated and inspected on the outside of the lining as opposed to tunnels. Although the subsurface conditions of buried pipes are not the same as they are for tunnels, the similarities are enough that indications can be drawn upon the effects of lining voids.

Finally, there will be a review of efforts to numerically model this condition. Meguid and Dang (2008) and also Tan and Moore (2008) have conducted numerical investigations on the effects of soil erosion voids on tunnels and pipes respectively. These models can give interesting insight into what might be expected from experiments using a physical model.

2.1.1 Tunnelling Basics

There are three major stages to tunnel construction; the excavation of the ground, the installation of the tunnel lining as a permanent support structure and finally the resolution of the surrounding ground around the tunnel lining. When ground is excavated for tunnel construction, the loss of soil support causes a redistribution of stresses in the remaining ground. The stages to tunnel construction are show in Figure 2.1 below. This can also cause a loss of ground and settlement unless the soil is immediately supported with tunnel lining. When Tunnel Boring Machines (TBM) are used the size of the excavation is usually more than the diameter of the tunnel lining to be installed afterwards. This creates a gap or a tail void between the tunnel lining and the surrounding ground (Lee et al., 1992). This gap generally has a crescent shape starting directly above the tunnel lining and stretching around to the bottom of the tunnel where the lining rests. Subsurface conditions, machinery and tunnelling expertise are all factors that determine the size of the gap. After excavation, soil will settle towards the lining, finally resting upon contact with the extrados of the lining. Conventionally the principal points of a tunnel are referred to as the *crown*, which is the very top of the tunnel, the *springlines*, which are the extreme horizontal edges of the tunnel, and the *invert*, which is the point at the very bottom of the tunnel. These points will be referred to throughout this thesis and are illustrated in Figure 2.2.

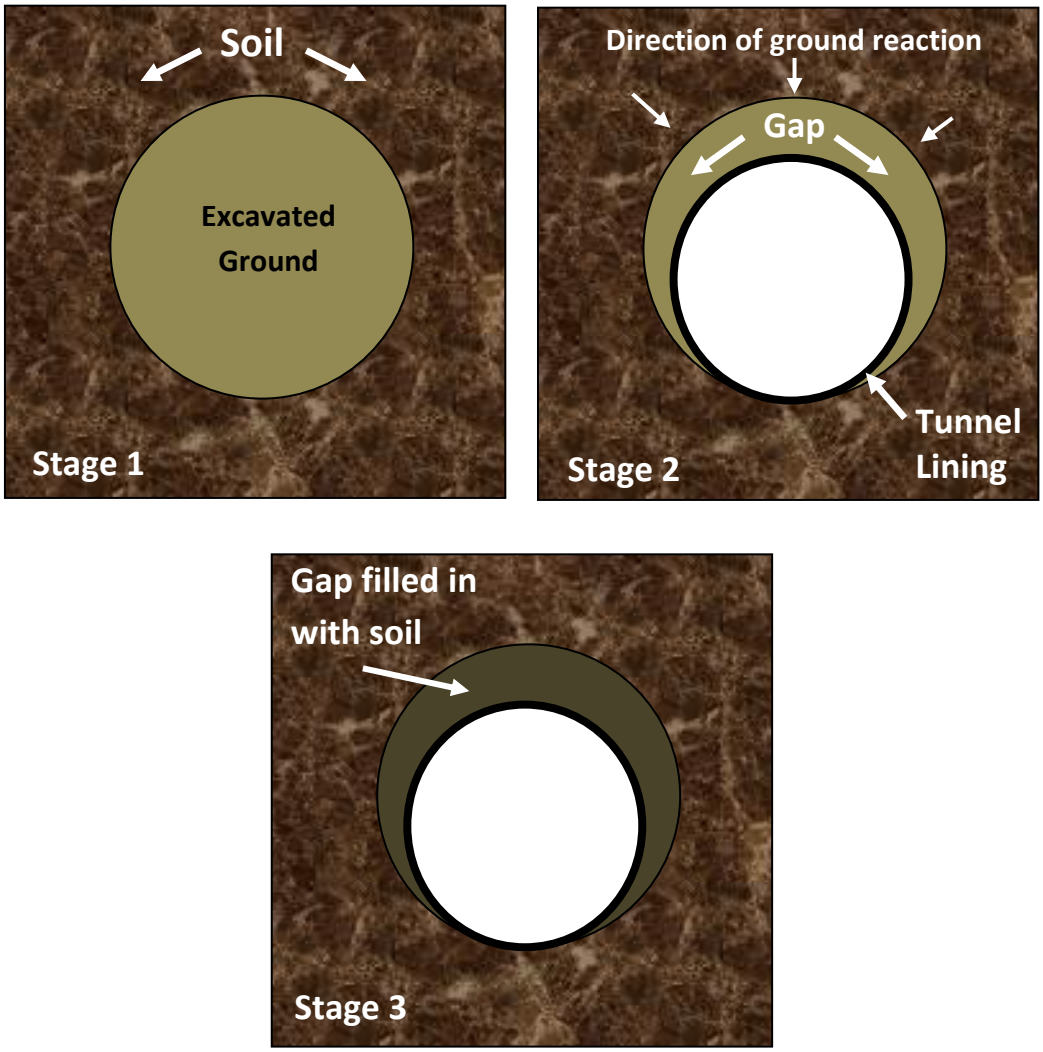

Figure 2.1: The stages of tunnel construction

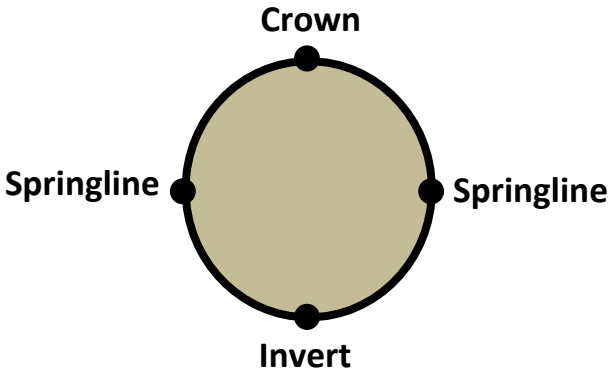

Figure 2.2: Principal points of a tunnel.

2.1.2 Lining Response to Soil Pressures

Peck (1969) described two theoretical situations with typical circular tunnel linings to illustrate soil-lining interactions. These linings are initially filled with soil so as to counteract the outside soil pressure. They are located at depth *z* from the ground surface. The coefficient of lateral earth pressure (K_o) is assumed to be less than 1.

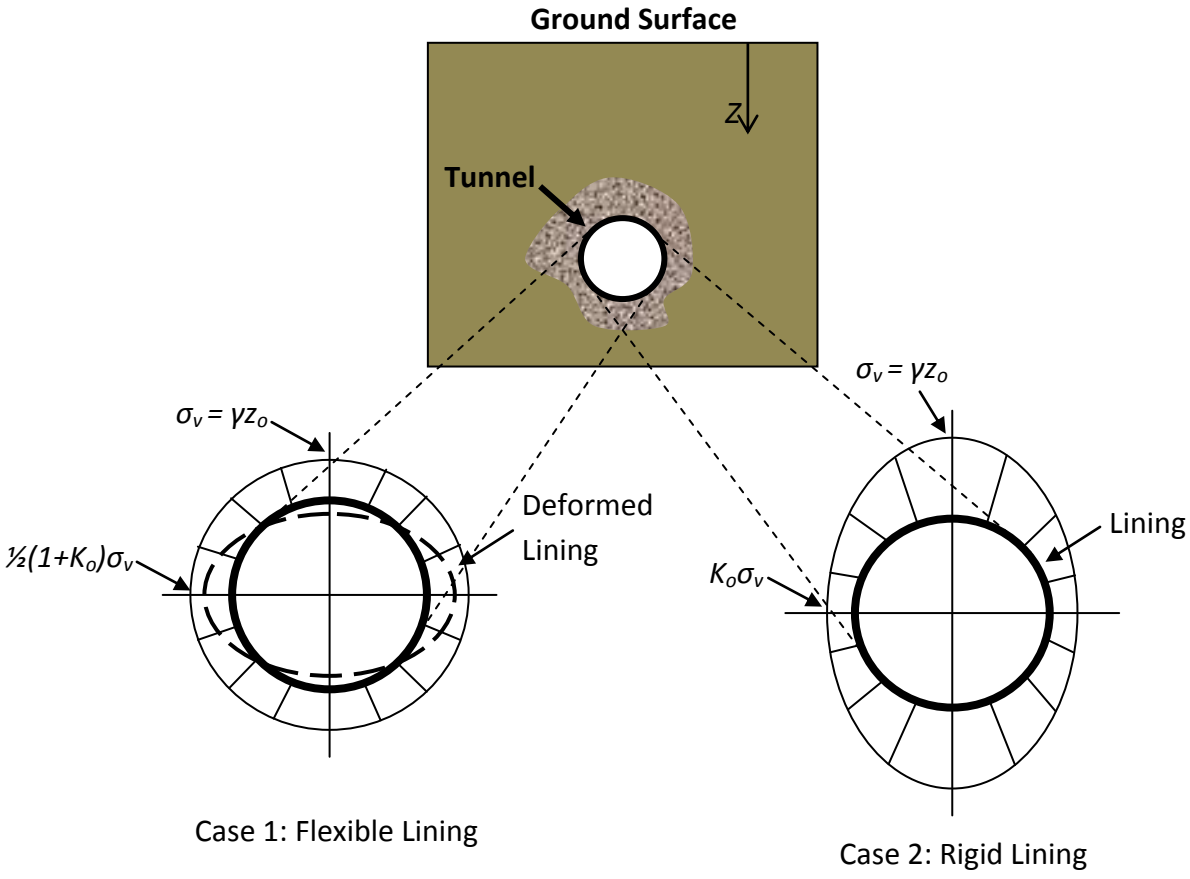

Figure 2.3: Earth pressure distribution on tunnels in flexible and rigid linings

This is a reasonable assumption since naturally occurring subsurface conditions in soft ground rarely have a K_o greater than 1. In one of these tunnels, the lining is completely rigid and exceptionally strong. In the other, the lining is supposed to be entirely flexible but able to withstand the substantial compression stresses. In both

cases, shear and tangential stresses are considered insubstantial. In the currently described state, the system is in equilibrium. But if the soil were to be removed, the system would have to readjust to maintain equilibrium. In the flexible lining this would result in the compression of the vertical axis of the lining and an extension of the horizontal axis. Figure 2.3 shows the earth pressure present in each of the described cases. For rigid linings, the earth pressure would not distort the lining in shape but instead bending moments would be induced. These bending moments would be negative at the crown and invert and positive at the springlines. Figure 2.4 shows the bending moment distribution induced by earth pressure on a rigid lining.

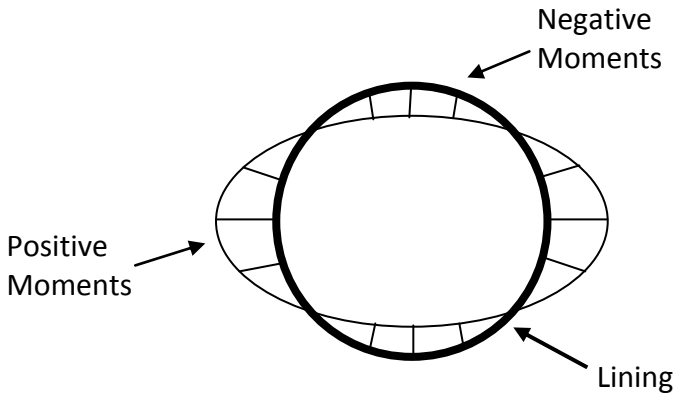

Figure 2.4: Induced bending moments on a rigid lining

Now visualize the tunnel lining in a two dimensional form with an arc length l and the thickness of the tunnel lining t. If elements of the lining with a length dl and thickness dt were considered so that the length dl were so infinitely small that they would cease to be curved, they could be regarded as straight. Then it can be imagined that at the element on the lining right at the crown under negative bending moments would experience compression on the outer surface of the lining and tension on the inner surface. Conversely, an element right at the springline of the tunnel would have tension on the outer surface of the lining but compression on the inner surface. This is illustrated in Figure 2.5.

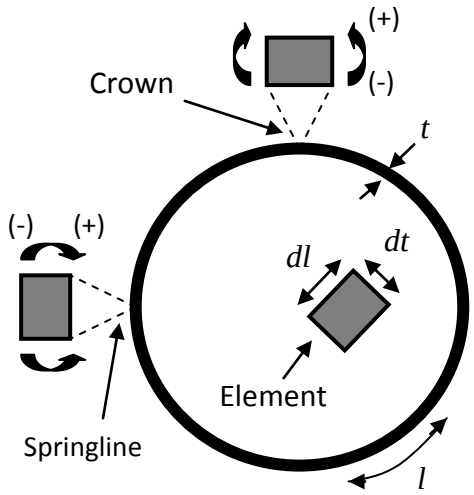

Figure 2.5: Lining elements from the crown and the springline

The previous situations describe the response of tunnel linings to earth pressures in idealised subsurface conditions. While they are helpful in understanding soil-lining interactions, real tunnel linings are very rarely completely rigid or flexible. They are generally a combination of the two and can exhibit qualities of both. Thus a superposition of the two reactions gives the general state of a tunnel lining. This is a state in which the lining may have slight deformation but will also sustain bending moments.

Along with earth pressures, there are also other modes that contribute to the deformation of tunnel linings. These other mechanisms can also effect the distribution of earth pressure around the tunnel. Gonzales and Sagaseta (2001) outlined these other modes and explained that the final earth pressure state and lining condition is a sum of the following:

- The radial inward movement of soil towards the lining, also known as the gap closure, usually as a result of the tail void being left by the TBM after the excavation of the tunnel.

- The deformation of the lining independent of ground loss (no surface settlement).
- The translation of the tunnel in a uniform vertical manner independent of distortion.

Figure 2.6 shows each mode.

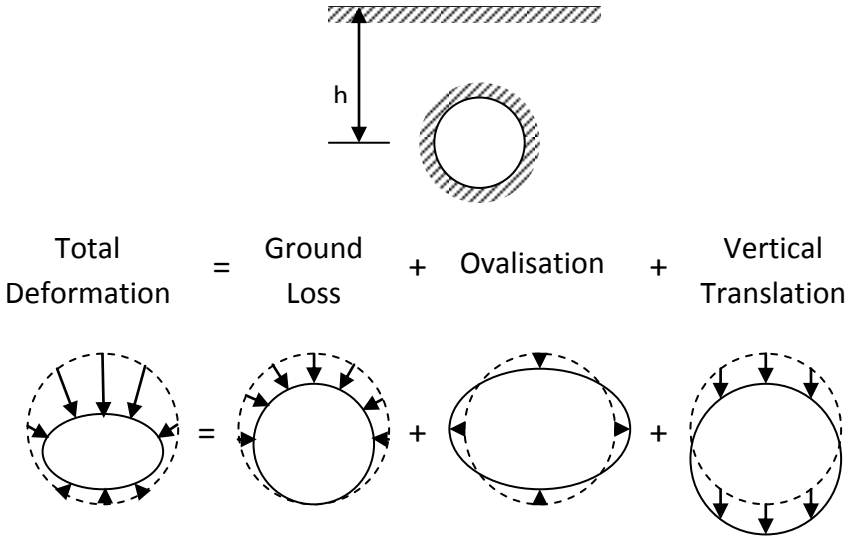

Figure 2.6: Summary of modes of tunnel deformation (Adapted from Gonzalez and Sagaseta, 2001)

2.1.3 Plane-strain State

So far the ground lining reaction to tunnel described shows the stages of tunnel from excavation to ground settlement and lining deformation. These are the movements of both soil and lining reaction that lead to a state of equilibrium. As the tunnel face excavation advances, radial displacements of soil take place in the tunnel lengths behind it. Section A-A in Figure 2.7 shows the tunnel face and the direction of advance. Eventually, once the progression of the tunnel face is of a sufficient distance away, the soil will converge unto the tunnel lining as soil reaches the maximum

movement (U_{max}). Once this has occurred, major soil movements will cease. The length of tunnel following this section can, assuming similar subsurface conditions, be described as under plane-strain conditions. Section B-B, in Figure 2.7, shows this region on the length of the tunnel as well as a plane-strain cross section. Plane-strain conditions assume that any cross section along the length of tunnel to be effectively similar. Therefore whole sections of tunnel can be analysed as a single or a few cross sections.

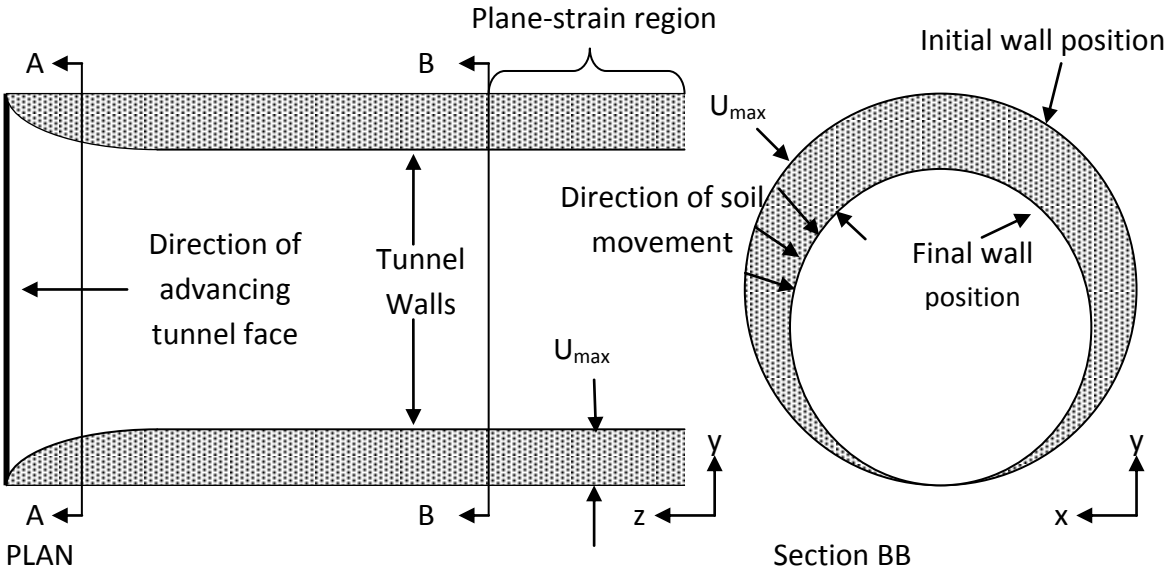

Figure 2.7: The advance of tunnel excavation and the development of a plane-strain region with the convergence of U_{max} (left); the cross section of a plane-strain region (right).

2.1.4 Analysis of Tunnel Linings

Mindlin (1940) investigated the effect of a boundary in an elastic medium on different stress distributions acting upon a circular void. Prior to this, the situation had only been investigated in infinite boundless conditions. Peck (1972) published a state of the art in soft ground tunnelling that set definitions of flexible versus rigid tunnel linings as related to the stiffness of the ground soil. Schmidt (1969) described the ground loss

or the settlements caused by shield driven tunnelling as fitting a profile much like a normal distribution curve. Subsequent work on tunnels has lead to more finely developed closed-form solutions and analyses to calculate the stresses and displacements. Contributors to this field include Muir Wood (1975), Einstein and Schwartz (1978), Sagaseta (1987), as well as Loganathan and Poulos (1998).

Bobet (2001) produced an analytical solution to shallow tunnels that determined the stresses, moments and thrusts for soil-lining interactions. This solution could be applied to a variety of conditions including dry or saturated ground, with or without tail voids, and for short or long term analysis. In developing this solution, the following assumptions were made:

- Circular cross section
- Plane strain conditions in the direction orthogonal to tunnel cross section
- There is a gap or tail void with a magnitude (*w*) which is defined by the equation $w = \frac{\text{loss}(\%)}{200} \cdot r_o$. *Loss* is the percentage difference in area between the excavation and the final tunnel lining installed. r_o is the outer radius of the tunnel lining.
- The shear stress (τ) is assumed to be zero at the interface between the lining and the ground
- The depth of the tunnel must be at least 1.5 times its radius in order to mitigate the effects of the ground surface
- The underground media is considered to be both isotropic and homogenous

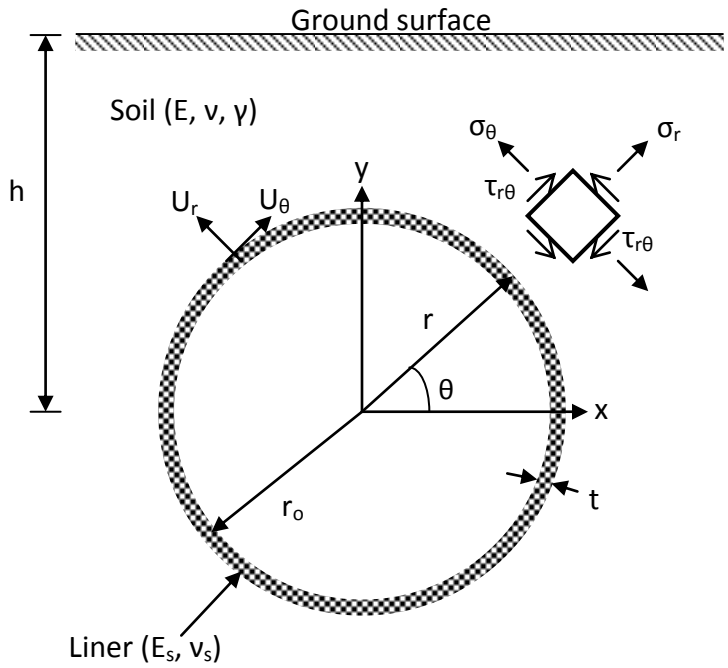

Figure 2.8: Circular tunnel (Adapted from Bobet, 2001)

Figure 2.8 shows the conditions in which the tunnel was considered by Bobet. The liner and soil is characterised by the parameters E, the modulus of elasticity, and ν, Poisson's ratio. With the soil there is an additional parameter of γ, the unit weight. Other dimensions referred to are U for displacement, r for radius, t for thickness, h for height above the tunnel springline, σ for stress and τ for shear stress. The subscripts of 'r' and 'θ' stand for the radial and tangential directions of action. The angle θ was measured in a counter clockwise direction with the positive X-axis as the starting point.

In Bobet's analysis, he considered many different subsurface conditions. The base scenario was the case of a shallow tunnel in dry ground. This condition is the one that most closely resembles the conditions that are modelled in this thesis. Therefore the general solution to the stresses (σ), thrusts (T) and moments (M) in this case are presented below. In deducing these solutions Bobet revisited a notion proposed by Peck (1969) that had been stated previously. That is the idea of a flexibility ratio (F) of a liner. This is a comparative factor that relates the elastic modulus of the liner and the

surrounding ground soil to determine whether the lining can be considered flexible or rigid. For the solution, the liner was considered both perfectly flexible yet completely incompressible. For a completely flexible liner, radial stresses are constant along the whole perimeter of the lining soil boundary. The stresses are given by the equation:

$$\sigma_{r=r_o} = \frac{E}{1+\vartheta} \cdot \frac{w}{r_o} - \frac{1}{2}\gamma h(1+K_o) \tag{2.1}$$

The solution for the moments is:

$$M = -\frac{3}{2}\frac{3-4\vartheta}{(1-\vartheta)F+3(5-6\vartheta)}\gamma h(1-K_o)r_o^2 \sin 2\theta + \frac{3-4\vartheta}{(1-\vartheta)F+8(7-8\vartheta)}\gamma(1-K_o)r_o^2 \sin 3\theta \tag{2.2}$$

Finally, the solution for the thrust is:

$$T = \frac{1}{2}\frac{\left[2E\frac{w}{r_o} - \gamma h(1+K_o)(1+\vartheta)\right](C+F)}{(C+F)(1+\vartheta)+(1-\vartheta^2)CF}r_o - \frac{3}{2}\frac{3-4\vartheta}{(1-\vartheta)F+3(5-6\vartheta)}\gamma h(1-K_o)r_o \cos 2\theta + \frac{3-4\vartheta}{(1-\vartheta)F+8(7-8\vartheta)}\gamma(1-K_o)r_o^2 \sin 3\theta \tag{2.3}$$

Where: γ = soil unit weight

h = depth below ground surface

ϑ = poisson's ratio of soil

C = compressibility

θ = angle of internal friction

2.1.5 Tunnel Boring Machine (TBM)

The Tunnel Boring Machine method was first developed in late 19th century England. While several engineers developed different parts, the first tunnel boring machine is credited to J. Price in 1896-1897. This was built to construct the Central London Railway Line (Guglielmetti et al, 2008). The modern tunnel boring machine is a highly versatile and adaptable machine. It can tunnel through hard rock or soft clays. The main features to a tunnel boring machine are its cutting head, a central driveshaft, a conveyor to transport excavated material and grippers so that the machine can advance itself. TBMs excavate circular cross sections on the whole tunnel face. These cross sections typically range in diameter from 2.5 – 12 m and are sometimes even larger (Girmscheid & Schexnayder, 2003). Additional features of TBMs are shielded bodies to prevent tunnel collapse in soft grounds and pressurised hydroshields for tunnel face support. Tunnel boring machines are extremely costly pieces of equipment and can be economically prohibitive except for complicated or longer tunnelling projects. The main benefits of using a tunnel boring machine are the safety of the workers and the support of the tunnel face and sides.

Tunnel construction using tunnel boring machines (TBM) has become increasingly commonplace as machines become more adaptable to varying underground strata and changing conditions. Tunnel boring machines have also increased speed, capacity and safety, which make them attractive choices. They also have the added benefit of sparing dense urban areas from the disruption of traditional cut and cover methods.

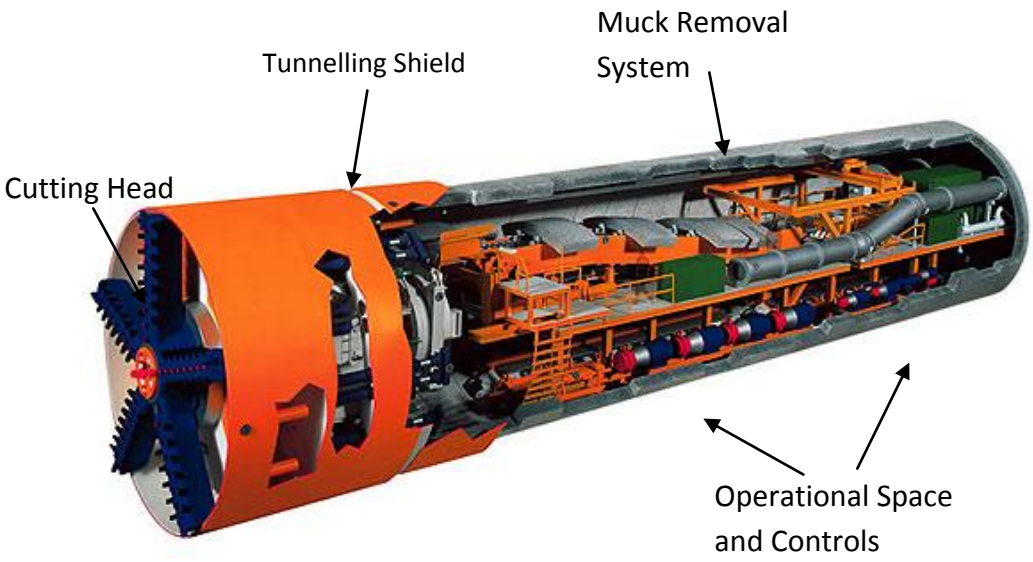

Figure 2.9: Diagram of a shielded TBM
(http://www.urbantransport-technology.com/projects/westerschelde/westerschelde5.html)

2.2 Groundwater Seepage in Tunnels

Many tunnels under the water table are constructed with drainage systems that dissipate the pore water pressure acting on the tunnel lining. The inclusion of a drainage system is most important in deep tunnels because of the significant pore water pressure that can develop. This pressure can cause considerable tensile strain on the tunnel linings, and consequently lead to increased leakage or cracking of the lining (Shin et al., 2009). Therefore, many tunnels built beneath the water table have drainage systems that reduce the pore water pressure right at the outer lining. A typical drainage system could take water all around the circumference of the lining and direct it towards drains located near the invert of the tunnel. Figure 2.10 shows a typical tunnel drainage system.

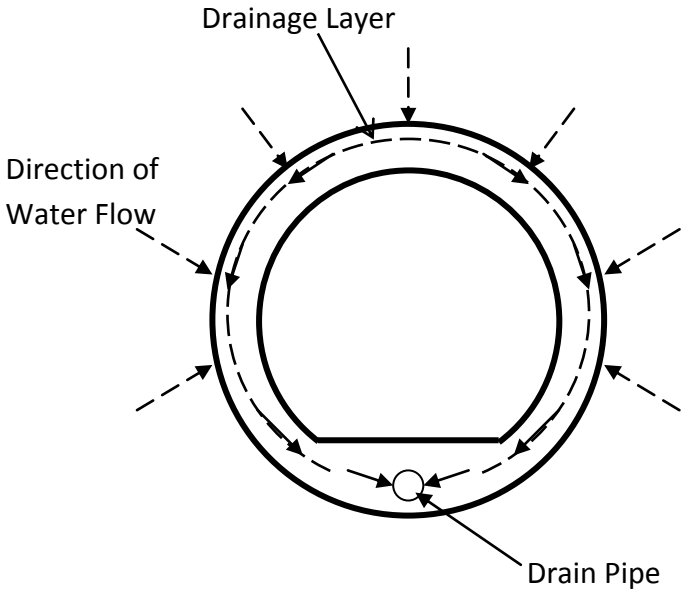

Figure 2.10: A typical tunnel drainage system (Adapted from Shin et al., 2009)

The rate of water flow into a tunnel is important for tunnel engineers because it can induce seepage forces, ground settlements or erosion. The problem with finding a solution to water seepage has been pursued by many researchers who have built upon the work of their predecessors. Goodman (1965), Freeze and Cherry (1979), Meiri (1985), Zhang and Franklin (1993), Lei (1999), El Tani (2003) and Hwang and Lu (2006) have all made significant contributions. Kolymbas and Wagner (2006) proposed an exact analytical solution to groundwater ingress into tunnels. In their solution, the rate of water flow into a drained tunnel is determined.

The Kolymbas and Wagner solution was derived under the following assumptions:

- Circular tunnel cross section
- Subsurface permeability that is both isotropic and homogeneous
- Steady flow at a constant head

While these are indeed idealised subsurface conditions and may not be realistic in most cases, they can still provide an estimate that can be useful in tunnel design.

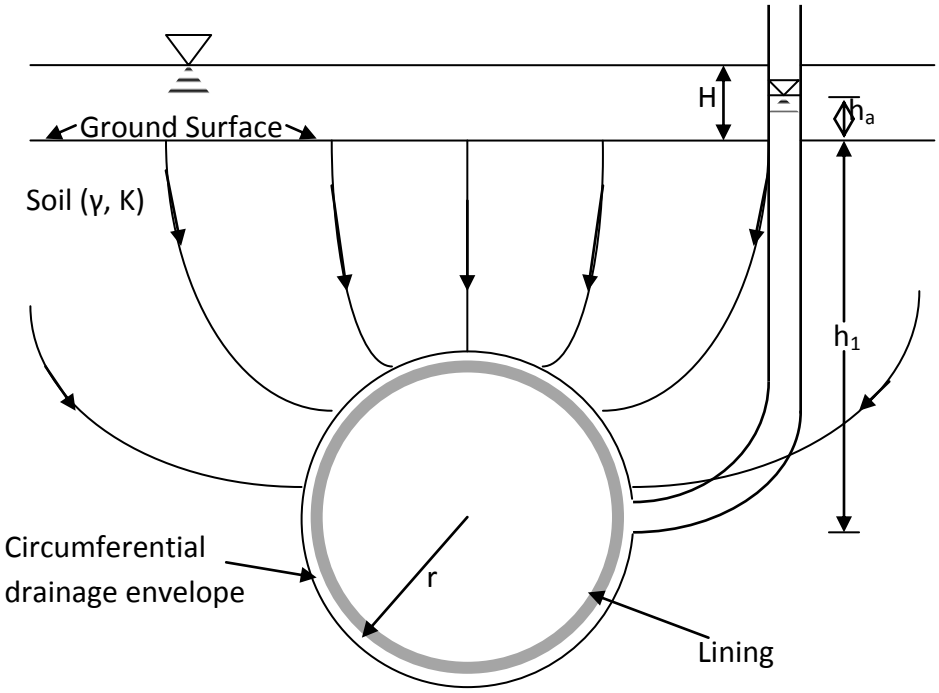

Figure 2.11: Idealised seepage flow (Adapted from Kolymbas and Wagner, 2006)

Figure 2.11 shows the conditions imagined by Kolymbas and Wagner. The water table is located above the ground surface indicating that the tunnel is underneath a body of water thereby providing a constant head. H denotes the height of water above the ground surface, h_1 is the height of the ground surface above the tunnel springline, h_a is the energy head in the drainage system around the lining and r is the radius of the lining. The solution to the flow was given by the equation below:

$$q = \frac{2\pi K(H - h_a)}{\log(\frac{h_1}{r})} \tag{2.4}$$

Where: q = drainage flow

K = soil permeability

r = tunnel radius

H, h_a, h_1 are head factors defined in Figure 2.11

Seepage force is another action of water ingression that needs to be considered. In drained or leaking tunnels this force acts on the soil that the water needs to flow through. In the tunnel lining, seepage forces can push soil sediments into the drainage filters eventually clogging them and rendering them ineffective (Shin et al., 2005). While tunnel drains can reduce pore water pressure, seepage forces can actually increase the stresses the soil skeleton imparts on the lining. Seepage forces will also cause settlement of ground away from the tunnel lining. Nam and Bobet (2005) showed numerically that ground displacements increase with distance away from the tunnel. While tunnels with drainage systems will experience less axial force and stress upon the lining, at greater depths there is a noticeable increase in moment experienced (Lee and Nam, 2006).

Park et al. (2008) developed an analytical solution to determine the subsurface seepage forces around a circular tunnel. This solution was considered for two cases of drained tunnels; with no water pressure at the lining, and with a constant total head. As with Kolymbas and Wagner's solution, it was assumed that the ground surface is below a body of water and therefore exists a constant head, H, above. While Park et al. presented solutions for two different cases, it was concluded that the first case was too idealised and would not exists in actual drained tunnel linings. The second case, with constant total head, would be more realistic and applicable to field situations.
The seepage force acting on a lining with constant total head is expressed as follows:

$$F = i\gamma_w = \gamma_w \frac{1 - 2\alpha\cos\theta + \alpha^2}{2\alpha A} \frac{H - h_a}{\ln[\left(\frac{h}{a}\right) + \sqrt{\left(\frac{h^2}{a^2}\right) - 1}]} \tag{2.5}$$

Where: F = seepage force

i = hydraulic gradient around the tunnel circumference

γ_w = unit weight of water

a = tunnel radius

h = depth from ground surface

α, A = conformal mapping parameters related to tunnel radius

2.3 Erosion Voids around Tunnels and Pipes

Erosion voids are a well noted occurrence within tunnel maintenance and rehabilitation literature. That being said, there has been surprisingly few studies into the nature of this problem. This includes case studies done into the possible pattens of formation and the effects of these erosion voids on the surrounding ground soil and/or tunnel lining. In fact, many papers make no more than a passing mention of the problem. Nevertheless, when erosion voids are mentioned in tunnels, most define an erosion void as an area of weakened soil caused by the inflow of water through cracks in the tunnel lining (Asakura and Kojima, 2003). As the water leaks into the tunnel it carries with it fine soil particles from the surrounding soil. Over time, this action can severely weaken an area around the crack on the tunnel lining. This action may lead to ground loss should the overburden pressure cause the void to collapse. The erosion void may also lead to changing earth pressure distribution and bending moments on the tunnel lining as the soil stresses readjust to the erosion void in a process known in geotechnics as arching. This can also lead to ovalisation of the tunnel and possibly cave-ins (ITA, 1991). MacDonald and Zhao (2001) described soil support as integral to subsurface infrastructure and that void formation causing a loss in soil support can lead to premature failures. They also stated that the types of subsurface soil that are at greatest risk of this mode of deterioration are sands and silts. This is because these soil types may contain particles small enough to pass through cracks but permeable enough to allow for high seepage flows. Delatte et al. (2003) states that there are many tunnels that are built to traverse under bodies of water. Tunnels in such locations are more susceptible to the dangers of water damage and the consequences potentially more severe if tunnel failure were to occur. Figure 2.12 shows the formation of erosion voids on the outer surface or extrados of a tunnel lining.

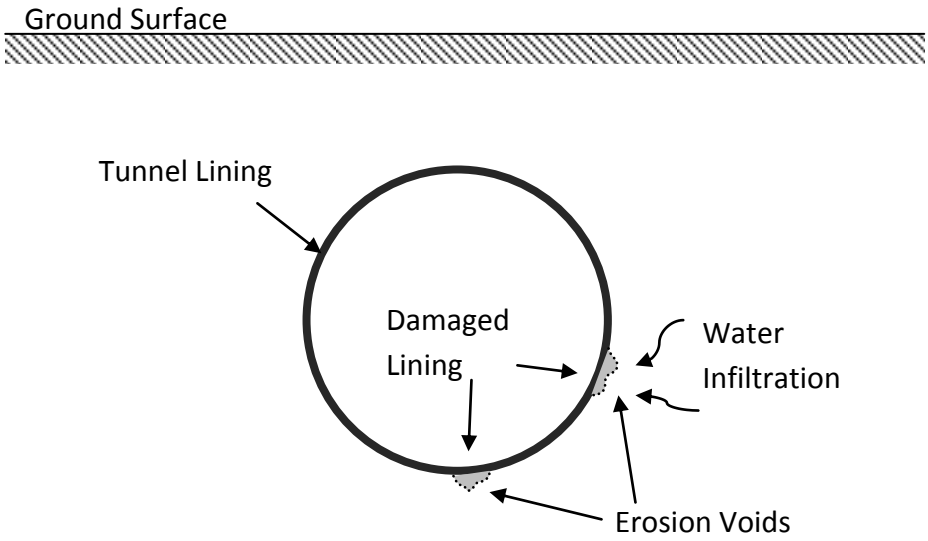

Figure 2.12: Erosion voids forming at cracks the tunnel lining

There have been many recorded cases of soil erosion occurring in soil on the extrados of a tunnel lining. In some cases, these voids that are detected before any damage occurs to the tunnel lining. In others, they are only discovered during a post failure forensic investigation. In an International Tunnelling Association report published in 1991 (ITA,1991) providing and detailing case studies of the damaging effects of water on tunnels, at least four cases are mentioned whereby a tunnel suffered damage because of "a loss of support due to the transport of fines". Two of these tunnels were sewage tunnels and one was a water tunnel (all in the U.S.) and the last one was a transportation tunnel in Japan. The transportation tunnel was built without sufficient waterproofing because of unforeseen water levels. Soon after the tunnel was completed large amounts of leakage began to take place at the lining segment joints carrying in extensive amounts of soil. While this indicated substantial soil support loss at the tunnel springline, no noticeable damage occurred because the leak was promptly sealed and grouted. In all three cases in the U.S. the tunnels were built in silty or sandy soils. Each case experienced a loss of soil support on the sides and inverts of the tunnels. Loss of support at the tunnel invert was followed by increased cracking

circumferentially and loss of support at the sides caused ovalisation and longitudinal cracking. Further erosion at the invert caused settlement of the tunnel resulting in further damage to the linings. Two out of three of the tunnels were repaired using grouting or pipe jacking. In the third, the amount of sediment that had flowed in through the lining forced the tunnel to be abandoned.

Davis et al. (2005) conducted tunnel lining inspections using non-destructive testing (NDT) methods. These methods included impulse response or transient dynamic response and impulse radar. They were employed on a section of a water supply tunnel in Buenos Aires, Argentina. In this case the voids behind the lining were caused not by water erosion but by improper grouting. Davis et al. (2005) used impulse radar to determine whether the voids were of a sufficient size to prevent hoop stresses from fully developing in the tunnel lining. The results did show some voiding occurring near the springline of the tunnel lining but it was concluded that it was not large enough to cause significant damage to the lining. Figure 2.13 shows the reported impulse radar image.

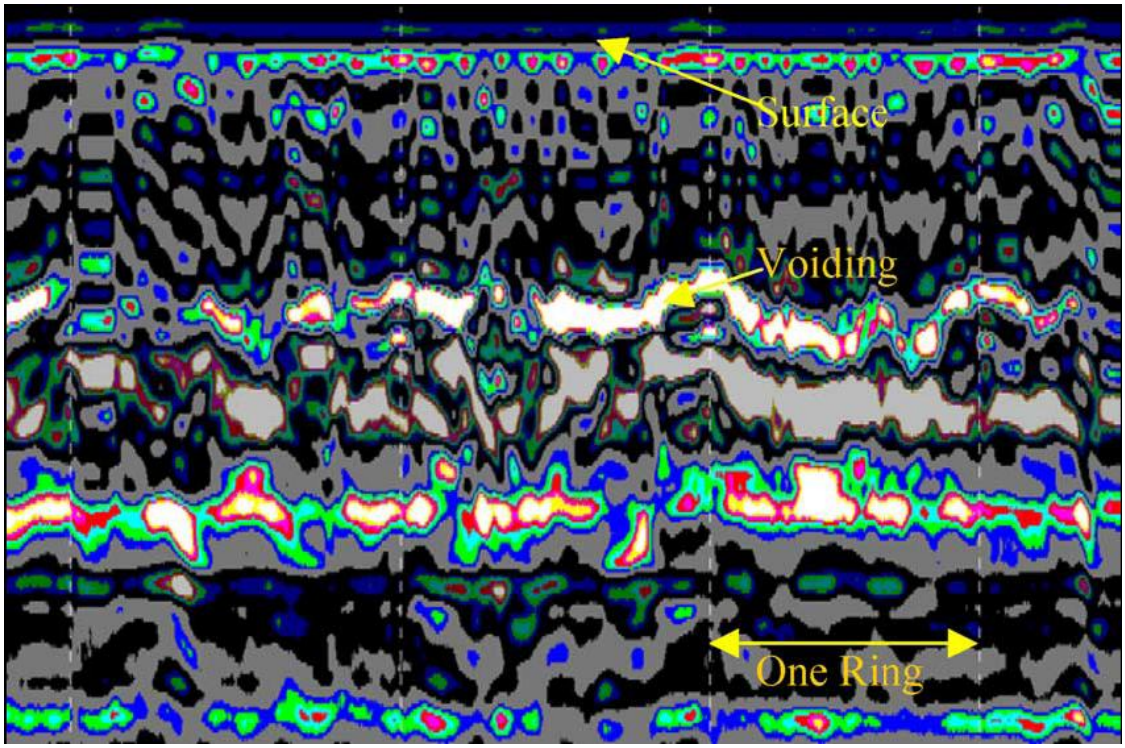

Figure 2.13: Impulse radar image detecting soil voids (Davis et al., 2005)

Pipe infrastructure provides many good examples of the formation of the destructive potential of erosion voids. This is because there is vastly more underground pipe infrastructure, especially those that are in a dire state of disrepair. It is also generally easier to dig up and replace failed pipes. Although there are differences in the earth pressure experienced by pipes and by tunnels, generally due to the differing modes of construction, the similarities are close enough to merit comparison between the two situations. The mode of failure experienced by pipes due to erosions voids can be quite similar in tunnels.

Helfrich (1997) conducted a study into a failed 0.3 m diameter sewer pipe. In this particular case the pipe was made of vitrified clay and was buried at depths from 3 to 6 m. Due to incomplete subsurface investigation prior to the pipe design and installation there was substantial settlement under the invert of the pipe. Some sections of pipe dropped up to 50 mm and were therefore unable to maintain service. Major sections of the pipe had to eventually be replaced with a thicker layer of backfill bedding underneath the invert. Talesnick and Baker (1999) also detailed a situation whereby a pipe failed because of large settlements beneath the invert of the pipe. As in the previous case, the pipe failed due to inadequate backfill beneath the invert. The pipe was a composite of concrete and steel with a diameter of 1.2 m. It was built in a stratum of clay over a bed of granular backfill. The pipe failed due to unsustainable vertical deflection within a year of installation and was never put into service. Post failure investigation found that parts along the length had gaps under the invert up to 200 mm. While the loss of soil support for the pipe in the examples above may not have been due to erosion void formation, they still illustrate the possible disastrous consequences of a loss in soil support.

Davies et al. (2003) compiled a report that catalogued the various factors that can lead to the deterioration of rigid sewer pipes. This comprehensive study detailed many conditions which promote or mitigate the formation of erosion voids near pipes. They also summarise the stages of sewer deterioration. Erosion voids are not the only outlined form of sewer pipe deterioration, but they are, however, quite prevalent and

can lead to other serious problems. Accordingly, Davies et al. (2003) included a thorough analysis of this issue.

The stages of sewer failure have been well documented by various authors including Hoffman and Lerner (1992), Serpente (1994) and Fenner (2000). There are three major stages as described by Davies et al. (2003). The first stage involves a small, usually unnoticed defect or crack caused by either excessive overburden or construction oversight. These cracks often occur at the principal points of the tunnel located at the invert, crown and springlines by reason of the disproportionate bending moments at those locations. Stage one defects are minor and the sewer still maintains its structural integrity and complete soil support. However, they allow further degeneration to occur.

The second stage of sewer failure is the ongoing and sometimes rapid decline of the sewer lining. This is primarily because of the loss of side support due to water infiltration and ensuing transport of fines out from the surrounding soil. This can also cause significant ground loss and the formation of pot holes should a road surface lie above. Eventually the loss of side support can turn the previous cracks into ever larger fractures on the sewer lining, allowing ever more seepage infiltration. Stage two can also be noticed by a possible slight ovalisation of the pipe.

The third and final stage of failure is the ultimate collapse of the sewer. This happens when further deformation movement of the sewer lining exceeds 10% of the original positions. At this point the sewer is at a high probability of collapse. Failure itself is generally not caused by soil erosion mechanisms described above. Instead, it is caused by an abrupt change of conditions on the sewer pipe such as a sudden excessive surcharge or nearby excavation causing the release of supporting soil stresses. Prior to failure, the presence of large erosion voids around the outside of the lining can be expected. This loss of soil support for the pipe structure is the reason for the increased chance of failure. At this point, the pipes will cease to function properly and be in dire need of repair or replacement Figure 2.14 shows the development of the three stages of sewer failure.

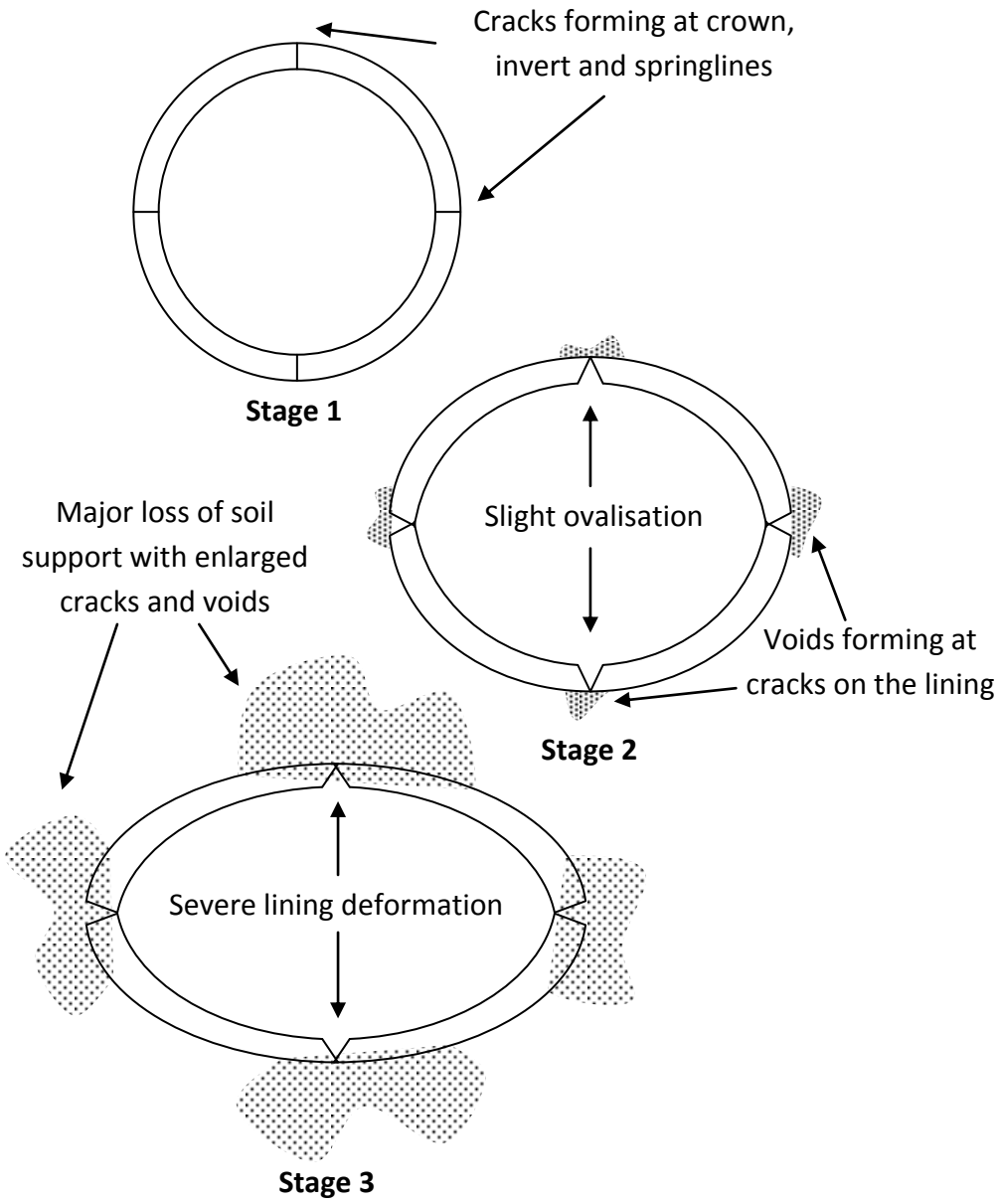

Figure 2.14: The stages of sewer pipe failure (Adapted from Davies et al. 2003)

2.4 Analysis of Soil Voids around Tunnels and Pipes

Tan (2007) conducted a finite element analysis to investigate the effect of soil voids on the circumferential forces and bending moment of a pipe lining. Soil voids of varying magnitudes at the springline of a rigid pipe were investigated under plane strain conditions. A finite element model (FEM) was developed that considered both linear elastic and elasto-plastic representations of the soil material. The soil voids were modelled as idealised circular shapes at contact angles on the pipe surface of 30°, 60°, and 90°. The soil material was considered to be granular and the voids represented included those up to the maximum size observed before ground settlement and surface changes were noticed (Spasojevic et al. 2006). Figure 2.15 shows the size and shapes of the modelled voids.

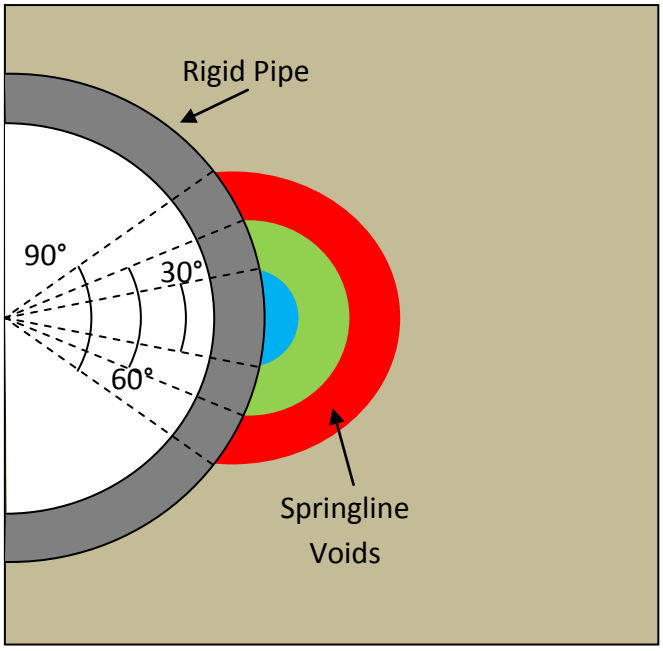

Figure 2.15: FEM voids on a pipe springline (Adapted from Tan and Moore, 2007)

The results of the finite element analysis were presented by Moore (2008). The controlling factor through all simulations was the contact angle on which the voids intersected the pipes. For the void angle, it was found that as the angle grew, so did the stresses and bending moments in the pipe structure. At the largest contact angle simulated, the increase of stresses exceeded 100% of the original stress on the pipe. It was concluded that since most pipes are constructed with a factor of safety in the order of 2, an increase of over 100% should be sufficient to instigate cracks in the pipes. Figure 2.16 shows an example of one of the simulations. The graph maps the changes in circumferential tension and compression stresses on the crown of the pipe as the contact angle with the erosion void increases.

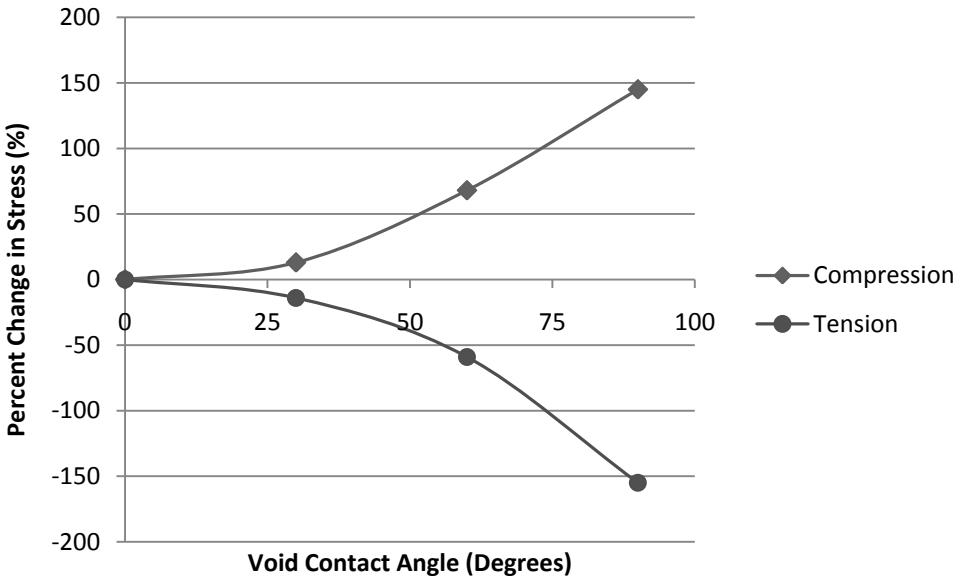

Figure 2.16: Circumferential stress changes at the crown (Adapted from Moore, 2008)

Meguid and Dang (2008) conducted numerical simulations into the action of erosion voids on tunnel linings. As with the simulations conducted by Tan and Moore (2007), the tunnel linings were investigated using finite element analysis under plain strain conditions. In this case, voids occurring on both the springline and invert of the tunnel were considered. The erosion voids were represented as a series of circular shapes arising on the surface of the tunnel. These varied in size by the percentage of the tunnel circumference that they encompass, from 3% to 15%. For this particular model, the tunnel was considered to be a shielded bored tunnel that was constructed in soft ground. The model tunnel had a diameter of 4 meters and was located at 10 meters below ground surface. Meguid and Dang (2008) also considered the flexibility ratio of the tunnel lining, accounting for the effect of erosion voids on tunnel linings of differing flexibility. Finally, the model assumed a tail void volume loss of 1% which is consistent with observed field values. Figure 2.17 shows the simulated lining voids.

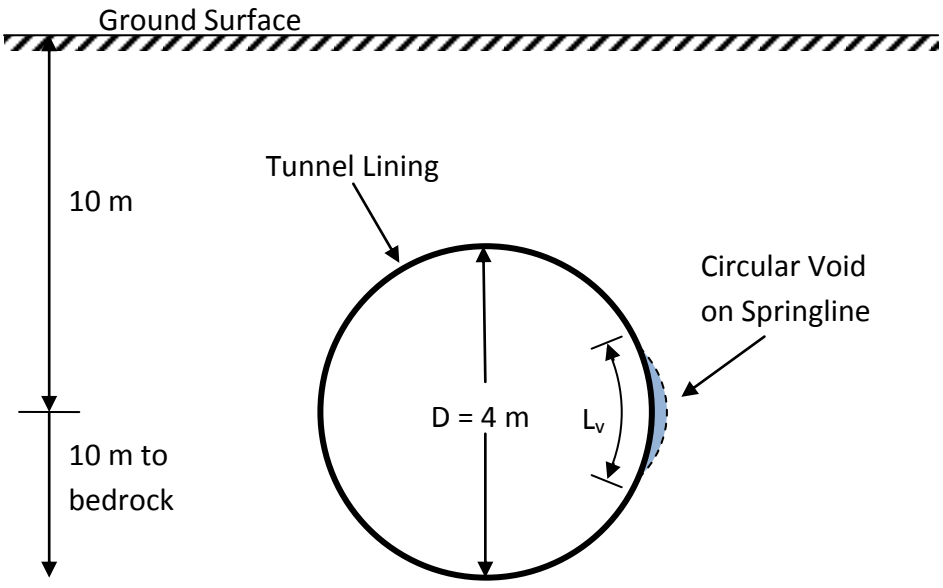

Figure 2.17: FEM tunnel with voids (Adapted from Meguid and Dang, 2008)

The results show that erosion voids can cause unaccounted for changes in the thrust forces and bending moments on tunnel linings. These changes were found to be largely dependent on the void size and the value of the lateral earth pressure coefficient. Changes in bending moment were more pronounced than thrust. The springline experienced large increases in bending moment whereas there was a reversal from negative bending moments to positive at the invert. This is a critical finding because the portion of the tunnel lining that is designed to resist compression loads could easily fail under tension. It was concluded that careful consideration should be given to identify and repair erosion voids in existing tunnels due to these findings. Also noted is that these finite element models are just simulations and need to be confirmed with physical testing. Figures 2.18 – 2.20 show some of the findings from these simulations.

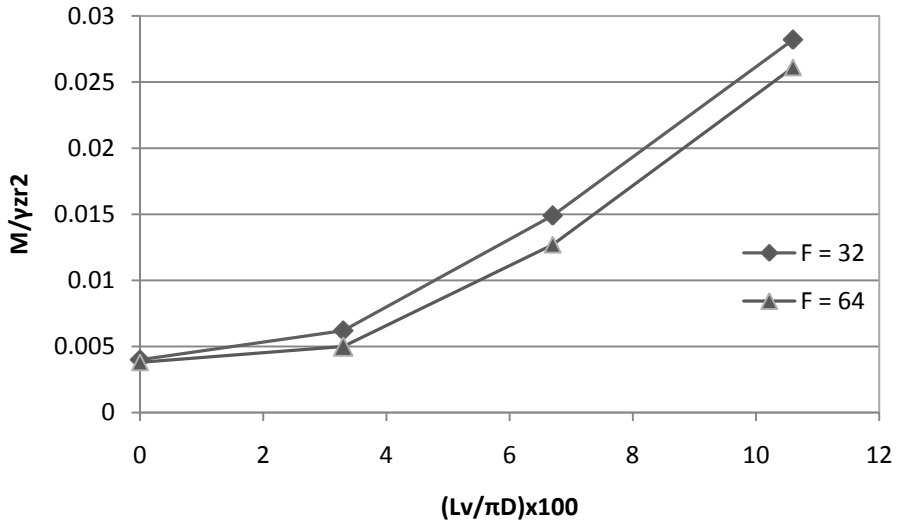

Figure 2.18: Change in bending moment at springline with void size and flexibility ratio (Adapted from Meguid and Dang, 2008)

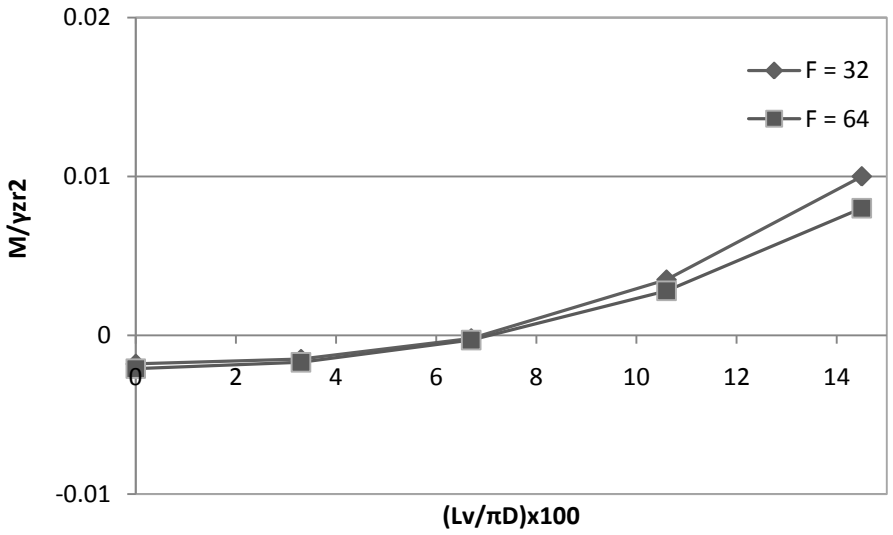

Figure 2.19: Change in bending moment at invert with void size and flexibility ratio (Adapted from Meguid and Dang, 2008)

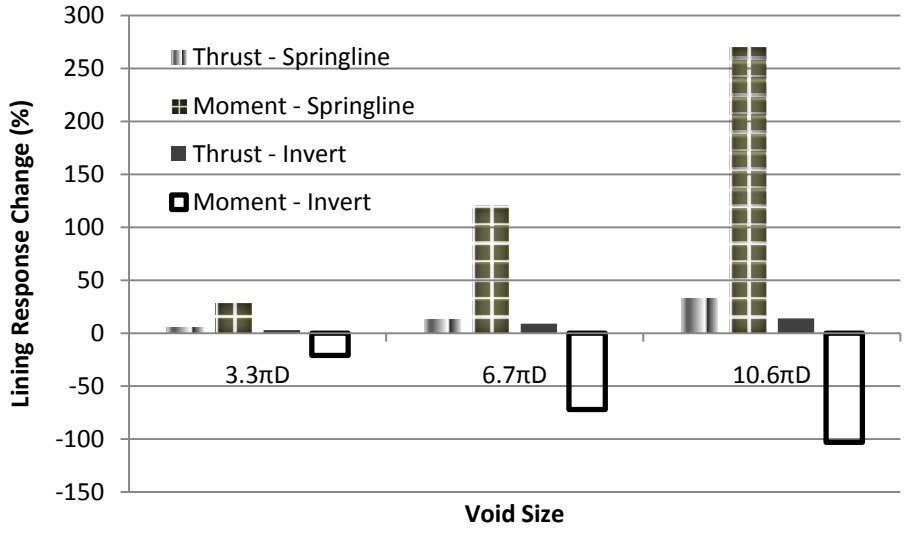

Figure 2.20: Summary of lining response changes with void size (Adapted from Meguid and Dang, 2008)

2.5 Literature Review Summary

The review of literature regarding the thesis topic showed that significant pore water pressures can develop around tunnel linings even if they have drainage systems. In fact, drained tunnels create greater water seepage forces in surrounding soils. These forces are often sufficient to move and carry away loose soil particles, causing voids.

Many case studies regarding the appearance and effects of erosion voids have been documented. In many of these cases voids were the cause of or a major contributing factor to eventual failure of underground pipes and tunnels. It was also noted that the erosion voids occurred most often at tunnel extremities, where fractures in the lining were most common.

Even with so many recorded cases of erosion voids, minimal research and experimentation have been conducted. The only research papers found regarding erosion voids were numerical analysis conducted to examine their effect on pipes and tunnel linings. Both these papers concluded that soil pressures would increase in the areas adjacent to erosion voids.

In regards to laboratory experimental simulations, no published papers were found for the study of erosion voids. An experiment to physically simulate erosion voids on a tunnel lining was therefore necessary.

Chapter 3 – Experimental Setup and Procedure

3.1 Introduction

Physical modelling of underground works is an economical and effective way of investigating geotechnical phenomena. This has been for many years the main method by which geotechnical theories are tested. There are a few different ways in which to conduct physical models. There are experiments conducted on scale models as opposed to full sized structures. There are also experiments that are run under accelerated gravity centrifuge versus 1g conditions. Meguid et al. (2007) conducted a comprehensive review of the methods of physical modeling of tunnels in soft ground. While each of these variations has its own benefits, for this experiment, a scale tunnel model under 1g conditions was applied. It is important to note that a scale model cannot truly simulate the in-situ stresses of a full sized application. It can however offer insight into the possible trends and reactions in a full scale situation.

An important aspect of laboratory modelling is establishing the correct boundary conditions that will effectively isolate the interested parameters in the test from external effects. Careful planning and consideration went into the design of this experiment in order to account for all boundary conditions and to effectively simulate the two-dimensional action of a soil erosion void on a tunnel lining. The most important and also most difficult aspects of the design and realisation of this experiment include: accurately simulating tunnel excavation, inducing the soil movement around the lining as a result of the gap closure, and ensuring that the tunnel was 'floating'.

Lastly, all experiments need a dependable way in which the test can be carefully monitored and data efficiently recorded. In this case, a combination of load cells converted into pressure sensors and linear variable differential transformers (LVDT) were used to track changes in the test conditions. Each sensor needed to be precisely positioned and calibrated. All were then connected to a data acquisition system and a computer to record the readings.

The goal of this test was to physically model a bored tunnel in sand and then introduce soil erosion voids onto the tunnel lining. This chapter will outline in detail the complete experimental program. This will include the tunnel model, the sensors and data acquisition system, the strongbox in which the test was conducted, the material properties of the soil used, and the procedure by which the experiment was carried out.

3.1.1 The Tunnel Model

The tunnel model developed for this experiment needed to be able to mimic the action of a tail void during the construction of bored tunnels. This was based on the design of Lee and Bassett (2006). In the paper, the authors attempted to model the shear and displacement patterns of tunnel construction near piles. The model used aluminum rods as idealised granular soil. The tunnel model consisted of six segments representing a tunnel 100 mm in diameter. Two tapered cones on either end of the tunnel could be controlled by a dial that caused the tunnel to reduce in diameter. Figure 3.1 shows the tunnel model used by Lee and Bassett (2006).

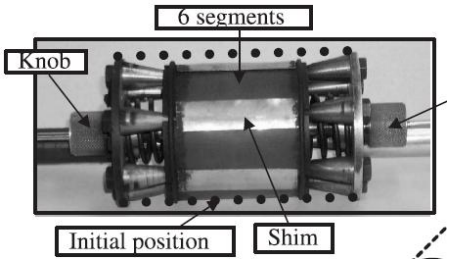

Figure 3.1: Variable diameter tunnel model (Lee and Bassett, 2006)

A similar device was also used by Tobar (2009) in order to model the ground lining interaction of excavated shafts. The defining mechanism of this model was the ability to evenly reduce its diameter in order to produce a tail void in the soil. The model tunnel had three main parts; the tunnel lining, the internal mechanisms, and the tunnel end which connected the two previous parts together. The general dimensions of the circular tunnel were 6 inches (152 mm) in outer diameter and 2 feet (610 mm) in length.

3.1.2 The Tunnel Lining

For the tunnel model, a fully rigid tunnel lining was desired and therefore a 1 inch (25 mm) thick cold rolled steel pipe was chosen to be made into the tunnel lining. The steel had a Young's modulus (E) of about 200 GPa. This would ensure that the model tunnel could be considered fully rigid. The tunnel lining was constructed from a pipe length with an outer diameter of 4.5 inches (114 mm) and an inner diameter of 3.5 inches (89 mm). At the ends, inside edges of the pipe were milled to have a diameter of 4 inch (102 mm) to a depth of 2 inches (51 mm). This was done to accommodate end tracks that would hold each tunnel section in place. The pipe was then cut into 6 equal sections that would represent a 43° arc of the final 6 inch (152 mm) outer diameter tunnel. The gaps in between the pipe sections were covered by thin steel shims that were screwed in to one side of the tunnel sections at equally spaced points. This was done to allow the shims to slide over top of the thicker sections to adjust to the reducing diameter of the tunnel and thus shrinking circumference. Each shim is 1.5 feet (457 mm) long and was rolled in order to conform to the circular shape of the tunnel. The small gaps between the shims and the lining were sealed with clear silicone caulking so that the fine sand particles could not enter and damage sensors. Figure 3.2 shows drawings of the tunnel lining and Figure 3.3 shows a picture of the lining as made.

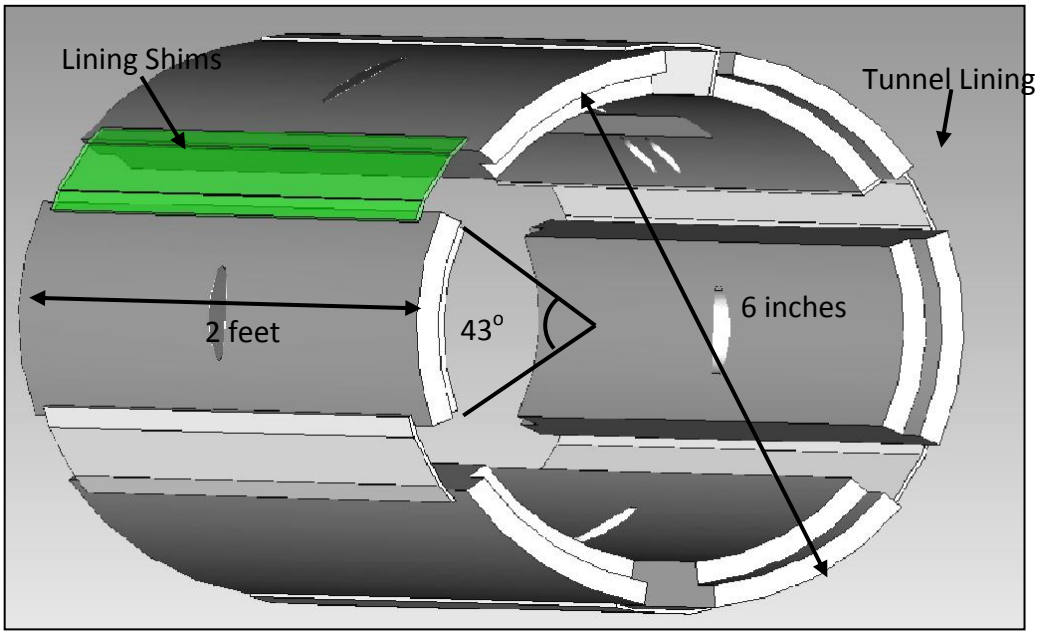

Figure 3.2: Drawing of tunnel lining

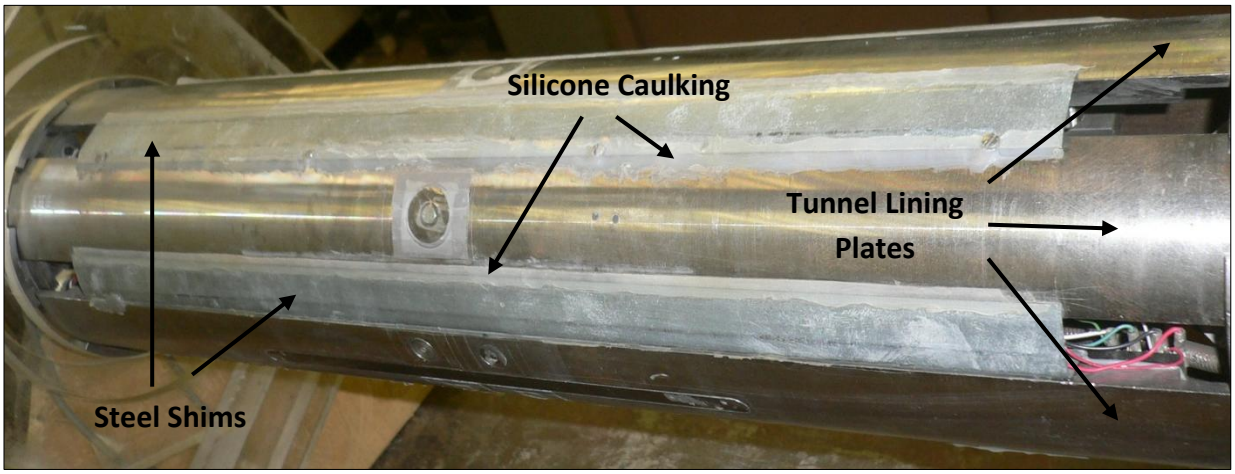

Figure 3.3: Photograph of the 'as built' tunnel

3.1.3 Tunnel Inner Mechanics

The tunnel lining pieces needed to be held in place in a circular fashion. This was achieved by a configuration of six steel pie shaped pieces that acted like a circular track to keep the thick steel parts of the tunnel lining in place. There was one set of steel tracks on each of the two ends of the tunnel lining. Each set of tracks was cut from a single circular steel disk and each track piece measured 1 ¾ inches (44 mm) long radially, had an arc length of 1.92 inches (49 mm) and an angle of 37°. Figure 3.4 shows a drawing of one set of the tracks and some dimensions.

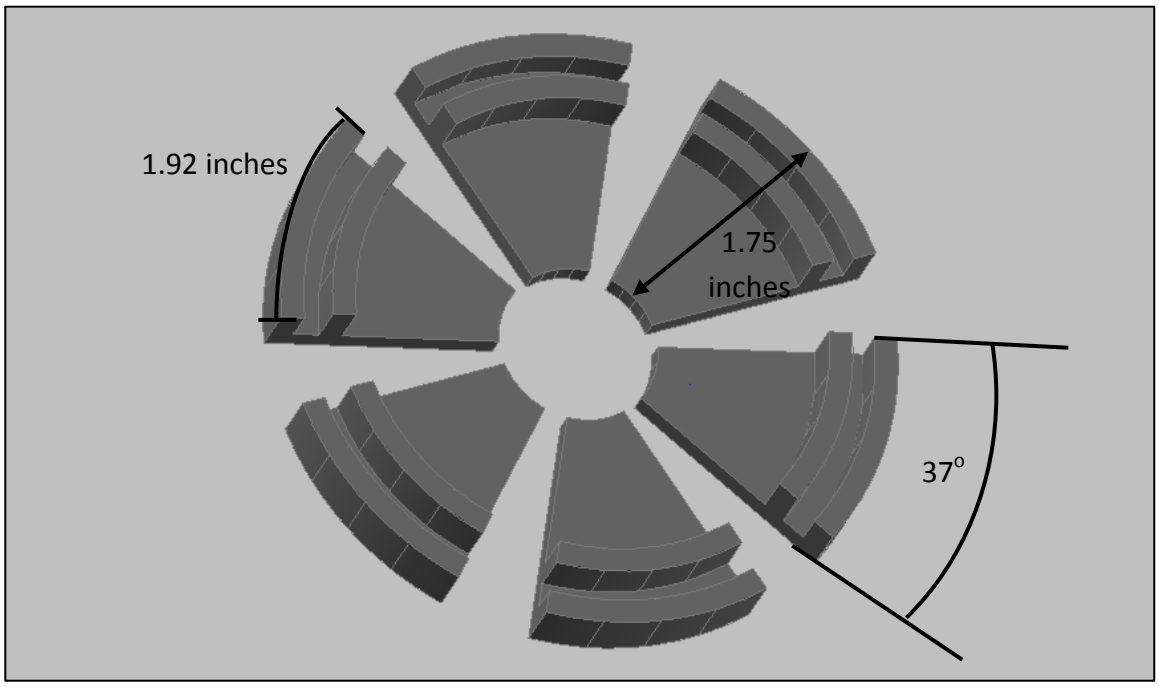

Figure 3.4: Drawing of lining end tracks

The track pieces of the tunnel served to hold the tunnel lining in place, but it also allowed the tunnel to contract in order to simulate a tunnel tail void. This contraction was accomplished by a mechanism in the tunnel interior that would simultaneously pull all the track pieces inwards, thereby contracting all the tunnel lining pieces inward and reducing the tunnel diameter. This mechanism consisted of two threaded rods of 1.5 inch (38 mm) diameter and 1.5 feet (457 mm) in length. One of the rods was threaded in a right handed direction and the other was threaded in a left handed direction. They ran down the center of the tunnel and were attached by a custom made coupling nut. A corresponding six sided nut was placed at the end of each of these rods. Custom made hinges attached on each face of these nuts to connect them to each of the six pieces of the lining tracks. In order to contract the tunnel lining, the center rod would have to be turned which would cause the nuts to move towards the coupling nut in the middle of the length of the tunnel. This would, in turn, pull the hinges and the track pieces radially toward the center of the tunnel, thus causing the lining to contract and reduce the diameter of the tunnel. Also attached to the threaded rods were two plastic guides that ensured that each of the lining plates stayed in place and contracted radially. These guides were held in place by smaller rods fixed to outer Plexiglas casings for the tunnel which will be described later. The plastic guides worked aligning small plates welded to the lining plates. The whole tunnel was designed to be able to contract a maximum of 10 mm in diameter. This would have translated into a volume loss of about 13%. This action could be controlled by the amount that the center rods were turned. All plates were checked for equal and even contraction by LVDTs that are accurate to the 0.01 mm. Figures 3.5 and 3.6 show the internal mechanisms of the tunnel lining.

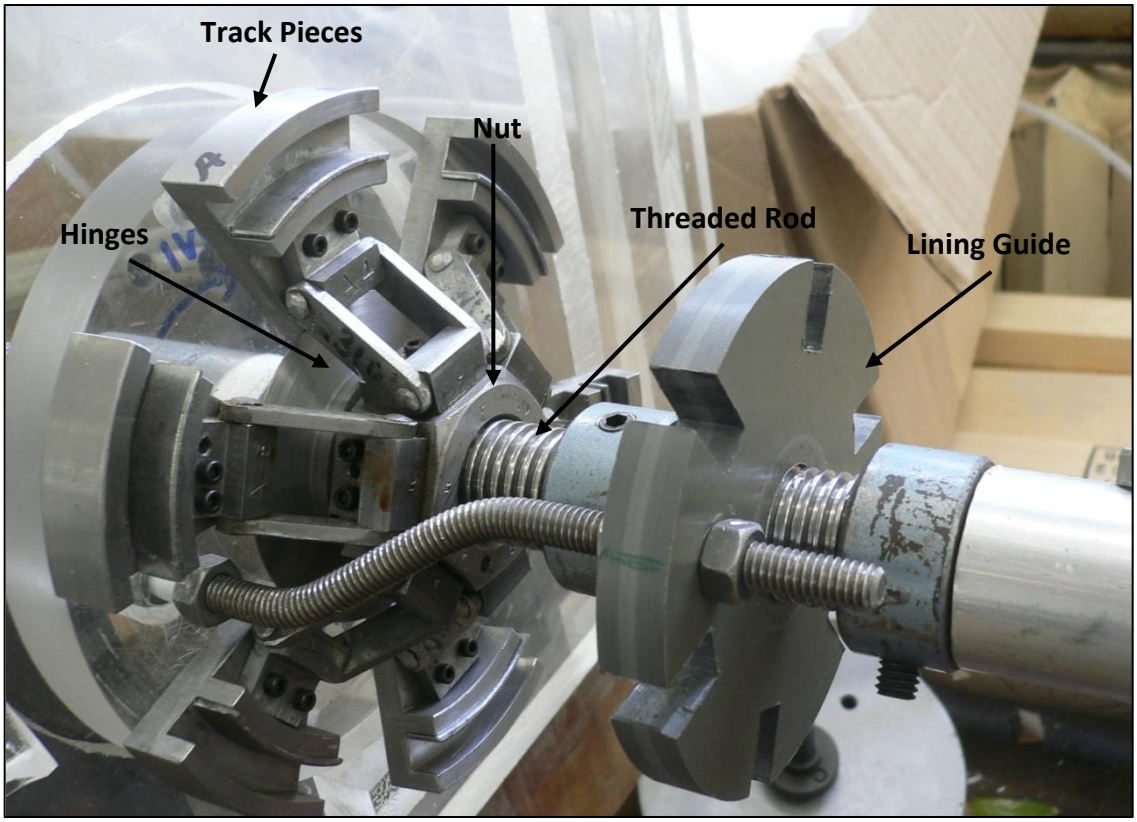

Figure 3.5: Inner tunnel parts without lining

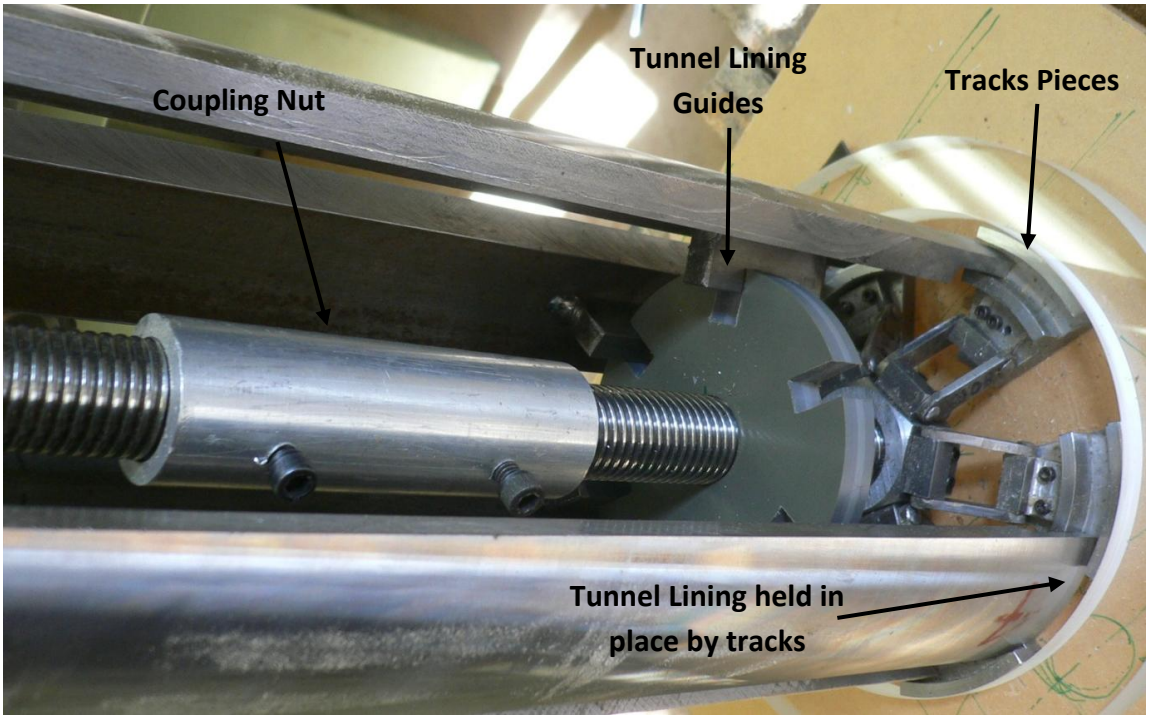

Figure 3.6: Inner tunnel with lining plates partially installed

3.1.4 Tunnel End Frame

The ends of the tunnel model were held in place by Plexiglas frames. The frames included a tunnel end caps and casings. These frames were placed to serve several purposes. The end caps held the steel tracks in place against the lining plates. The casings were to provide a point by which the tunnel could be mounted on the strong box for testing. Lastly, the casings also restricted movement of the tunnel lining to only vertical motion.

The end caps were 1 inch (25 mm) thick and cut into a hexagonal shape so that the tunnel could be placed at three different positions for testing. On one of the ends there was a removable end cap and, using a small circular temporary cap, the tunnel could be installed in to the strongbox through a small circular hole. The end caps were held in place by a bent threaded rod that was attached to the plastic lining plate guides inside the tunnel. The plastic plate guides and the end caps were both mutually reinforcing. Figures 3.7 and 3.8 show the end frames of the tunnel lining.

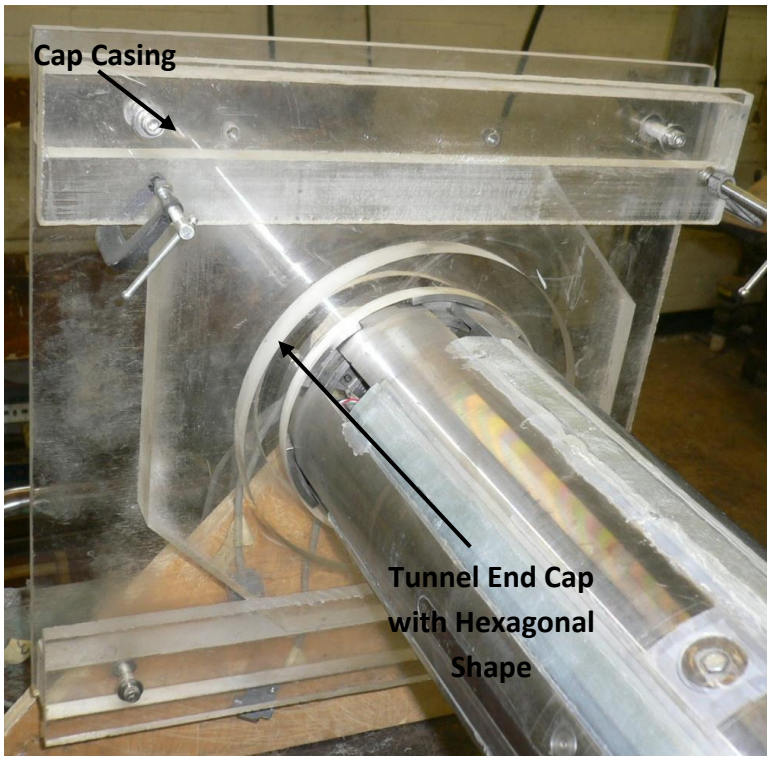

Figure 3.7: Casing with hexagonal end cap

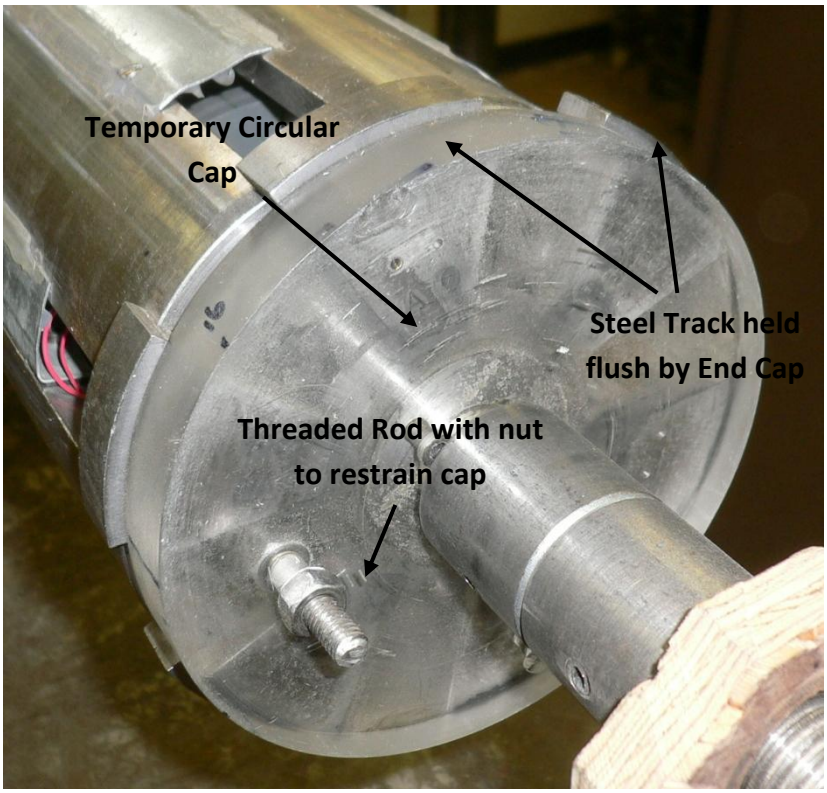

Fig 3.8: Circular end cap with restraining rod

3.1.5 The Retractable Window

To simulate the action of a surface erosion void on the tunnel lining, a small retractable window was installed on one of the thick lining plates. This small window measured 0.4 inch (10 mm) by 10 inches (254 mm). This area would equate to an $Lv/\pi r^2$ of about 1.5% and a void angle of 5.1° as compared to Meguid and Dang (2008) and Tan and Moore(2007) respectively. The retraction method of the window was a miniature version of the tunnel contraction mechanism, the difference being that in the case of the window, only one small plate need be retracted. Otherwise the action included two small threaded rods of opposing directions that were connected together at the center of the plate by a small custom made coupling nut. On each rod was a small nut on which a small custom made hinge attached the nut to the window plate. Three restraining guides were attached to the lining plate to secure the threaded rods from any axial movement. A leaf spring kept the window plate taut against the threaded

rods. To move the window, a threaded rod was turned, causing the hinges to move towards the coupling nut and thusly the window inwards. The window was able to retract to a maximum of 3.5 mm. The window was calibrated to retract exactly 1.5 mm per full (360°) rotation. The tunnel was designed so that the window could be positioned at the springline, invert and at a 45° angle in between. Figure 3.9 shows the main components of the retractable window.

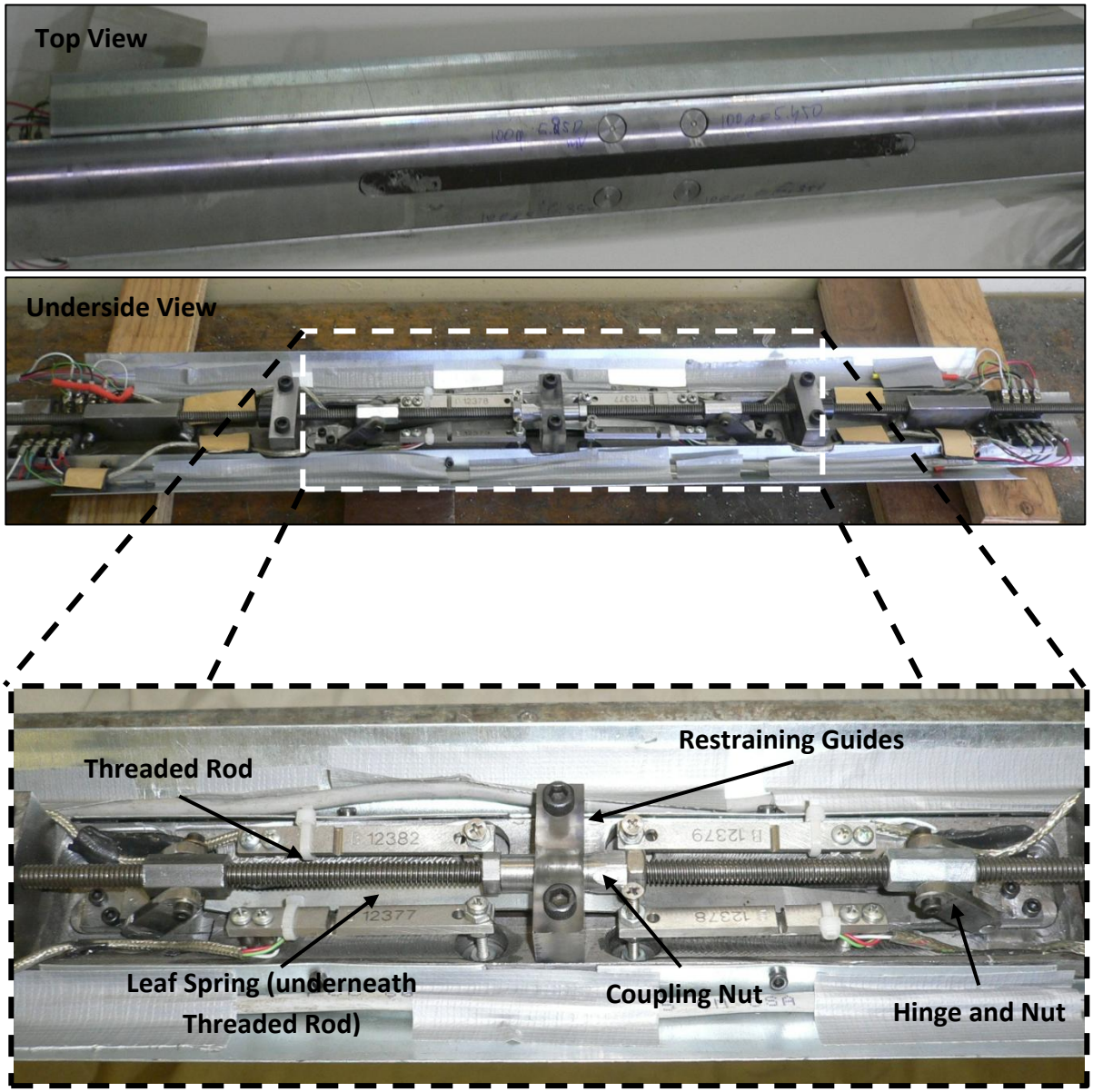

Figure 3.9: Retractable window details and parts

3.2 Sensors and Data Acquisition System

In order to acquire data and monitor the test conditions, a monitoring system had to be installed including pressure sensors and linear variable differential transformers (LVDT). This system was also essential in establishing consistent initial conditions and monitoring the correct implementation of test procedures. Along with the sensors, the data acquisition system (DAS) also constituted an integral part of the test setup. This was a system to record all the readings from the sensors. This section will detail the system and all of its parts.

3.2.1 Pressure Sensor Assembly and Mounting

In order to detect changes in soil pressures on the tunnel lining surface, a series of pressure sensors were constructed and mounted. In total, eight pressure sensors were used. These sensors were made from cantilevered load cells of two different sizes. The load cells work by applying small strain gauge bridges to cantilever beams so that minor deflections could be translated into loads. Four sensors were small, low capacity load cells installed surrounding the window to measure changes in pressure immediately around the window. The other larger capacity sensors were installed on four other lining plates to monitor soil pressures on the rest of the tunnel. The smaller sensors had a capacity of 220 grams and a circular pressure area ½ inch (13 mm) in diameter. They were installed surrounding the window in order to detect small changes in pressure when it was retracted. The larger sensors had a capacity of 500 grams and were each installed on four other lining plates. They also had a circular pressure sensing area of 1 inch (25 mm) in diameter.

The sensors were mounted to the underside of the lining plates. Holes of 1 inch (25 mm) and ½ inch (13 mm) diameters were drilled through the lining and equal sized disks were constructed and installed flush to the lining surface. Care was taken to make sure that a miniscule gap existed between the lining plate and the sensor surface to

allow for movement. In order to keep fine sand particles from entering the gap space around the sensors and interrupting readings, covers were made from invisible tape and plastic sheets. This effectively kept sand from entering the gaps while still allowing the sensors to obtain consistent readings. The sensors were calibrated using a set of bronze weights with the sensor covers on. Wires to connect the sensors to the DAS were extended along the tunnel and out through the end caps. All sensors were connected to the same DAS. Appendix B shows mounting instructions and specifications of the sensors used. Figures 3.10 and 3.11 show the installed sensors and their placement on the tunnel lining.

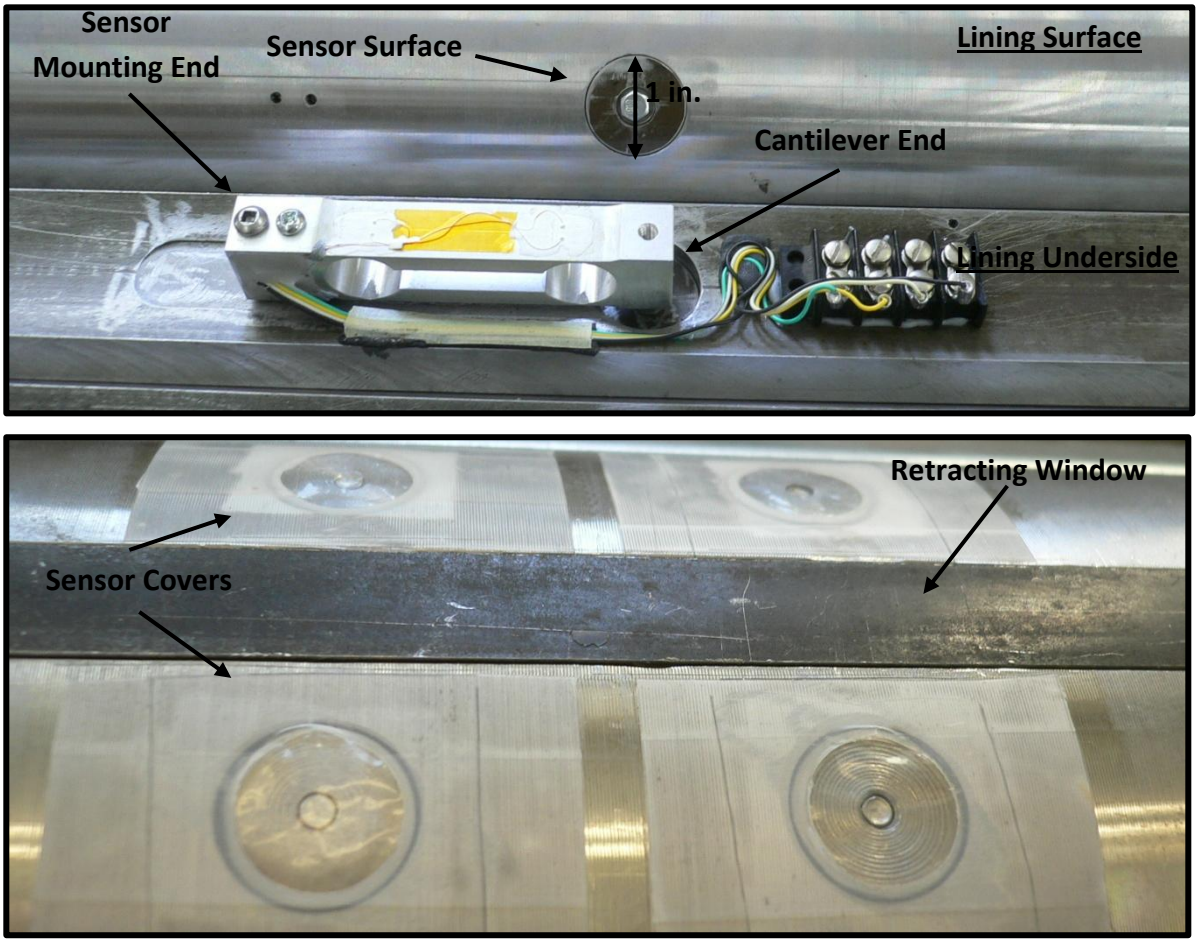

Figure 3.10: View of large sensors on the lining surface and mounted to the underside(Top), and smaller sensors with covers surrounding the window (Bottom)

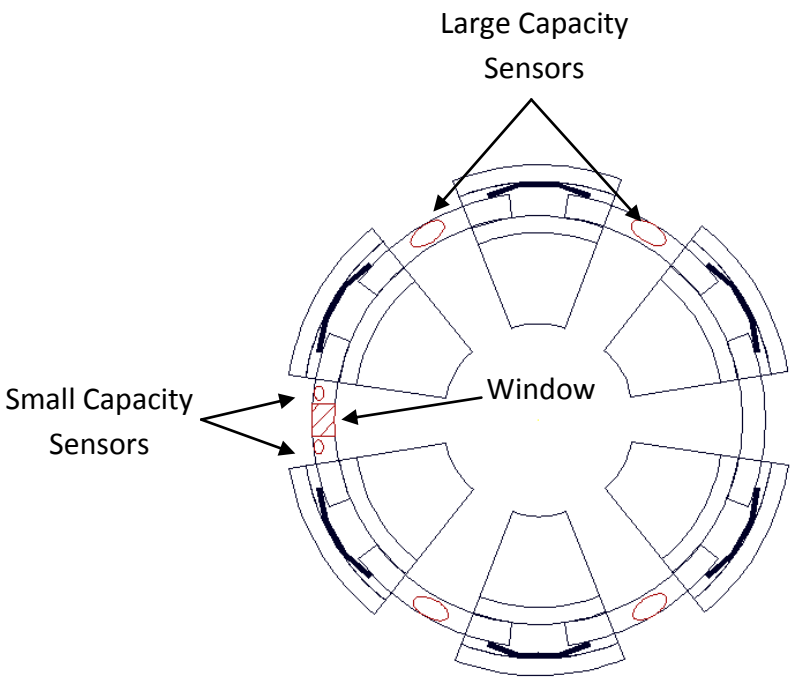

Figure 3.11: Sensor placement on the tunnel lining as shown in the plane-strain view

3.2.2 Linear Variable Displacement Transducer (LVDT)

LVDTs were used to monitor the radial contraction of the tunnel so that it would not exceed 1 mm. Two LVDTs on either end of the tunnel directed horizontally onto the tunnel lining were used for this purpose. They each had a range of 10 mm. Two more LVDTs, one on each of the Plexiglas tunnel casings, were pointed downward, resting on the tunnel end caps. These were used to monitor the vertical translation of the tunnel as a tail void was induced by contracting the tunnel. This was to ensure even vertical translation on both ends of the tunnel. All LVDTs were connected to the same DAS as the pressure sensors.

3.2.3 Data Acquisition System (DAS)

In total, there were 12 sensors that needed to be connected to a DAS so that the readings could be recorded. They were all connected by nine-pin connectors to a *Model 5100* scanner box. The scanner box had two strain gauge cards and two high voltage cards with a total of 20 connection ports. The 8 load cells transmitted loads through strain gauges and therefore were connected to the strain gauge cards. The LVDTs were connected to the high voltage cards. In addition to being ports in which the sensors could be connected, the scanner box also provided electrical power to initiate the sensors. The scanner box was controlled using *Strain Smart 4.3* software installed on a computer running the *Windows XP* operating system. The sensors were also calibrated using this software. Options such as the frequency and precision of the readings could be chosen. Data output came in the form of *MS Excel* spreadsheets.

3.3 Strongbox

The test was run in a strongbox that would contain both the tunnel and the soil as a closed system. This box was reinforced in order to withstand the pressures of large quantities of sand. It was designed such that the rigid boundaries would not influence the recorded readings.

The box is mostly made up of steel plates, bolts and beams. It was decided that one face would be made up of Plexiglas so that the test procedure could be observed. The Plexiglas face was ½ inch (13 mm) thick and the steel plates that make up the other walls of the box were ¼ inch (6 mm) thick. The internal dimensions of the box measured 55.5 inches (1410 mm) wide by 12 inches (305 mm) deep by 46 inches (1168 mm) high. The box was much wider and taller than deep because the model was to represent the two-dimensional plane strain condition. It is, however, deep enough to generate enough overburden pressure on the tunnel lining. All sides of the box were bolted together and the inner edges and corners were sealed with caulking. There were six 100

mm by 100 mm HSS beams bolted across the front and back face to prevent bulging of the surface during testing.

The box rested atop two footings made of 100 mm by 100 mm HSS pieces that were each 850 mm long. On the ends of each of these footings were adjustable levelling screws so that the box could stand level on slanted floors. In the middle of the base of the box was a trap door that would allow sand to be removed easily and quickly. To accommodate the tunnel, two holes 6 inch (152 mm) in diameter were cut through the box. One on the back steel plate and one on the front Plexiglas face. The centers of the holes were aligned with the vertical center line of the box and the bottom of the holes sat 305 mm from the base plate of the box. They were placed at this height in order to satisfy the boundary condition that the tunnel must be at least one diameter above the rough rigid base. The following sections will give a more detailed description of the strongbox components.

3.3.1 Box Elevation View

The three ¼ inch (6 mm) thick steel walls and one ½ inch (13 mm) Plexiglas wall all rested on a base plate that was also ¼ inch (6 mm) in thickness. Steel angle pieces 50 mm by 50 mm connected the walls to each other and to the base plate with a series of bolts and welds. The threaded bolts were 11 mm ($^{7}/_{16}$ inch) diameter and either 57 mm ($2^{1}/_{4}$ inch) long, or 152 mm (6 inch) long for those holding the HSS beams to the box face. The bolt heads were hexagonal in shape and measured 19 mm side to side. The nuts used to fasten the bolts had the same geometry as the bolt heads. In total, 13 bolts were used to fasten each corner of the box.

Three pairs of 100 mm by 100 mm HSS beams were used as forward and back face support. They were bolted horizontally to the edges of the box. The bottom most one stood at 177 mm (7 inch) from the base, the next one at 206 mm (8 inch) above the first and the last one was attached at 190 mm (7½ inch) above the second. The entry hole for the tunnel was cut between the lowermost and middle reinforcing beam.

Below the base of the box there were two footing beams, each 850 mm (2.8 feet) long, welded perpendicular to the face of the box. They sat at 442 mm (1.45 feet) from the center line of the box or at 884 mm (2.9 feet) apart from each other. On top of the footing beams, support frames for the end casings of the tunnel were constructed on the front and back of the box. The frame consisted of a 988 mm (3.2 feet) long HSS cross beam that was welded across the two footing beams and two 385 mm (1.2 feet) HSS beams were welded to the cross beam. The top two beams pointed away from the box and were 300 mm (1 foot) apart. Figures 3.12 and 3.13 show the front and back views of the strongbox.

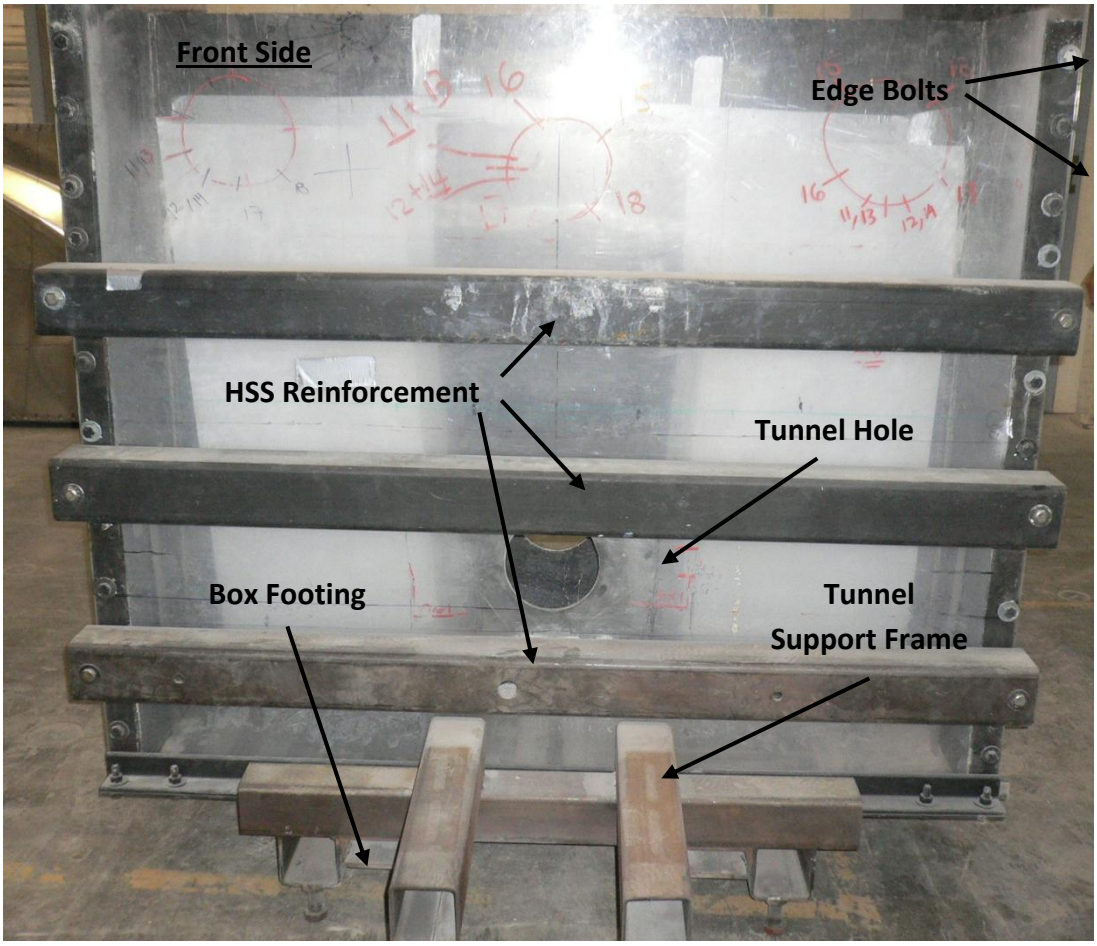

Figure 3.12: Strongbox front with labelled elements

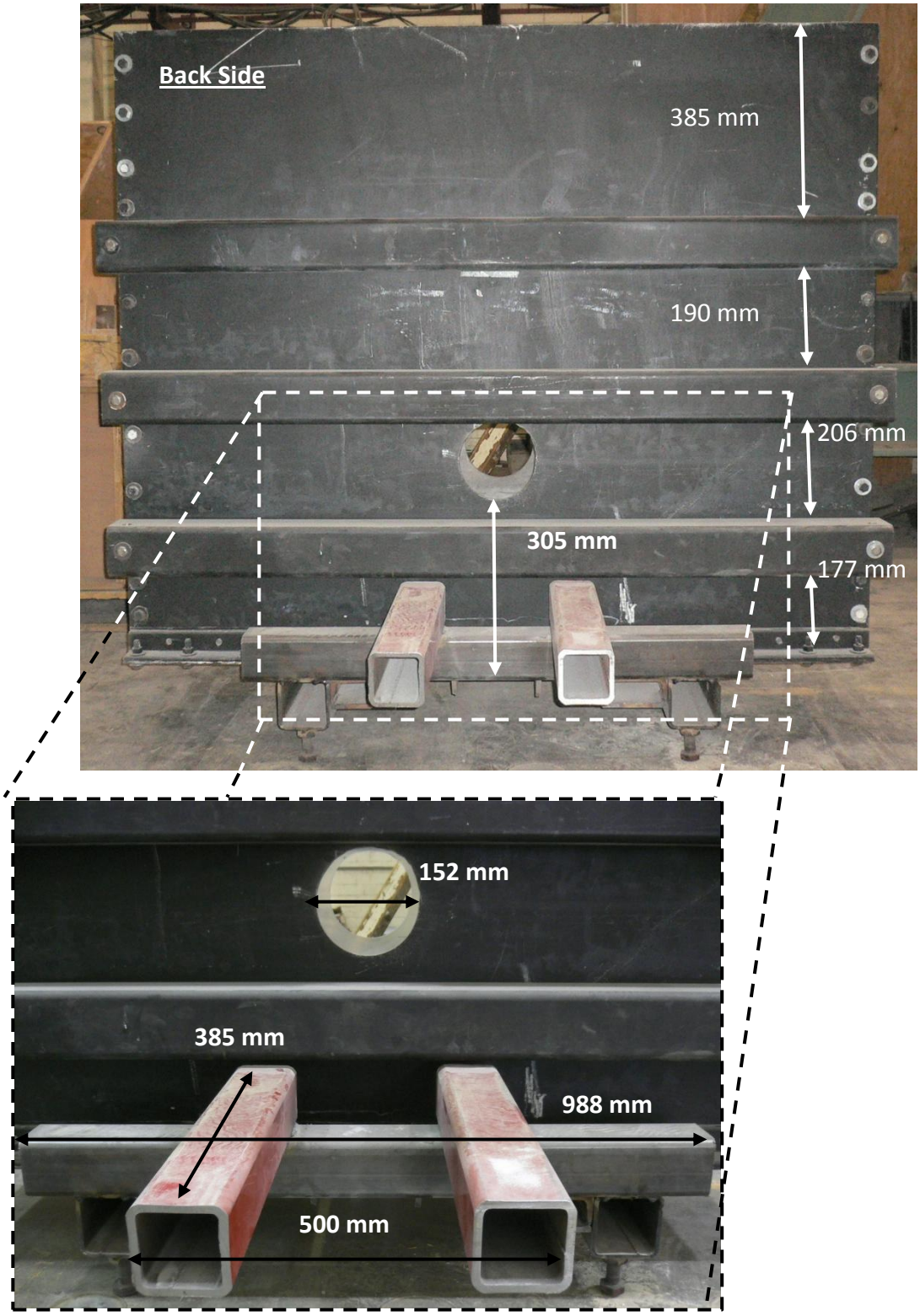

Figure 3.13: Strongbox back with reinforcement spacing and tunnel frame details

3.3.2 Box Side View

The side of the box shows the vertical angles that hold the walls together. There was one for each side that connected the front and back wall to the side wall. These two angles spanned the height of the box at 1524 mm (5 feet). There was also a 200 mm horizontal angle at the base of the box that connected the side wall with the base plate. The angles were all welded to the side wall by small welds of between 50 mm (2 inch) and 100 mm (4 inch) and were bolted to the front/back walls and base plate. There are also angles that run along the front and back of the base plate that held the bottom of the Plexiglas and back plate in place. Figure 3.14 show some of the side view details.

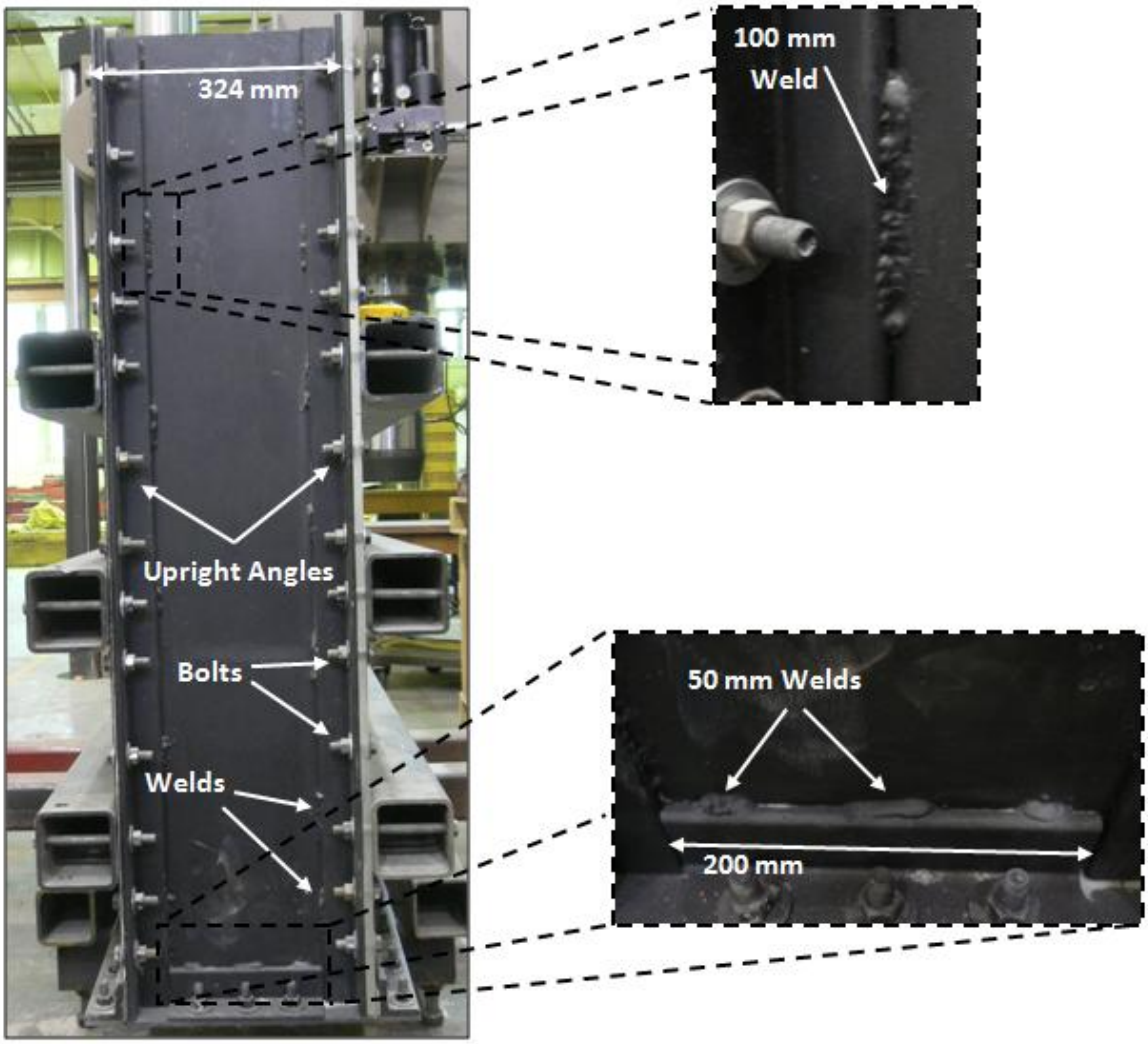

Figure 3.14: Side view details

3.3.3 Wall Insides and Trapdoor

The box had two more features that are important to note. Since the walls of the box were only 1 foot (305 mm) apart there was concern that skin friction from the walls could affect the test. Therefore the steel side of the wall was covered with plastic sheeting in order to reduce friction, whereas the Plexiglas side could be considered a smooth surface. There was also a small trapdoor in the middle of the tank base measuring ½ ft (152 mm) by 1 ft (305 mm). The door had two sliding screens to empty the sand. To be able to utilise the trapdoor the box had to be elevated on two stone blocks so that a large sand container could be placed under the box. Figure 3.15 shows the wall and the sheets.

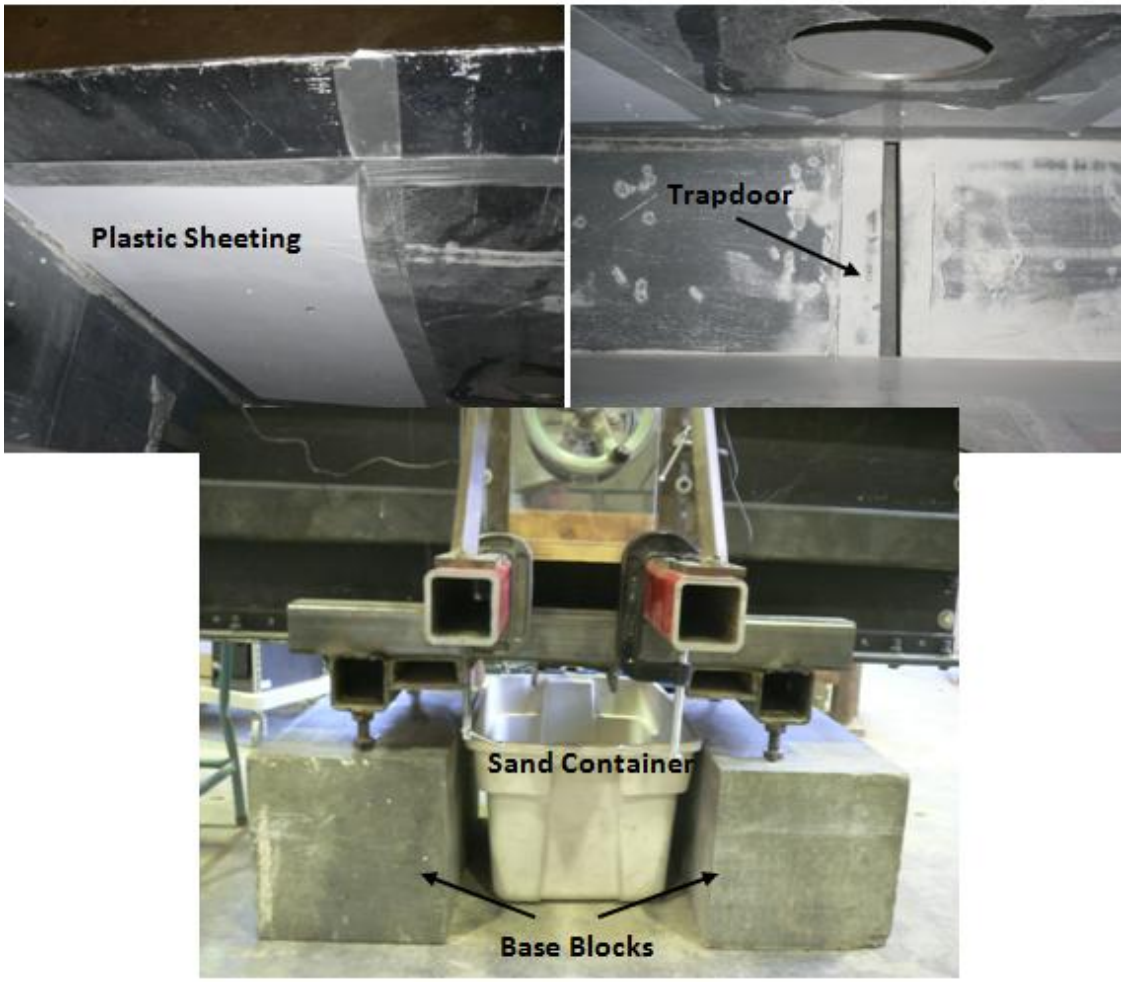

Figure 3.15: Plastic sheeting, trapdoor, base blocks and sand container

3.4 Soil Properties

Fine sand was chosen to be the soil medium for testing. This was because the small sensors were thought to be more reactive to smaller sand particles. The sand has a labelled grade of *Quartz Industrial 7030* meaning that 30% of the material would be retained in a No. 70 mesh. The specific gravity (G_s) of this sand was found to be 2.66 using the ASTM Standard D854-06. A sieve analysis was conducted according to ASTM D6913-04e1 and a particle size distribution was obtained. The coefficient of uniformity (C_u) was found to be 1.90 and the coefficient of curvature (C_c) to be 0.89. Table 3.1 below summarizes the soil properties of the fine sand used. Figure 3.16 shows the particle size distribution curve for the fine sand used. Appendix A includes the data from the soil properties tests.

Property	Value
Specific gravity	2.66
Coefficient of uniformity (C_u)	1.9
Coefficient of curvature (C_c)	0.89
Maximum dry unit weight (γ_{max})	15.7 (kN/m^3)
Minimum dry unit weight (γ_{min})	14.1 (kN/m^3)
Experimental dry unit weight (γ_d)	15 (kN/m^3)
Unified soil classification system	SP
Internal friction angle (ϕ)	38.5°
Cohesion (c)	0.2 (kPa)

Table 4.1: Soil Properties

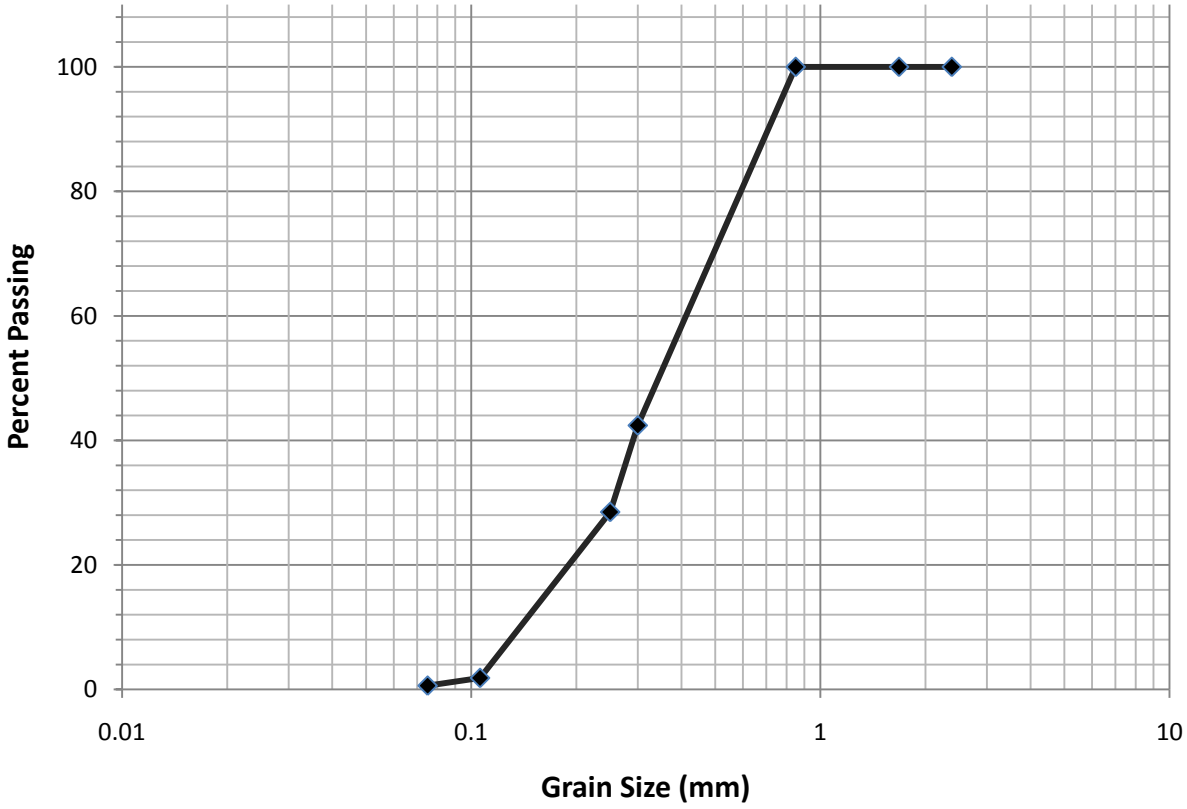

Figure 3.16: Sand grain size distribution

3.5 Test Procedure and Methodology

A thorough, detailed test procedure was developed in order to facilitate successful testing. The main goals in developing the testing program were to be able to perform as many tests as possible while keeping the procedure simple and repeatable. There were three different positions for which the retractable window can be placed. For this reason, it was decided that the test program would include nine tests, three for each position in order to ensure a degree of certainty with the results. This section will go through the test steps and procedure in detail.

3.5.1 Tunnel Test Positions

The three tunnel positions tested were with the window representing the erosion void at the springline, the invert and at the midpoint along the lining between the two. For reasons of symmetry, these positions were only tested for the right half of the tunnel and not the left half. The parts of the tunnel lining above the springline were not tested because voids formed in this area are likely to collapse before any appreciable arching would occur. Figure 3.17 shows the testing window positions.

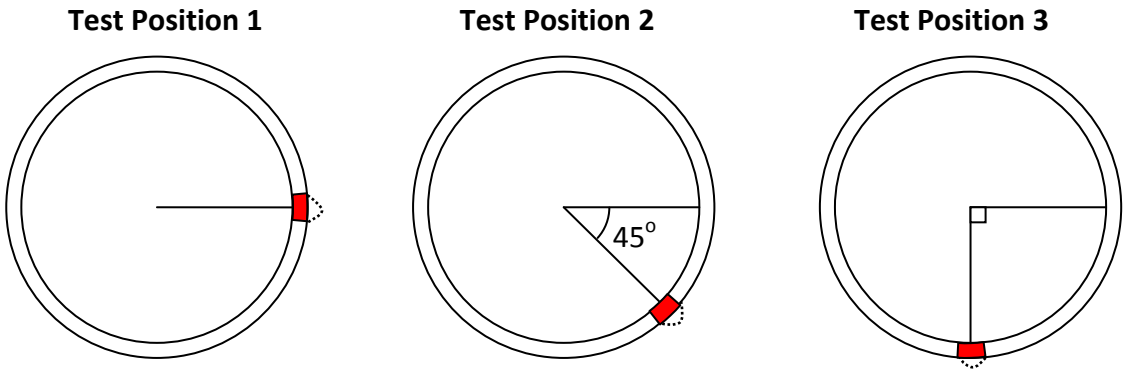

Figure 3.17: Window Test Positions

3.5.2 Test Materials

Several other materials were obtained and constructed for the purpose of conducting an efficient and successful test. To hold the large amount of sand that would be needed for the test, a wooden container was constructed. This container measured 4 feet (1219 mm) long by 2 feet (607 mm) wide by 2 feet (607 mm) deep. It was lined with plastic sheeting inside to prevent sand from leaking. There were also three plastic *Rubbermaid* boxes, like the one shown in Fig 3.15, that were used to empty the container.

Several tools were used for the sand filling process. Two rubber gaskets, 1/8 inch (3 mm) thick, were made to line the ends of the tunnel so that the sand would not escape out of the holes cut into the side walls of the strongbox. A shovel was used to move and level the sand deeper in the strong box and three tamping feet were constructed to compact the sand below the tunnel. Two tamping feet served as hand tampers and the third one was made specifically to be used with a hammer to compact the sand directly beneath the tunnel. Three sand sampling cups were used to check sand density. Appendix A shows the results of the sand density from the sampling cups used in the test. A wheel was attached to the threaded rod at the end of the tunnel so that contraction could be activated with minimal disturbance to the sand. Finally, due to the hazardous amount of sand dust created during testing, dust masks were worn at all times. Figure 3.18 shows some of the equipment used during testing.

Figure 3.18: Testing equipment (clockwise from top left: tampers, sand samplers, dust mask)

3.5.3 Test Pre-Preparation

Before testing could commence, the box was inspected and cleaned of all soil and sands. Then the tunnel was installed into the strongbox with the rubber gaskets on either end. The edges of the gaskets were duct taped onto the strongbox walls to ensure a tight seal. Next, the trap door was closed and sealed with a strip of duct tape. This was proven effective in preventing sand leaking from the bottom of the tank. After this, the LVDTs were installed all around the tunnel edges and all sensors were connected to the scanner box. Next, the tunnel lining was lifted from both ends and clamped into place. This was done so that the tunnel would eventually not rest on the holes in the box walls but instead be completely supported by the soil inside. The tunnel was then checked with a level and adjustments made as necessary. Finally the tunnel ends were covered on the outside with plastic sheeting and inside the box with a small towel to protect them from falling sand.

3.5.4 Strongbox Filling Procedure

The procedure in which sand was deposited into the strongbox was vital to the success of the test. Sloppy sand pouring and inconsistent compaction could create uneven areas in the sand that could affect the readings on the sensors during the test. Many false tests can result from this problem. Therefore the filling procedures were strictly followed for each test without exception.

The filling process was split into layers. There were three layers below the tunnel, two that span the width of the tunnel and two more on top of the tunnel. The sand was poured until it was at a level 2 times the diameter of the tunnel above the crown. At this level, the surface boundary effects are thought to be minimal. All layers were clearly marked out on the Plexiglas surface. The bottom three layers were also marked on the inside of the box because the lower marks were sometimes obscured by the HSS reinforcing beams. The bottom three layers were each 10 cm (4 inch) thick.

The two layers in the middle were 7.5 cm (3 inch) thick and the two layers at the top were 15 cm (6 inch) thick.

For each of the bottom layers, sand was filled by hand and then levelled using the shovel. Next, the sand was compacted rigorously using the hand tamper. If the sand compacted to a level below the marked lines, more sand was poured, levelled and compacted. Once the sand reached the level of the tunnel invert, it was compacted by hammering on the tamping foot in the area directly beneath the tunnel. The layer above the invert was then filled up to the springline of the tunnel. Some sand was gently pushed into the space below the springline under the tunnel. Then the layer was compacted lightly. Once the sand was filled to the level of the crown of the tunnel, it was again lightly compacted. The last two layers were simply filled to the line and levelled off without any compaction. The backfill procedure used was similar to standard practices. In the middle of each layer, a sand sampling cup was placed to check the density of the sand at different layers. They were removed after the completion of the test and weighed. Once this was completed the test is ready to be run. Figure 3.19 shows how the strongbox was filled.

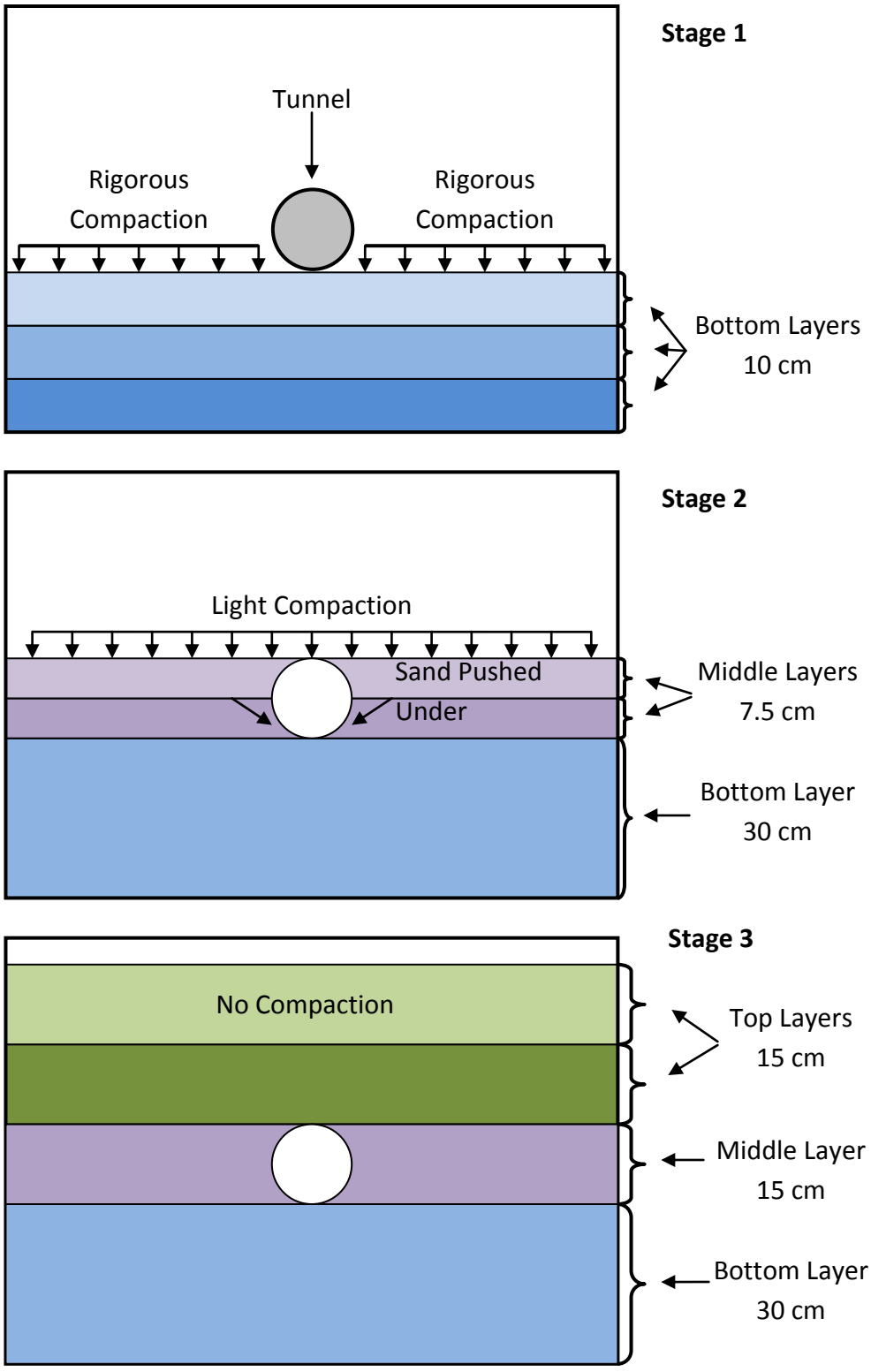

Figure 3.19: The Stages of Sand Placement

3.5.5 Test Procedure

After the box was filled with sand, the first step in the test was to release the clamps on the Plexiglas casings that held the tunnel up. This set the tunnel lining onto the sand so that it was freely floating on the soil medium. Next, the sensor readings and time were noted as the initial conditions of the test. The sensors on the top of the tunnel should have similar or lower readings than the sensors beneath. Also, twinned sensors, such as the small sensors above and below the window should have very similar initial readings. Once the initial conditions were established, the next step was to contract the tunnel to induce radial soil movement. This was done by turning a wheel connected to the threaded rod on the tunnel. The contraction was carefully monitored by the LVDTs until a decrease of 2 mm in diameter. After this, the sand was allowed to settle around the tunnel. Once the sensor readings stabilised, the data and time were noted before advancing to the next step. Retracting the window to simulate a local support loss was the last step of the test. Since the window could retract up to 3 mm, this action was split into two parts wherein each retraction would move the window 1.5 mm away from the sand. After each retraction, the sensor readings were recorded and the test completed. Finally, after the test, while the box was being emptied, the sand sampling cups were recovered and sand density measured.

Chapter 4 – Results and Analysis

4.1 Introduction

This chapter will present the results of the experiment as well as some analysis. This will include observations as well as supporting data. While all data will be presented, emphasis will be placed on the change in earth pressure before and after tunnel window retraction inducing support loss. Normalised values were used because they best represented the changes in pressure during the test and allowed for quick and easy comparison of results.

4.2 Setting of Initial Conditions

The initial conditions of the test were considered once the tunnel was contracted to initiate soil pressure change. Sensors were inspected to ensure that symmetrical ones had similar readings. The tunnel lining reduced in diameter by 2 mm. After this reduction, given some time for the sensor readings to settle pressures were noted. With the window at the springline, both sensors near the invert increased in pressure while sensors near the crown decreased. When the window was placed at the invert, all sensors would decrease in pressure with the exception of the small ones near the window. With the window at 45° between the springline and invert, most sensors decreased in pressure except the one closest to the invert. In general, while the sensors near the invert showed an increase in pressure, those away from the invert show a decrease. This could be because lining contraction causes the soil above the springline to settle downward but below this the soil does not heave upwards.

Figures 4.1 – 4.3 show the changes in initial pressures that followed the reduction in lining diameter. Since the sensors changed position depending on the position of the window, a diagram indicating sensor placement accompanies each graph. The vertical axis represents the change in pressure (P) over the initial pressure (Po). Figure 4.1 shows the change in pressure with the window at the springline. The upper sensors, 15 and 16, showed pressure reductions of 35% and 57% respectively. Conversely, the lower sensors 17 and 18 increased in pressure by 38% and 40%. This is attributed to the fact that the induced soil movement due to the tunnelling simulation is occurring above the invert area leading to pressure relaxation at 15 & 16. Figure 4.2 shows the changes with the window at the invert. In this case, all sensors showed a drop in pressure. The sensors above the springline, 15 and 18, showed pressure readings of 75% and 70% of the initial pressures. The sensors below the springline, 16 and 17, recorded pressures that are 47% and 37% of the initial pressures. In Figure 4.3 with the window at the 45^{o} angle between in the invert and the springline sensor 15, near the crown, showed a decrease of 74%. Near the springline sensor 16 decreased by 62% and sensor 18 decreased by 73%. Near the invert, sensor 17 increased by 88% from the initial measurements.

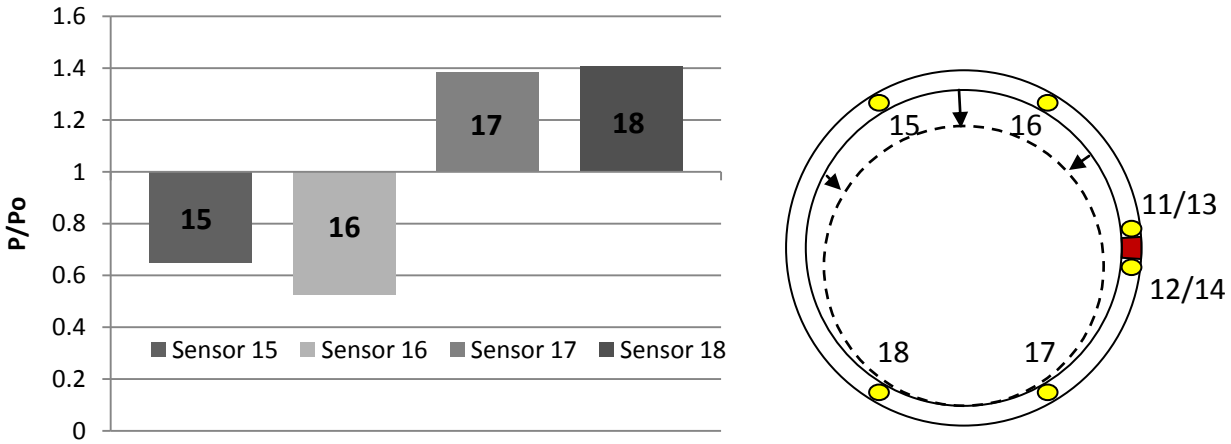

Figure 4.1: Lining contraction pressure changes with window at tunnel springline

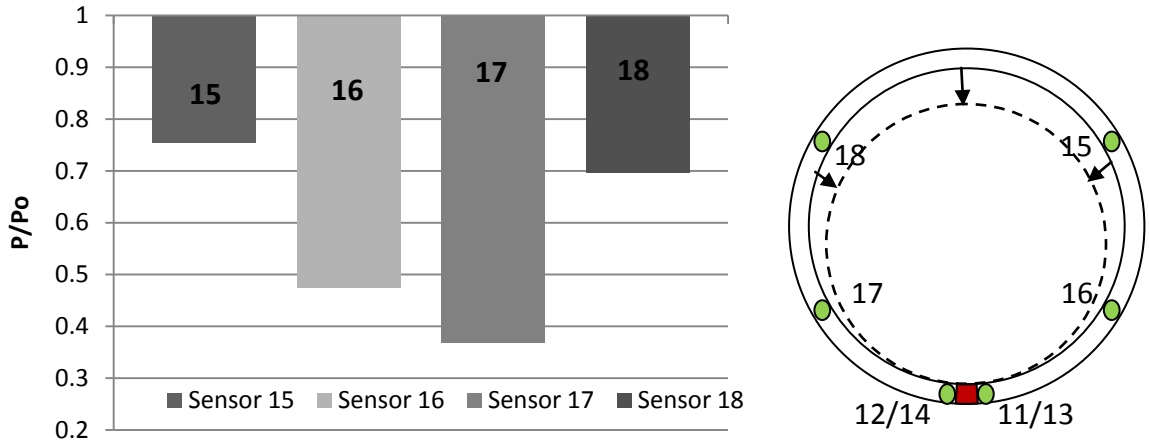

Figure 4.2: Lining contraction pressure changes with window at tunnel invert

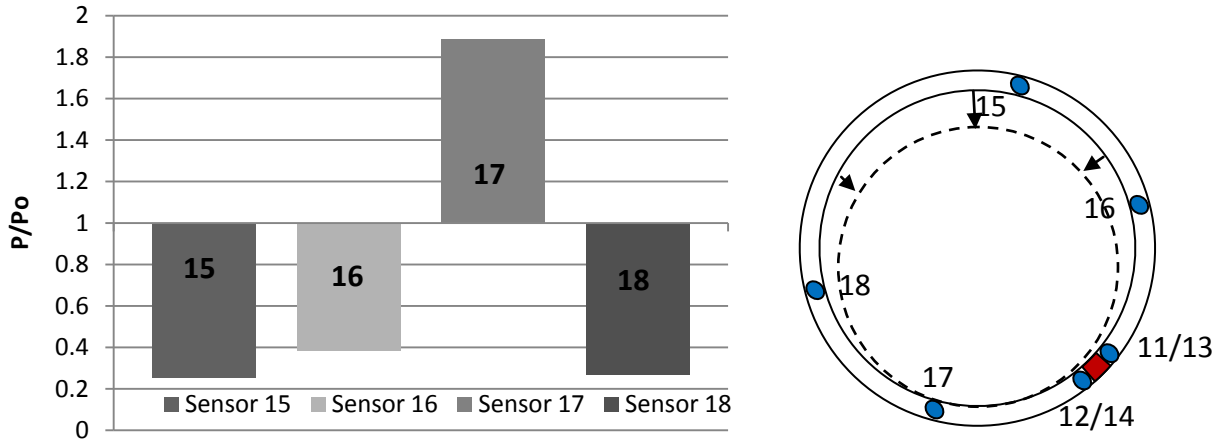

Figure 4.3: Lining contraction pressure changes with window at 45^{o} angle

4.3 Window Retraction

Three tests were conducted at each position of the window. Each set of tests showed a consistent change in earth pressure experienced by the small sensors closest to the window. In all tests, the change in pressure of the larger sensors away from the window was minimal. This was likely due to the short width of the window representing a small erosion void. Since the larger sensors did not register change in pressure with the retraction of the window, their data are not presented. Each position of the window induced a different and distinct reaction from the soil when it was retracted. This was to be expected because of the differences in vertical and lateral earth pressures along the tunnel lining. When data from all three positions are put together a pattern can be surmised.

4.3.1 Test Data: Window at Springline

The first position is with the window at the springline. The retraction of the window and subsequent arching of the soil produced different reactions between the sensors surrounding the window. In sensors 11 and 13 above the window, the pressures decreased when the window was retracted. The pressure in sensors 12 and 14 below the window either increased marginally or stayed about the same. The decrease in pressure of the upper sensors averaged to about 40% of the pre-retraction pressures. The reason for a decrease in pressure above the window and minimal change below could be because once the window was retracted, the small area of soil around the upper sensor settled downwards releasing pressure from that area on the lining.

Figures 4.4 through 4.6 show the results of each of the three tests. Figure 4.4 is the first test at the springline position. With the window retracted 1.5 mm, there was minimal change in pressure. At 3 mm retraction, there is a marked pressure change from sensors 11 and 13 above the window, from sensors 12 and 14 below the window. The sensors above (11/13) decreased by 72 – 76%. Those below (12/14) showed an increase in pressure of 13 – 20%. Figure 4.5 presents the results from the second test at the springline position. In this test, the upper sensors (11/13) began to decrease in pressure even when the window only retracted 1.5 mm. But when it was retracted the full 3 mm all sensors recorded a significant drop in pressure. The two sensors above (11/13) had a final pressure that was 41 – 49% of the initial pressure. The two sensors below (12/14) decreased to 88 – 91% of the initial pressure. The third test shown in Figure 4.6 indicates an increase in pressure when the window was retracted only 1.5 mm. But the reaction at 3 mm follows the pattern of the first test where sensors 11/13 dropped in pressure while sensors 12/14 stayed near initial conditions. Figure 4.7 shows the average of the three tests and the overall trend with the window positioned at the springline.

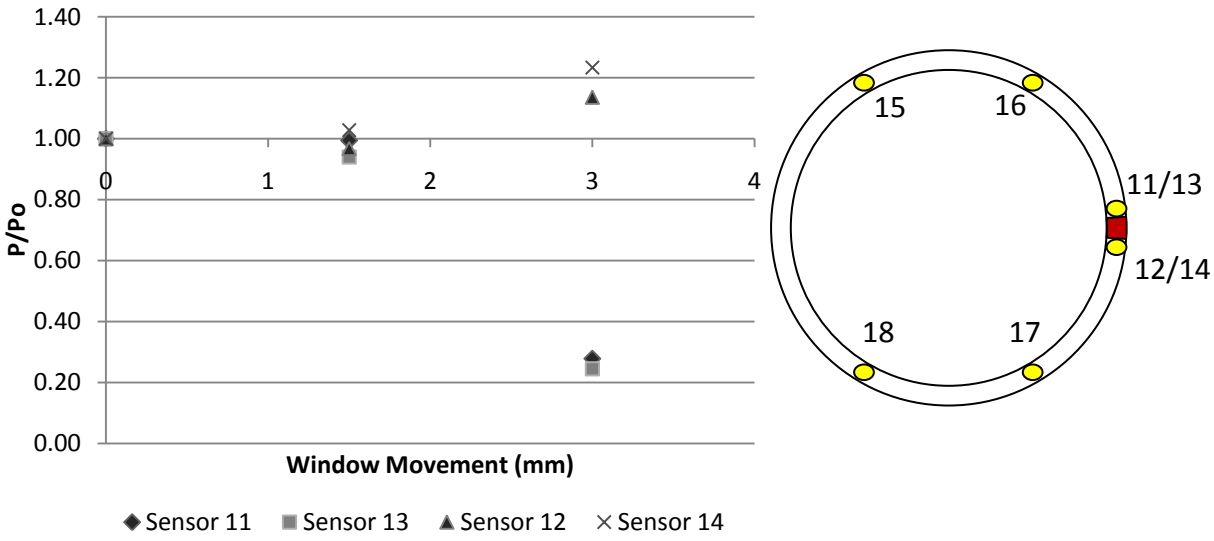

Figure 4.4: Change in pressure with the retraction of window at springline (Test 1)

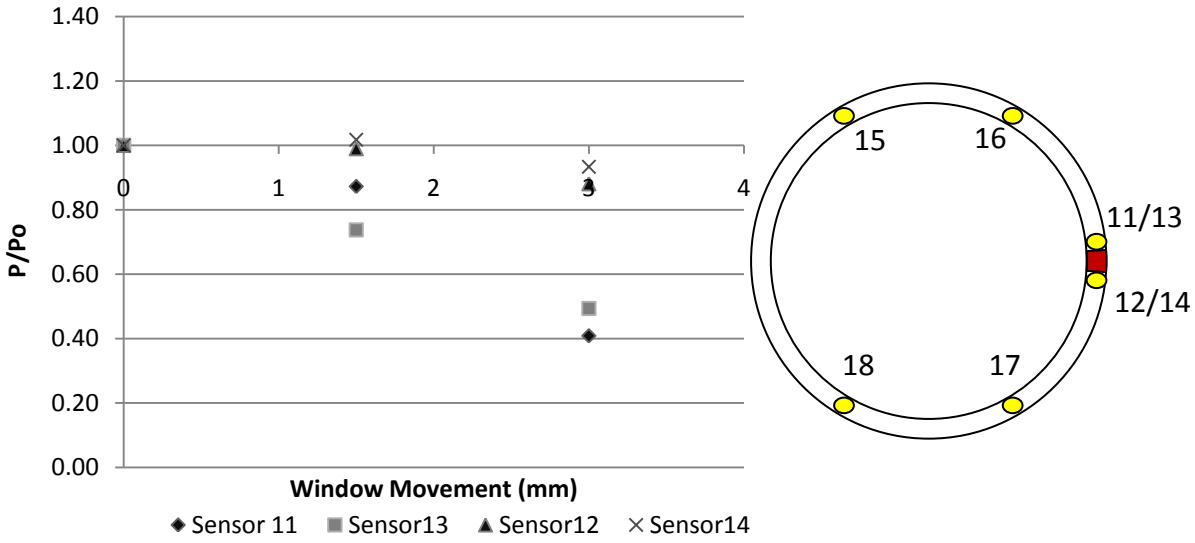

Figure 4.5: Change in pressure with the retraction of window at springline (Test 2)

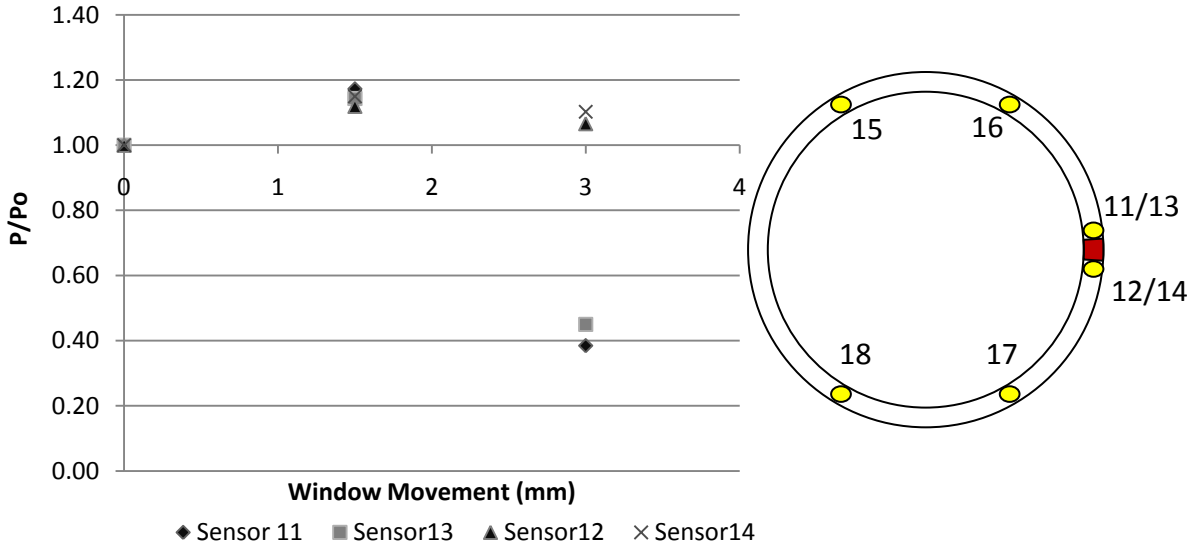

Figure 4.6: Change in pressure with the retraction of window at springline (Test 3)

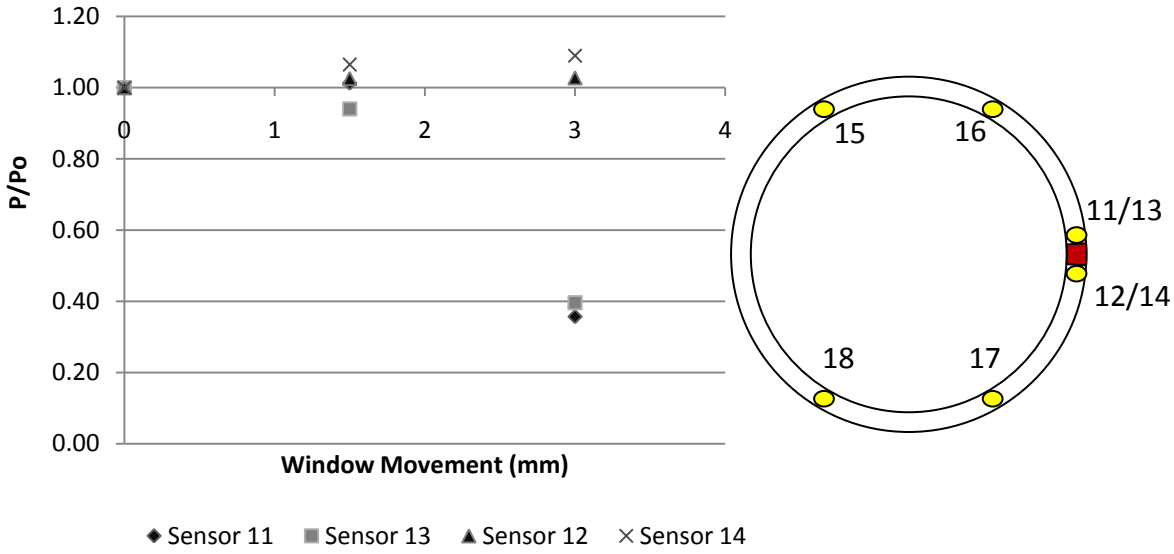

Figure 4.7: Average of all tests change in pressure with the retraction of window at springline

4.3.2 Test Data: Window at Invert

When the window was positioned at the invert of the tunnel, all four smaller sensors should have been symmetrical and therefore have similar readings. In all tests, sensors measured increase in pressure with the retraction of the window. The increase ranged from 3% to 23%. The average increase was about 13% of the original pressures. The data from this set of tests was not as consistent as the prior set but the trend of increase was evident. Figures 4.8 through 4.10 show the results from the tests at the invert. Figure 4.8 depicting the results from the first test is missing the data from sensor 11, which was not functioning properly at the time and thus ignored. However, the test was kept because sensor 13 was in an identical placement and the total profile can still be interpreted. In this test the sensors increased in pressure from 4 to 23% with sensor 12 measuring the smallest pressure increase and sensor 14 with the greatest pressure. Figure 4.9 shows the second test with the window at the invert. In this instance, the increase in pressure recorded range from 3 – 16% with sensor 11 being the lowest and

sensor 14 the greatest. In the third test shown in Figure 4.10 the range of increase was from 13 – 23%. In this case the greatest increase was recorded by sensor 11 and the least was in sensor 14. Figure 4.11 shows the average of the three tests.

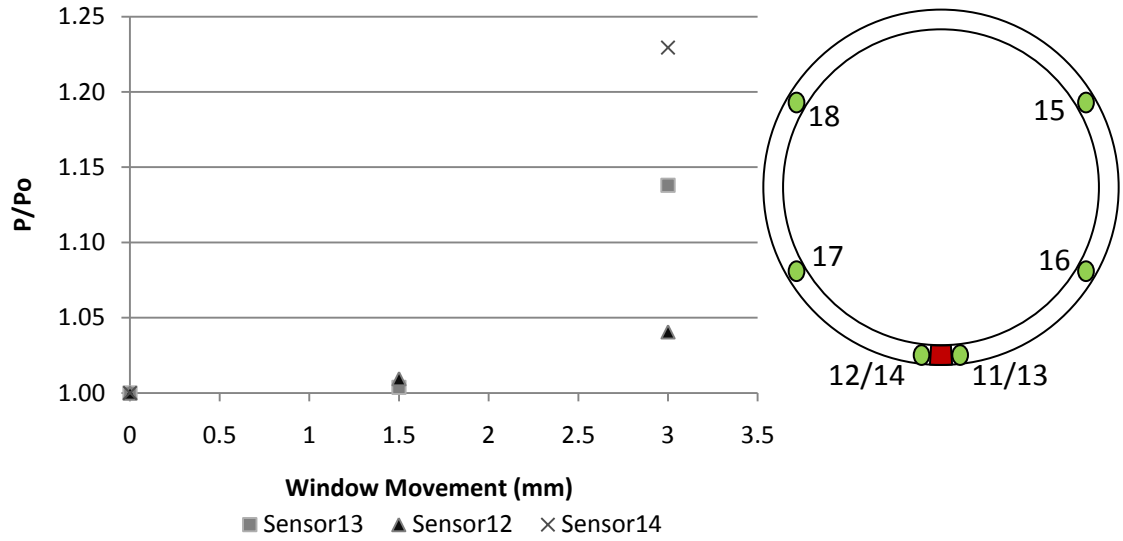

Figure 4.8: Change in pressure with the retraction of window at invert (Test 1)

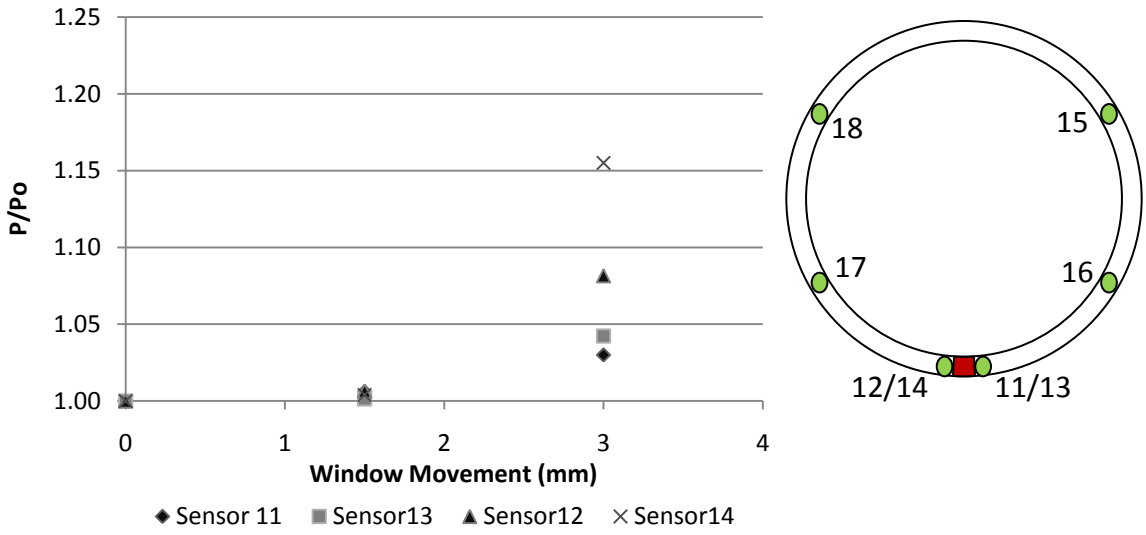

Figure 4.9: Change in pressure with the retraction of window at invert (Test 2)

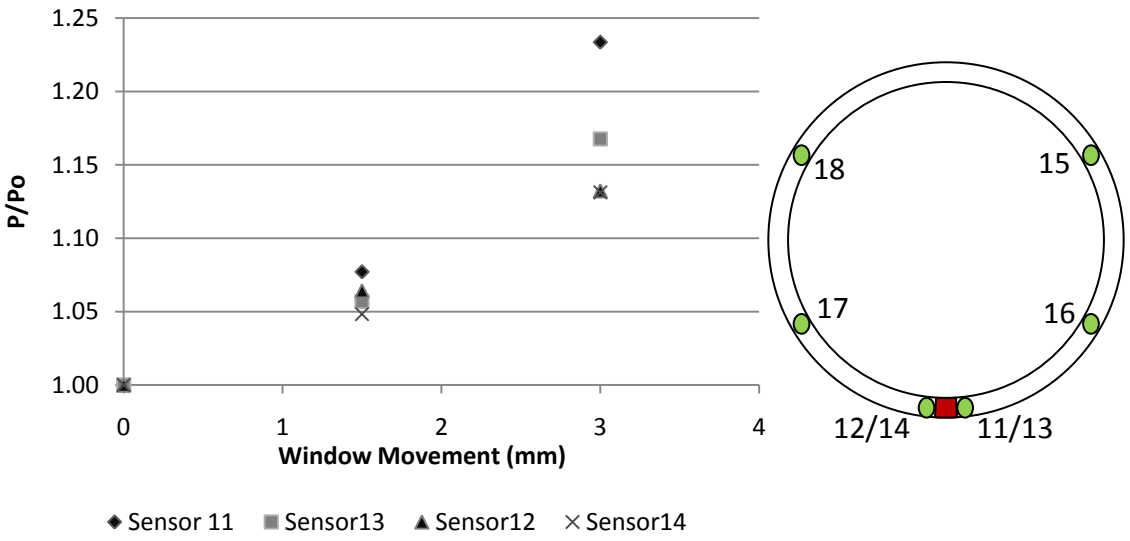

Figure 4.10: Change in pressure with the retraction of window at invert (Test 3)

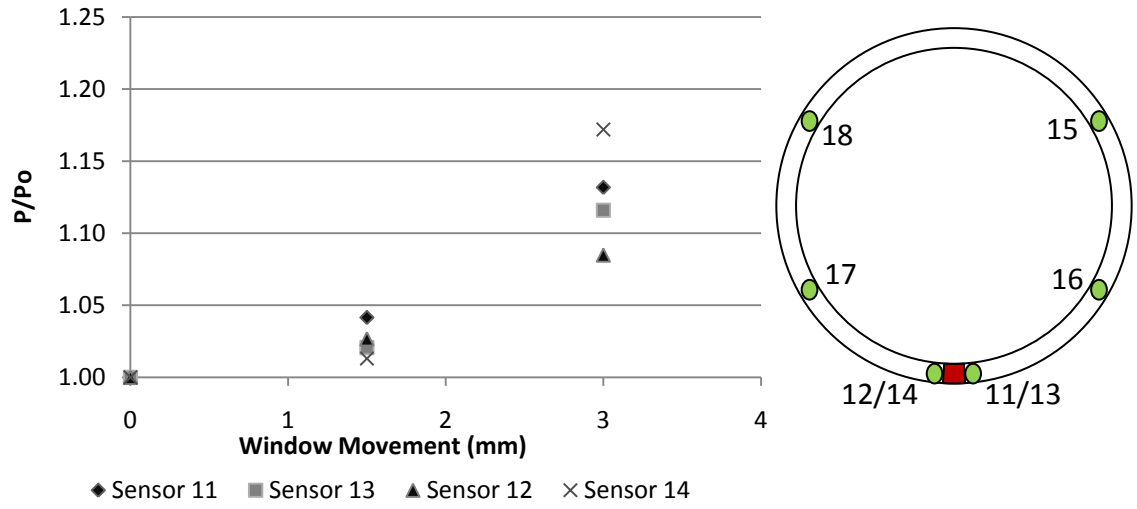

Figure 4.11: Average of all tests change in pressure with the retraction of window at invert

4.3.3 Test Data: Window at 45^{o} Angle

The last position tested was with the window positioned at the bisecting 45^{o} angle between the springling and the invert. When the window was placed at this position, all the sensors still showed pressure increases as the window was retracted. But unlike the invert position, the sensors above the window showed indisputably different reactions than the sensors below. The sensors below the window (sensors 12/14) showed a small magnitude increase. The three tests had increases ranging from 3% to 7%. The upper sensors (sensors 11/13) saw increases ranging from 12% to 29%. The average increase in the lower sensors was about 4%, whereas the upper sensors had an average increase of about 18% percent. In test number 3 of this position, the upper sensors showed a drop in pressure from when the window was retracted 1.5 mm to when it was in the final 3 mm retraction. This could be because local soil movement or settlement shifted pressures away from the sensors. Figures 4.12 through 4.14 show the results from test position 3.

Figure 4.12 shows the first test. In this graph, all the sensors recorded pressure increases with the window retracted 1.5 mm. Sensors 11/13 increased 19 – 25% and sensors 12/14 increased 4 – 7%. These increases declined minimally as the window retracted to 3 mm. The second test presented in Figure 4.13 indicates that the sensors measured increases in pressure as the window was retracted to 1.5 mm. Again, sensors 11/13 measured the greater increases of 13 – 20%. Sensors 12/14 recorded a change of only 2 – 4%. These increases declined slightly as the window retracted to 3 mm. Figure 4.14 shows the results of the last test where sensors 11/13 measured increases in pressure of 25 – 29% when the window was at 1.5 mm. The pressures then dropped to 14 – 15% as the window moved to 3 mm. Sensors 12/14 increased by 4% and stayed relatively constant.

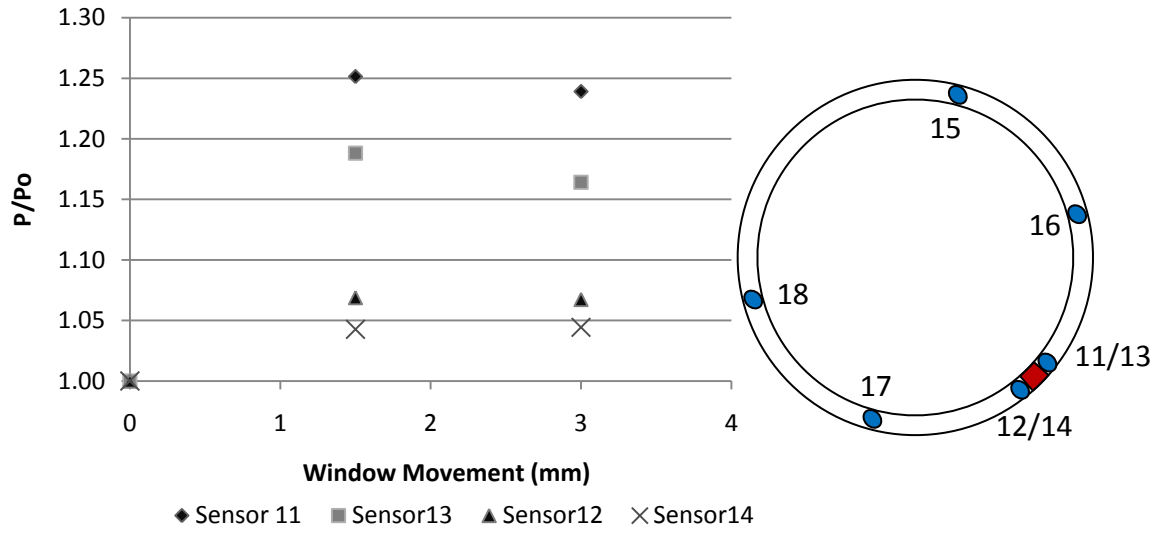

Figure 4.12: Change in pressure with the retraction of window at 45^{o} angle (Test 1)

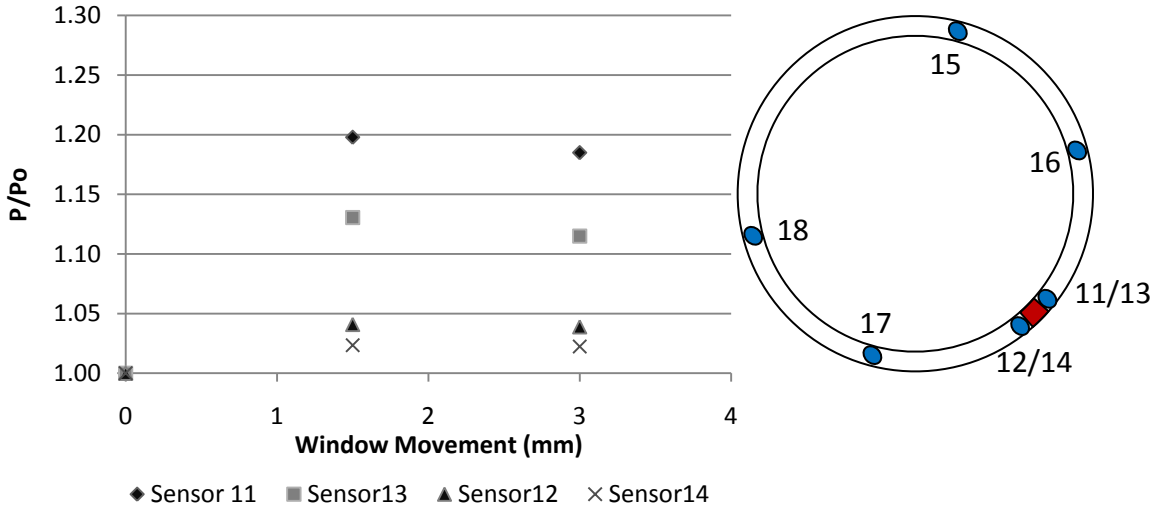

Figure 4.13: Change in pressure with the retraction of window at 45^{o} angle (Test 2)

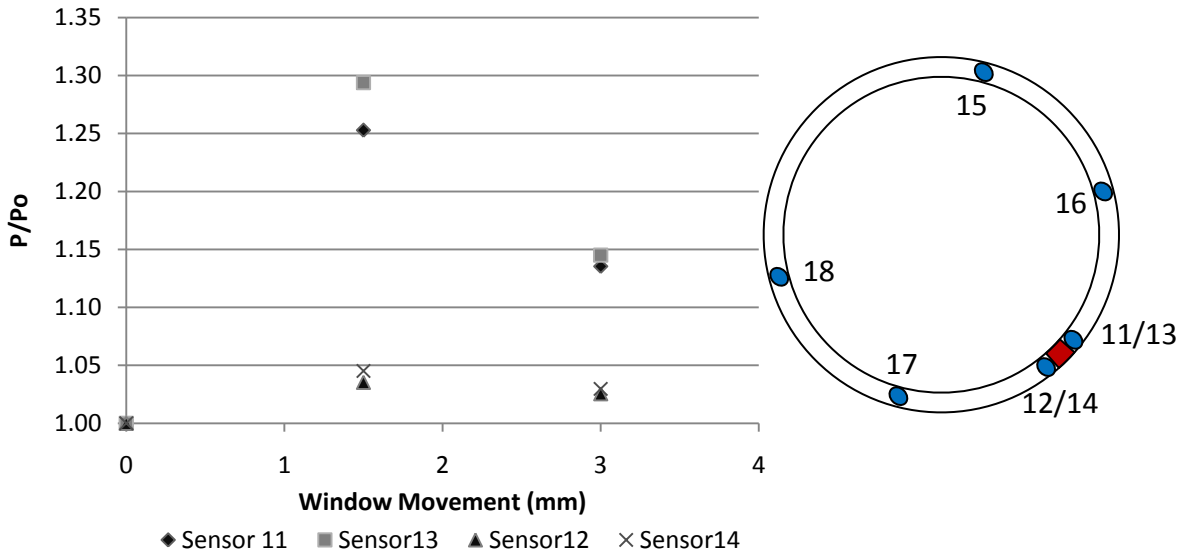

Figure 4.14: Change in pressure with the retraction of window at 45^{o} angle (Test 3)

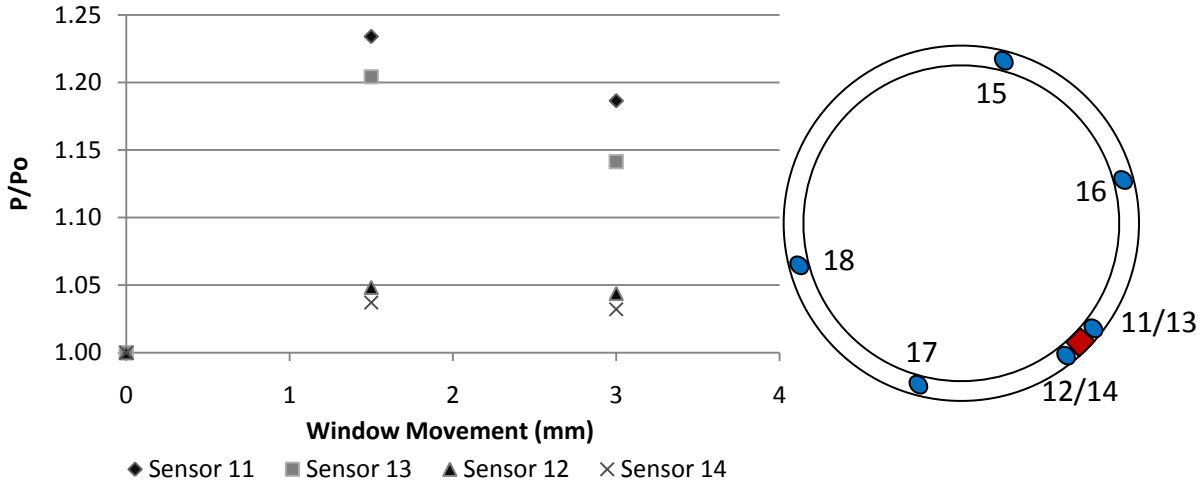

Figure 4.15: Average of all tests change in pressure with the retraction of window at 45^{o} angle

4.4 Discussion

From looking at all test results in all three positions, a few points of interest can be noticed. Firstly, while obvious, it is important to state that all points under the springline on the tunnel circumference experienced an increase in pressure when the window was retracted. This seems to lend evidence to the fact that arching was indeed induced and that at least some of the pressure was redistributed to the areas directly adjacent to the window. Another point of interest was the sensitivity of the soil and sensors to the window retraction. In the first two sets of tests with the window at the invert and springline, the window had to be retracted the full 3 mm before the maximum pressure change was obtained. For the window position at a 45^{o} angle, the sensors measured a maximum change in pressure when the window was retracted only halfway at 1.5 mm. This shows that the soil was seemingly more sensitive to changes at that position.

The greatest change in pressure was seen at the springline with a drop of about 60% of the original pressures at the sensors above the window. A possible explanation for this would be sand settling into the retracted window, and a void occurring right over the spot where the upper sensors were placed. Figure 4.16 illustrates this hypothetical scenario. The greatest increase in pressure occurred at the 45^{o} angle position, where the sensors above the window saw changes of up to 29% in pressure. This indicates that when arching was induced in the soil, most of the soil pressures relocated onto the sensors above the window, causing a much greater change than the ones below.

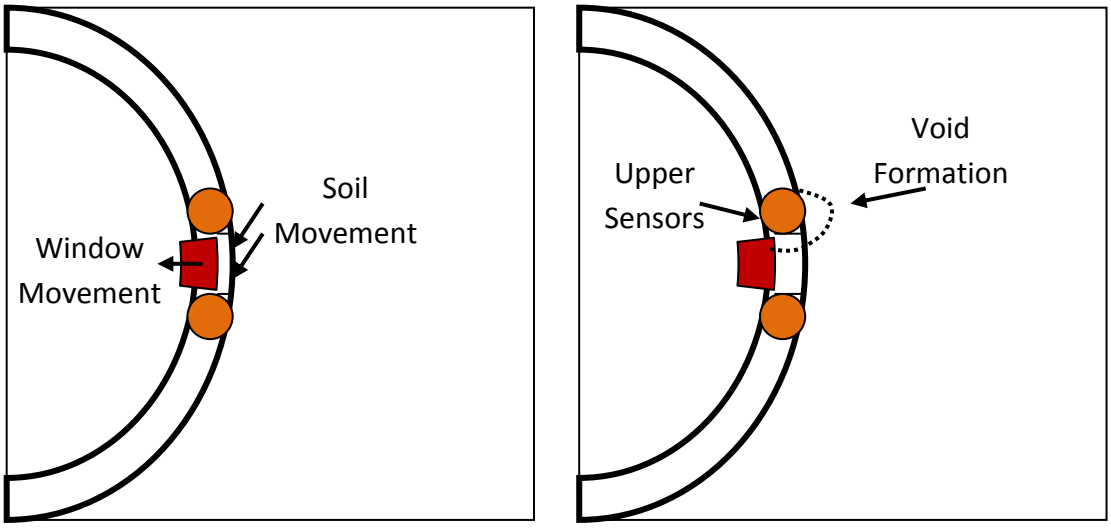

Figure 4.16: Hypothetical soil movement when window is at springline

4.5 Sources of Error

As with any experiment, it is important to note areas of the testing that may give rise to inaccurate results. While great care was taken to minimise the impact of such faults, it is not always possible to eliminate them. The following are possible areas that may have adversely affected the experiment.

1. The tunnel model attempted to simulate the tail void by decreasing the diameter of the tunnel and allowing the soil to settle upon it. To accurately simulate a tail void, this model depended on the tunnel invert to move downwards into the sand as the lining was contracted. In real tunnel construction, however, soil generally moves towards the installed lining except at the invert as it is usually the supporting point of the tunnel lining.
2. While the procedure in which the sand was placed into the tank was careful and meticulous, it is still very difficult to have sand that was completely homogenous and isotropic throughout. This problem is further aggravated by the small size of the sensors used as this would have made them even

more sensitive to particle size and compactness of the sand. The fine sand size helped mitigate but not eliminate this problem.

3. The mechanism that contracts the tunnel lining requires that a wheel be turned at the end of the tunnel. Although it does not take much force to turn this wheel, it may still impart a moment onto the tunnel lining that can affect the readings from the sensors.
4. The tunnel model was not perfectly round since it consisted of several long pipe arc segments that were aligned together to make a cylindrical tunnel. Because of this, the soil may have behaved differently upon this lining than on an actual tunnel.

Despite these possible errors, it would seem from the data that some definite conclusions can be reached with a degree of certainty. The values obtained and the soil reactions were consistent enough to validate discussion.

Chapter 5 – Summary and Conclusions

5.1 Summary

The experiment succeeded in being able to measure the change in radial pressures upon a tunnel lining with the introduction of a simulated erosion void on the TBM bored tunnel surface. This likely induced an arching effect that forced the redistribution of soil pressures on the tunnel circumference. Soil erosion was simulated at three different positions along the tunnel circumference and produced distinctly different subsurface reactions. Only positions from the springline to the invert of the tunnel were considered because erosion voids above this point would collapsed before appreciable soil arching could occur.

TBM constructed tunnel conditions were achieved by producing a model tunnel that could simulate the soil action to the introduction of a tail void. This was accomplished by constructing a tunnel model that could reduce its diameter, thus creating an artificial tail void within the soil. The pre-determined conditions of the experiment, testing in plane strain conditions and using fine dry sand, were chosen to limit extraneous factors and isolate the factors under investigation. With this in mind, the experiment was able to produce interesting and noteworthy indications of the subsurface reactions to erosion voids upon the tunnel lining.

5.2 Conclusions

The following conclusions were reached from the experimental program:

1. The introduction of the soil void on the tunnel lining surface caused increased pressure on areas of the tunnel below the springline directly adjacent to the erosion void. This may be because the soil support that was lost with the creation of the void was at least partially redistributed onto the areas next to it.

2. The subsurface reaction differed depending on the position of void. Voids at the 45^{o} bisecting angle between the springline and the invert produced the greatest increase in pressure, of +29%, while voids on the springline produced the greatest change with a -60% decrease.
3. Due to the small size of the erosion void induced, ($1.5\pi D\%$), the tests did not notice changes in pressure elsewhere on the tunnel lining.
4. A window on the lining surface was retracted to simulate erosion voids. It was retracted incrementally at 1.5 mm, and then 3.0 mm. In most cases, the window had to be retracted the full 3 mm before the maximum pressure change was reached. Because of the way the model simulated erosion voids, this may indicate the transition from at rest to active earth pressures and finally to no soil pressures on the window area.

5.3 Limitations and Recommendations

As the literature review reveals, investigations into the subsurface reaction to erosion voids on tunnel linings are scarce. This leaves many other avenues of discovery to be explored on the subject. The following list makes a few recommendations in areas of research that call for further study.

1. The size of the void, as predicted by Meguid and Dang (2008), may have a significant impact on the soil reaction to erosion voids. Therefore it would warrant further physical modelling onto voids of varying sizes. The size of the void can vary as the percentage of the tunnel circumference it encompasses or the volume size of the void. The void size at which the soil collapses and ground loss occurs can also be determined.
2. This investigation only tested the void position at three different points along the lining and found distinctly different reactions. To get a complete picture of the erosion void effects, all positions along the tunnel circumference can be examined. This can include positions above the springline.

3. The limitations of the tunnel model only allowed for placement of sensors and certain points along the lining circumference. This restricted the pressure changes to only be evident at a these points. A complete pressure profile mapping the changes along the whole tunnel circumference would be extremely valuable. This could be accomplished with a model where the pressure sensors were movable or one where multiple sensors covered the entire lining.
4. Another factor that is likely to have an impact on the reaction of erosion voids is the type of soil in which the voids are present. The soil types can be different in terms of other homogenous soils like clays and sands or mixed soils types. Various soil layers can also be examined. Because of the different ways in which other soil types transmit pressures, it can be expected that varying soil properties can affect major differences.
5. The effect of submersion and pore water pressure should also be investigated. This is because water leakage is the main cause of erosion voids in the first place, meaning that most erosion voids occur in tunnels which are either submerged or experience pore water pressure. This would require a tunnel model and sensors that are water resistant.
6. Finally, a full scale model can be tested so that the effects of scaling need not be a concern. This may be the most difficult to artificially test and a more realistic approach may be to install sensors and monitors on an existing tunnel or tunnel project. While erosion voids should not be induced, selecting sections of tunnels where they are likely to occur may be possible.

5.4 Summary of Contributions

The purpose of this thesis was to attain a method by which erosion voids could be simulated on a tunnel lining. An original experimental method was developed. Furthermore, the method was used to produce specific experimental results. The contributions of this thesis therefore include the development of an experimental method of simulating erosion voids on tunnel linings, as well as obtaining findings from the test results.

Detailed contributions are summarised in the following list:

1. In experimentally simulating the action of erosion voids on a soil lining, this thesis developed an original method of retracting a small section of the tunnel lining. This enables the reproduction of loss of soil support as well as the soil arching that likely accompanies erosion voids. It does not, however, simulate the soil volume loss of erosion voids.
2. For experimentally simulating the tail void in bored tunnels, this thesis adapted the model of a collapsible tunnel lining. This was proven to be a workable method.
3. Test results found evidence that when soil support in sand is removed from a section on the surface of a lining, the ground pressures were at least partially redistributed unto adjacent areas.
4. It was also discovered that the mode of redistribution is largely dependent on the location of the loss of soil support and is likely due to soil arching.
5. The test results of this thesis provide a framework from which numerical models and analyses can be developed to further advance knowledge regarding erosion voids on tunnel linings.

References

Asakura, T., and Kojima, Y. (2003). "Tunnel Maintenance in Japan." *Tunnelling and Underground Space Technology,* 18, pp 161 – 169.

ASTM. (2007). "ASTM D6913-04e1 (Standard Test Methods for Particle-size Distribution (Gradation) of Soils Using Sieve Analysis)"

ASTM. (2007). "ASTM D854 (Standard Test Methods for Specific Gravity of Soil Solids by Water Pycnometer)"

Bobet, A. (2001). "Analytical Solutions for Shallow Tunnels in Saturated Ground." *Journal of Engineering Mechanics.,* 127(12), pp 1258 – 1266.

Davies, J. P., Clarke, B. A., Whiter, J. T., and Cunningham, R. J. (2001). "Factors Influencing the Structural Deterioration and Collapse of Rigid Sewer Pipes." *Urban Water,* 3, pp 73 – 89.

Davis, A. G., Lim, M. K., and Petersen, C. G. (2005). "Rapid Economical Evaluation of Concrete Tunnel Linings with Impulse Response and Impulse Radar Non-Destructive Methods." *Non-Destructive Testing and Evaluation International,* 38, pp 181 – 186.

Delatte, N., et al. (2003). "Application of Nondestructive Evaluation to Subway Tunnel Systems." *Transportation Research Record,* Vol. 1845, 127 – 135.

Einstein, H. H., and Schwartz, C. W. (1978). "Simplified Analysis for Tunnel Supports." *American Society of Civil Engineers, Journal of the Geotechnical Engineering Division,* 105(4), 499 – 518.

El Tani, M. (2003). "Circular Tunnel in a Semi-Infinite Aquifer." *Tunnelling and Underground Space Technology,* 18, pp 49 – 55.

Fenner, R. A. (2000). "Approaches to Sewer Maintenance: A Review." *Urban Water,* 2, pp 343 -356.

Freeze, R. A., and Cherry, J. A. (1979). *Groundwater.* Prentice – Hall, Englewood Cliffs, New Jersey.

Girmsheid, G., and Schexnnayder, C. (2003). "Tunnel Boring Machines." *Practice Periodical on Structural Design and Construction,* ASCE, Vol. 8, No. 3, pp 150 – 163.

González, C., and Sagaseta, C. (2001). "Patterns of Soil Deformations around Tunnels. Application to the Extension of Madrid Metro." *Computers and Geotechnics,* Vol. 28, pp 445 – 468.

Goodman, R. (1965). "Groundwater Inflows During Tunnel Driving." *Engineering Geology,* 2 (2), pp 39 – 56.

Guglielmetti, Vittorio, Piergiorgio Grasso, Ashraf Mahtab and Shulin Xu. (2007). *Mechanized Tunneling in Urban Areas*. London, UK: Taylor & Francis Group.

Helfrich, S. C. (1997). "Investigation of Sewer-Line Failure." *Journal of Performance of Constructed Facilities*, pp 42 – 44.

Hoffman, M. And Lerner, D. (1992). "Leak Free Sewers: Who Needs Them." *Water and Waste Treatment Journal,* Vol. 35, No. 8, pp 18 – 19.

Hwang, J-H., and Lu, C-C. (2007). "A Semi-Analytical Method for Analyzing the Tunnel Water Inflow." *Tunnelling and Underground Space Technology,* 22, pp 39 – 46.

ITA. (1991). "Report on the Damaging Effects of Water on Tunnels During Their Working Life." *Tunnelling and Underground Space Technology,* Vol. 6, No. 1, pp 11 – 76.

Kolymbas, D., and Wagner, P. (2007). "Groundwater Ingress to Tunnels – The Exact Analytical Solution." *Tunnelling and Underground Space Technology,* 22, pp 23 – 27.

Lee, I-M., and Nam, S-W. (2006). "Seepage Force Considerations in Tunnelling." *International Symposium on Underground Excavation and Tunnelling,* pp 21 – 27.

Lee, K. M., Rowe, R. K., and Lo, K. Y. (1992). "Subsidence owing to tunnelling. I. Estimating the gap parameter." *Canadian Geotechnical Journal*, Vol. 29, pp 929 – 940.

Lee, Y-J., and Bassett, R. H. (2006). "A Model Test and Numerical Investigation of the Shear Deformation Patterns of Deep Wall-Soil-Tunnel Interaction." *Canadian Geotechnical Journal,* NRC, 43, pp 1306 – 1323.

Lei, F. Z. (1999). *Applied Mathematics in Hydrogeology.* Lewis Publishers, Boca Raton, Florida.

Loganathan, N., and Poulos, H. G. (1998). "Analytical Prediction for Tunneling-induced Ground Movements in Clays." *Journal of Geotechnical and Geoenvironmental Engineering,* 124(9), pp 846 – 856.

MacDonald, S. E., and Zhao, J.Q. (2001). “Condition Assessment and Rehabilitation of Large Sewers.” *International Conference on Underground Infrastructure Research,* University of Waterloo, Ontario, pp 361 – 369.

Meguid, M.A., and Dang, H.K. (2008). “The effect of erosion voids on existing tunnel linings.” *Tunnelling and Underground Space Technology,* 24, pp 278 – 286.

Meguid, M. A., Saada, O., Nunes M. A., and Mattar, J. (2007). “Physical Modeling of Tunnels in Soft Ground: A Review.” *Tunnelling and Underground Space Technology,* Vol. 23, No. 2, pp 185 – 189.

Meiri, D. (1985). “Unconfined Groundwater Flow Calculation into a Tunnel.” *Journal of Hydrology,* 82, pp 69 – 75.

Mindlin, R. D. (1940). “Stress Distribution around a Tunnel.” *Trans. ASCE*; 105:1117 – 40.

Moore, I. D. (2008). “Assessment of Damage to Rigid Sewer Pipes and Erosion Voids in the Soil, and Implications for Design of Liners.” *North American Society for Trenchless Technologies Conference and Exhibition,* C-2-01.

Muir Wood, A. M. (1975). “The Circular Tunnel in Elastic Ground.” *Géotechnique*, 25, pp 115 – 127.

Nam, S-W., and Bobet, A. (2006). “Liner Stresses in Deep Tunnels Below the Water Table.” *Tunnelling and Underground Space Technology,* 21, pp 626 – 635.

Park, K-H., Lee, J-G., and Owatsiriwong, A. (2008). “Seepage Force in a Drained Circular Tunnel: An Analytical Approach.” *Canadian Geotechnical Journal,* 45, pp 432 – 436.

Peck, R. B., Hendron, A. J., and Mohraz, B. (1972). “State of the Art of Soft-Ground Tunneling.” *Rapid Excavation and Tunneling Proceedings,* Vol. 1, pp 259 – 286.

Peck, R. B. (1969). “Deep Excavations and Tunneling in Soft Ground.” *Proceedings of the Seventh International Conference on Soil Mechanics and Foundation Engineering,* Mexico City, pp 225 – 290.

Sagaseta, C. (1987). “Analysis of Undrained Soil Deformation Due to Ground Loss.” *Géotechnique,* 37(3), 301 – 320.

Schmidt, B. (1969). “Settlements and Ground Movements Associated with Tunneling in Soil.” Ph.D. Thesis*,* University of Illinois, Urbana.

Serpente, P. E. (1994). “Understanding the Modes of Failure for Sewers.” *Urban Drainage Rehabilitation Programs and Techniques Selected Papers on Urban Drainage Rehabilitation from 1988 – 1993.* New York: ASCE.

Shin, H-S., Youn, D-J., Chae, S-E., and Shin, J-H. (2009). “Effective Control of Pore Water Pressures on Tunnel Linings using Pin-Hole Drain Method.” *Tunnelling and Underground Space Technology,* 24, pp 555 – 561.

Shin, J. H., Potts, D. M., and Zdravkovic, L. (2005). “The Effect of Pore-Water Pressure on NATM Tunnel Linings in Decomposed Granite Soil.” *Canadian Geotechnical Journal,* NRC, 42, pp 1585 – 1599.

Spasojevic, A. D., Mair, R. J., and Gumbel, J. E. (2007). “Centrifuge Modelling of the Effects of Soil Loading of Flexible Sewer Liners.” *Géotechnique*, Vol. 57, No. 4, pp 331 – 341.

Talesnick, M., and Baker, R. (1999). “Investigation of the Failure of a Concrete-Lined Steel Pipe.” *Geotechnical and Geological Engineering,* Vol. 17, pp 99 – 121.

Tan, Z. (2007). “Effect of Soil Voids on Sewer Repair Using Liners.” MSc Thesis, Department of Civil Engineering, Queen’s University at Kingston, Ontario, Canada.

Tan, Z. and Moore, I.D. (2007). “Effect of Backfill Erosion on Moments in Buried Rigid Pipes.” Transportation Research Board Annual Conference, Washington D.C. January, 29.

Tobar Valencia, T. (2009). “An Experimental Study of the Earth Pressure Distribution on Cylindrical Shafts.” MEng Thesis, Department of Civil Engineering, McGill University in Montreal, Quebec, Canada.

U.S. Department of Transportation. (2005). *Federal Highway Administration. Highway and Rail Transit Maintenance and Rehabilitation Manual*, pp. 4-1–4-36. (Chapter 4).

Zhang, L., and Franklin, J. A. (1993). “Prediction of Water Flow into Rock Tunnels: an Analytical Solution Assuming an Hydraulic Conductivity Gradient.” *International Journal of Rock Mechanics and Mining Sciences and Geomechanics Abstracts,* 30 (1), pp 37 – 46.

Appendix A

Soil Properties Data

This appendix shows data from some of the soil properties tests. This includes the specific gravity tests and sieve analysis tests. All tests were done with ASTM standardised procedures. Figure A.1 shows the results of tests from 5 soil samples. The two outliers are ignored and the rest are averaged. Figures A.2 – A.4 are the results from the sieve analysis tests. Figure A.5 is the summary of the sieve analysis. Figure A.6 are the results of the soil samples taken using the sampling cups during testing. These determine the sand density at different layers of soil.

Test no.	1	2	3	4	5
Vol. Of flask at 20˚C	500 mL	500 mL	500 mL	500 mL	500 mL
Method of air removal	vacuum	vacuum	vacuum	vacuum	vacuum
Mass fl. + water + soil = M_{bws}	745.22	748.06	748.38	752.54	748.6
Temperature, ˚C	23	23	23	23	23
Mass fl. + water[b] = M_{bw}	682.91	673.55	673.99	677.72	673.75
Dish no.	1	2	3	2	3
Mass dish + dry soil	215	190.78	192.95	193.38	192.93
Mass of dish	115.42	73.65	73.16	73.77	73.25
Mass of dry soil = M_s	99.58	117.13	119.79	119.61	119.68
$M_w = M_s + M_{bw} - M_{bws}$	37.27	42.62	45.4	44.79	44.83
$\alpha = \rho_T/\rho_{20^\circ C}$	0.9993338	0.9993338	0.9993338	0.9993338	0.999334
Gs = αMs/Mw	2.67007406	2.74640939	2.63678846	2.6686831	2.667862
	Average	**2.660852**			

Figure A.1: Tests results from the Specific Gravity Tests

Soil Type: A 100 % Fine Sand 0 % Coarse Sand

Sample 1 Empty Plate Weight (kg) 0.13

Plate + Soil Sample Weight (kg) 2.115

Total Soil Sample Weight (kg) 1.985

Sieve #	Mass of each Sieve (kg)	Mass of each Sieve + Retained Soil (kg)	Mass of Soil Retained (kg)	Percentage on each Sieve (%)	Cummulative Percent Retained (%)	Percent Finer or Passing (%)
8	0.585	0.585	0	0.00	0.00	100.00
12	0.475	0.475	0	0.00	0.00	100.00
20	0.435	0.435	0	0.00	0.00	100.00
50	0.355	1.665	1.31	65.99	65.99	34.01
60	0.38	0.555	0.175	8.82	74.81	25.19
140	0.34	0.82	0.48	24.18	98.99	1.01
200	0.335	0.36	0.025	1.26	100.25	-0.25
Pan	0.365	0.38	0.015	0.76	101.01	-1.01

Figure A.2: Sieve analysis test 1

Soil Type: A 100 % Fine Sand 0 % Coarse Sand

Sample 2 Empty Plate Weight (kg) 0.13

Plate + Soil Sample Weight (kg) 1.64

Total Soil Sample Weight (kg) 1.51

Sieve #	Mass of each Sieve (kg)	Mass of each Sieve + Retained Soil (kg)	Mass of Soil Retained (kg)	Percentage on each Sieve (%)	Cummulative Percent Retained (%)	Percent Finer or Passing (%)
8	0.585	0.585	0	0.00	0.00	100.00
12	0.475	0.475	0	0.00	0.00	100.00
20	0.435	0.435	0	0.00	0.00	100.00
50	0.375	0.845	0.47	31.13	31.13	68.87
60	0.38	0.775	0.395	26.16	57.28	42.72
140	0.34	0.935	0.595	39.40	96.69	3.31
200	0.335	0.365	0.03	1.99	98.68	1.32
Pan	0.37	0.385	0.015	0.99	99.67	0.33

Figure A.3: Sieve analysis test 2

Sample 3 Empty Plate Weight (kg) 0.13

Plate + Soil Sample Weight (kg) 2.205

Total Soil Sample Weight (kg) 2.075

Sieve #	Mass of each Sieve (kg)	Mass of each Sieve + Retained Soil (kg)	Mass of Soil Retained (kg)	Percentage on each Sieve (%)	Cummulative Percent Retained (%)	Percent Finer or Passing (%)
8	0.585	0.585	0	0.00	0	100
12	0.475	0.475	0	0.00	0	100
20	0.435	0.435	0	0.00	0	100
50	0.375	1.945	1.57	75.66	75.66	24.34
60	0.38	0.52	0.14	6.75	82.41	17.59
140	0.34	0.68	0.34	16.39	98.80	1.20
200	0.335	0.35	0.015	0.72	99.52	0.48
Pan	0.365	0.375	0.01	0.48	100.00	0.00

Figure A.4: Sieve analysis test 3

Sample #		1	2	3	Average
Sieve #	Sieve Size (mm)	Percent Finer or Passing (%)	Percent Finer or Passing (%)	Percent Finer or Passing (%)	Percent Finer or Passing (%)
8	2.38	100	100	100	100
12	1.68	100	100	100	100
20	0.85	100	100	100	100
50	0.3	34.005	68.8742	24.3373	42.4055
60	0.25	25.1889	42.7152	17.5904	28.4982
140	0.106	1.00756	3.31126	1.20482	1.84121
200	0.075	0	1.3245	0.48193	0.60214
Pan	0	0	0.33113	0	0.11038

Figure A.5: Sieve analysis summary

		Weight Can + Soil (gr)	Weight Can (gr)	Net Soil Weight (kg)	Density (kg/m3)	Unit Weight (kN/m3)
Test #1	L 1 Can #2	294.40	99.23	0.20	1573.95	15.44
	L 2 Can #1	289.76	91.95	0.20	1585.02	15.55
	L 3 Can #3	259.12	78.13	0.18	1442.15	14.15
Test # 2	L 1 Can #2	291.47	99.26	0.19	1550.08	15.21
	L 2 Can #1	281.95	91.95	0.19	1522.44	14.94
	L 3 Can #3	264.94	78.14	0.19	1488.45	14.60
Test # 3	L 1 Can #2	292.66	99.32	0.19	1559.19	15.30
	L 3 Can #3	266.01	78.10	0.19	1497.29	14.69

Figure A.6: Soils densities from test sampling cups

Appendix B

Load Cell Specifications

This appendix has specifications of the load cells that were used in the experiments. This includes sensor mounting instructions, calibration factors and load and deflection factors.

SCAIME

AR: NOTICE DE MONTAGE
AR: MOUNTING INSTRUCTIONS

Les capteurs AR, sont des capteurs de faible portée, très fragiles, et des précautions de manipulation sont indispensables pour ne pas les détériorer (risques importants de surcharge et de décalage du zéro).
Faire attention en déballant les capteurs.
Tenir les capteurs à plat dans la main, jamais par une extrémité.

The AR series of load cells have extremely low capacities, are very fragile, and must be manipulated with a lot of care to avoid risk of damages (possible overloads and offset zero problems).
Be carreful when unpacking the load cells.
Carry the load cells flat on the hand, never take it from one of the end.

Encombrement & fixation / *Dimensions and fixing specifications.*

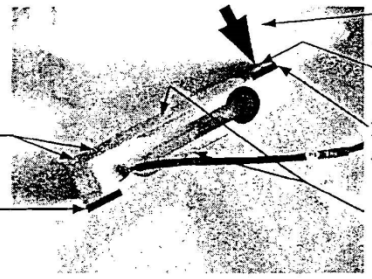

Montage du capteur sur la base :
Utiliser 2 vis M4x0.7, serrer au couple de 1mN, toujours maintenir le capteur du coté du câble pour éviter de le contraindre.

Base plate mounting :
Use 2 M4x0.7 screw, tighten torque 1mN, always hold the load cell from the cable side to avoid any extra strain.

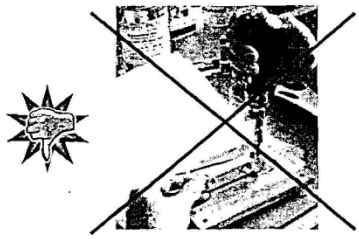

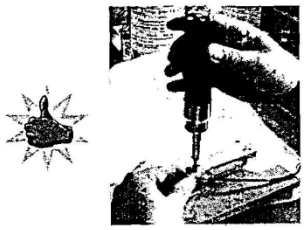

Montage du plateau :
Utiliser 1 vis M4x0.7, serrer au couple de 1mN, attention au poids de la clef dynamométrique (souvent supérieur à 800gr), se forcer à transmettre le couple de serrage en soulageant le poids de la clef.
Ne pas appuyer sur le plateau avec la clef.
Utiliser une cale ou ramener les butée de surcharge en contact chaque fois que cela est possible.
Toujours maintenir le plateau au moment du serrage, jamais la base, pour ne pas transmettre le couple au capteur.

Top plate mounting :
Use 1 M4x0.7 screw, tighten torque 1mN, pay attention to the weight of the torque wrench (usually higher than 800gr), apply the tighten torque keeping in mind to lighten weight of the torque wrench. ***Do not push down the plate with the torque wrench.***
Use a spacer or set the stop in contact with the load cell any time it's possible.
Always hold the plate (not the base) when screwing in order to avoid the transmission of a torque to the load cell.

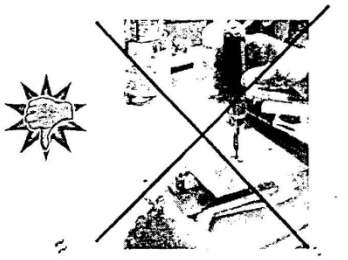

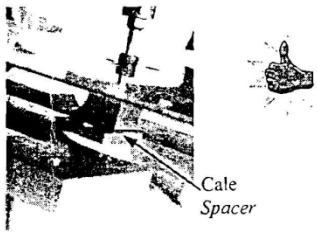

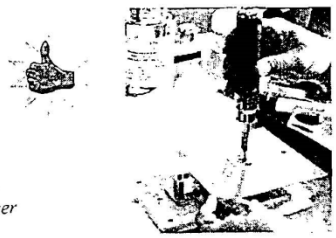

142701-A 1/1

SCAIME

CERTIFICAT DE CONTROLE FINAL
CONTROL CERTIFICATE

Contrôleur - *Inspector:* 17350
Date - *Date:* 2008/10/29
Modèle - *Model:* AR1.2
Référence - *Reference:* 400979
N° de série - *Serial N°:* 001855

CE

Capacité nominale - *Rated capacity* : (kg)	1.2
Sensibilité nominale, à Cn - *Rated output, at Cn* : (mV/V)	1.086
Zéro initial - *Zero balance* : (µV/V)	-7
Résistance d'entrée - *Input resistance* : (Ω)	405.0
Résistance de sortie - *Output resistance* : (Ω)	349.8
Résistance d'isolement - *Insulation resistance* : (GΩ/50V)	> 1
Plage de temp. compensée - *Compensated temp. range* : (°C)	+5 /+35
Degré de protection - *Protection class* :	IP 63
Durée garantie - *Warranty period* : (an/year)	1

Informations complémentaires - *Additionnal information*

Tension d'alimentation max - *Maximum excitation voltage* : (V)	12
Couple de serrage - *Tightening torque* : (Nm)	1
Longueur de câble - *Cable Lenght* : (m)	0.25
Taille de plateau maximum - *Maximum plateform size* : (mm)	150x150
Blindage raccordé au corps d'épreuve - *Shield connected to load cell body* : (Y/N)	N

Schema de câblage - *Wiring color code*

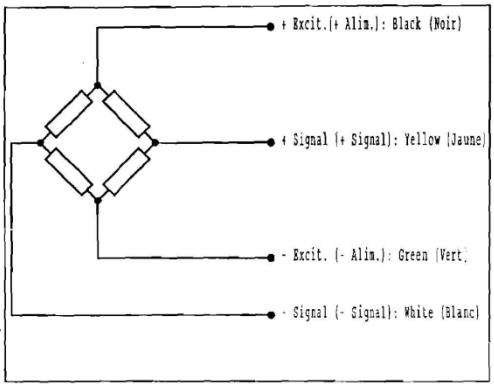

Caractéristiques métrologiques du certificat d'essai - *Test certificate metrology specifications*

OIML	NTEP
Délivré par - *Delivered by:*	
Class :	Accuracy class :
Emin :	Min. dead load :
Emax :	Max load cell capacity :
Elim :	Safe load limit :
n.max :	n.max single cell :
v.min :	n.max multiple cell :
Y :	v.min :
Z :	
Plc :	

Attention: ne pas couper le câble, cela peut modifier l'étalonnage, créer de l'instabilité et rendre le capteur non standard.
Beware: do not cut the cable, this may affect the calibration, iduce instability, turn the load cell into a non-standard version.

Fiches techniques, notices et accessoires de montage disponibles: consulter notre site web (www.scaime.com) ou notre département commercial au +33 (0)4 50 87 78 64.
Data sheet, mounting instructions and accessories also available: consult our website (www.scaime.com) or our sales department at +33 (0)4 50 87 78 64.

SCAIME

CERTIFICAT DE CONTROLE FINAL
CONTROL CERTIFICATE

Contrôleur - *Inspector:*	17350
Date - *Date:*	2008/10/29
Modèle - *Model:*	AR1.2
Référence - *Reference:*	400979
N° de série - *Serial N°:*	001840

CE

Capacité nominale - *Rated capacity* : (kg)	1.2
Sensibilité nominale, à Cn - *Rated output, at Cn* : (mV/V)	1.078
Zéro initial - *Zero bolonce* : (µV/V)	5
Résistance d'entrée - *Input resistance* : (Ω)	404.7
Résistance de sortie - *Output resistance* : (Ω)	349.9
Résistance d'isolement - *Insulation resistance* : (GΩ/50V)	> 1
Plage de temp. compensée - *Compensated temp. range* : (°C)	+5 /+35
Degré de protection - *Protection class* :	IP 63
Durée garantie - *Worranty period* : (an/year)	1

Schema de câblage - *Wiring color code*

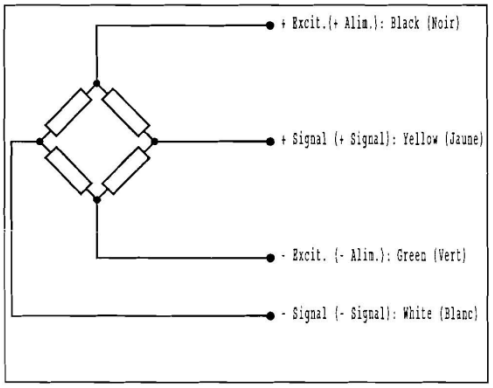

Informations complémentaires - *Additionnal information*

Tension d'alimentation max - *Maximum excitation voltage* : (V)	12
Couple de serrage - *Tightening torque* : (Nm)	1
Longueur de câble - *Cable Lenght* : (m)	0.25
Taille de plateau maximum - *Maximum plateform size* : (mm)	150x150
Blindage raccordé au corps d'épreuve - *Shield connected to load cell body* : (Y/N)	N

Caractéristiques métrologiques du certificat d'essai - *Test certificate metrology specifications*

OIML	NTEP
Délivré par - *Delivered by:*	
Class :	Accuracy class :
Emin :	Min. dead load :
Emax :	Max load cell capacity :
Elim :	Safe load limit :
n.max :	n.max single cell :
v.min :	n.max multiple cell :
Y :	v.min :
Z :	
Plc :	

Attention: ne pas couper le câble, cela peut modifier l'étalonnage, créer de l'instabilité et rendre le capteur non standard.
Beware: do not cut the cable, this may affect the calibration, iduce instability, turn the load cell into a non-standard version.

Fiches techniques, notices et accessoires de montage disponibles: consulter notre site web (www.scaime.com) ou notre département commercial au +33 (0)4 50 87 78 64.
Data sheet, mounting instructions and accessories also available; consult our website (www.scaime.com) or our sales department at +33 (0)4 50 87 78 64.

Scaime SAS - ZI de Juvigny - BP501 - 74105 Annemasse cedex
Tél. +33 (0)4 50 87 78 64 - Fax : +33 (0)4 50 87 78 46 - E-mail : info@scaime.com

FUTEK MODEL LBB200 (L1501) *CANTILEVER BENDING BEAM LOAD CELL*

Drawing Number: FI1049-B

INCH [mm] | R.O.= Rated Output

WIRING CODE (WC3)			
+Excitation	-Excitation	+Signal	-Signal
RED	WHITE	BLACK	GREEN
Shield			
FLOATING			

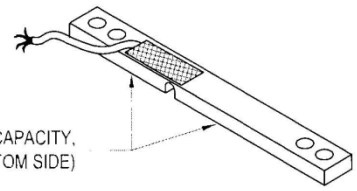

MODEL#, CAPACITY,
ID# (BOTTOM SIDE)

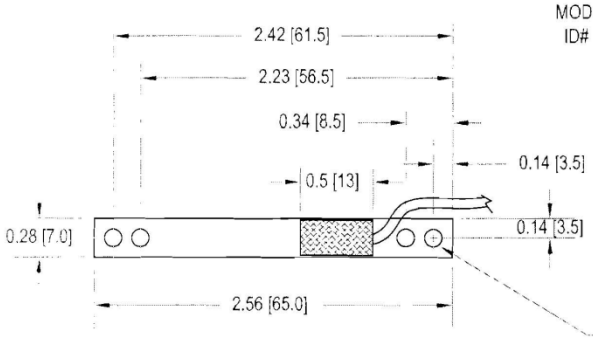

- OUTPUT
(COMPRESSION)

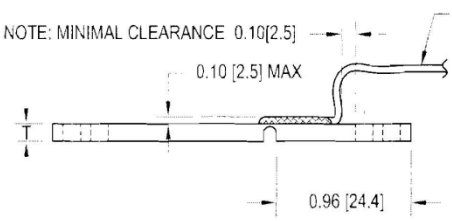

lb	CAPACITY lb	CAPACITY N	NOM. DEFLECTION	T
FSH00887	1/4	1.1	0.022 [0.56]	0.12 [3]
FSH00888	1/2	2.2	0.016 [0.41]	0.12 [3]
FSH00889	1	4.5	0.011 [0.28]	0.12 [3]
FSH00890	2	8.9	0.008 [0.20]	0.12 [3]
FSH00891	5	22	0.010 [0.25]	0.18 [4.6]
FSH00892	10	44.5	0.008 [0.20]	0.18 [4.6]
FSH00893	25	111	0.015 [0.38]	0.18 [4.6]

SPECIFICATIONS:

RATED OUTPUT	*1 mV/V nom.*
SAFE OVERLOAD	*150% of R.O.*
ZERO BALANCE	*±10% of R.O.*
EXCITATION (VDC OR VAC)	*18 MAX*
BRIDGE RESISTANCE	*1000 Ω nom.*
NONLINEARITY	*±0.05% of R.O.*
HYSTERESIS	*±0.05% of R.O.*
NONREPEATABILITY	*±0.01% of R.O.*
TEMP. SHIFT ZERO	*±0.02% of R.O./°F[0.036% of R.O./°C]*
TEMP. SHIFT SPAN	*±0.02% of LOAD/°F[0.036% of LOAD/°C]*
COMPENSATED TEMP.	*60 to 160°F [15 to 72°C]*
OPERATING TEMP.	*-45 to 200°F [-42 to 93°C]*
WEIGHT	*1 oz [28 g]*
MATERIAL	*17-4PH S.S.*
DEFLECTION	*SEE CHART*

CABLE: #26 AWG, 4 Conductor Spiral Shielded PVC Cable 1 ft [0.3 m] Long

FUTEK
ADVANCED SENSOR TECHNOLOGY, INC.

10 THOMAS
IRVINE, CA 92618 USA
1-800-23-FUTEK (38835)

INTERNET:
http://www.futek.com

Extraneous Load Factors

Equation: $\sigma_{max} \geq$ (A)Fx +(B)Fy +(C)Fz +(D)Mx +(E)My +(F)Mz

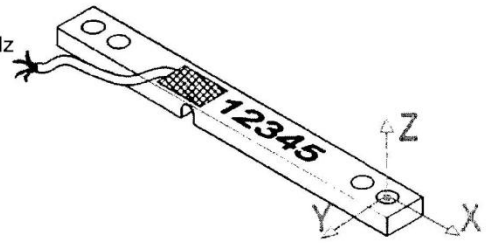

Material: 17-4 PH Stainless Steel

Material	Capacity (lb)	A	B	C	D	E	F
(S.S.*)	0.25	734.78	11769.63	97436.56	19525.03	68958.60	8374.34
	0.5	629.37	9717.03	69999.38	16184.95	49633.98	6912.28
	1.0	412.03	6116.87	26539.13	9413.14	18538.52	4271.47
	2.0	355.37	4617.90	19055.32	6845.69	13371.81	3222.67
	5.0	237.16	1863.48	5505.70	3816.56	6195.15	3339.65
	10	206.36	1261.25	2557.27	3001.74	3631.74	2493.52
	25	217.73	217.73	2007.15	2007.15	2107.61	2107.61

σ_{max} **Table**

Material	Static Load (=60% Y.S.)	Fatigue (Non Reversing Loads)	Fatigue (Full Reversing Loads)
17-4 PH S.S.	87,000	78,000	62,000*

*Value is 75% of Fatigue Strength based on 10-20 x 10^6 cycles and allow for factors that influence Fatigue such as surface finish, stress concentrations, corrosion, temperature and other variables for the production of the transducer, for infinite Fatigue Life (100 x 10^6) use 75% of values shown.

Deflection & Natural Frequency

Material	Capacity (lb)	Deflection (in.)	Natural Frequency (Hz)	β
(S.S.*)	0.25	0.007	150	0.0145
	0.5	0.010	180	0.0146
	1.0	0.009	270	0.0146
	2.0	0.012	330	0.0147
	5.0	0.007	570	0.0220
	10	0.009	700	0.0222
	25	0.020	730	0.0227

*FN results are based on calculation of deflection & weight scene on Sensor arm.

Natural Frequency & Frequency Response Equation's:

$$\text{Natural Frequency (FN)} = 3.13 \sqrt{\frac{1}{\frac{\beta}{Capacity} \bullet Deflection}} \text{ (Hz)}$$

$$\text{Frequency Response with load (FR)} = 3.13 \sqrt{\frac{1}{\frac{\beta + AppliedLoad}{Capacity} \bullet Deflection}} \text{ (Hz)}$$

*Where β values are obtained by Futek Engineers